INVESTIGATING THE ROLE OF TUMOUR NECROSIS FACTOR RECEPTOR ASSOCIATED FACTOR 1 (TRAF1) VARIANTS IN REGULATING INFLAMMATION IN MURINE MODELS OF LIPOPOLYSACCHARIDE-INDUCED SEPSIS

Sahib Singh Madahar

A thesis submitted to the Faculty of Graduate Studies
in partial fulfillment of the requirements
for the degree of

MASTER OF SCIENCE

Graduate Program in Biology
York University
Toronto, Ontario

June 2024

© Sahib Singh Madahar, 2024

Abstract

Sepsis, a life-threatening condition, is characterized by a dysregulated inflammatory response to an infection ultimately leading to severe organ dysfunction and progression to a stage of septic shock. Although the role of NF-κB in the pathophysiology of sepsis has been extensively investigated, the development of evidence-based therapies is limited, and treatment interventions are sparce. Tumor necrosis factor receptor (TNFR) associated factor 1 (TRAF1) is a signalling adaptor protein that is involved in regulating the activation of NF-κB. The TRAF1 protein has been implicated in several chronic autoimmune diseases characterized by persistent and abnormal inflammation such as rheumatoid arthritis (RA). Unpublished in vitro research from our lab has identified a single amino acid mutation in TRAF1, V203A, that can limit the activation of lymphocytes and reduce the production of pro-inflammatory cytokines in macrophages. However, whether these results translate to an in vivo model is not known. To this end, we have generated a knock-in mouse model where the same mutation was introduced into the TRAF1 gene by CRISPR/Cas12a, referred to as TRAF1 V196A. The primary focus of this thesis was to investigate whether the TRAF1 V196A variant reduces inflammation and protects mice from lipopolysaccharide (LPS)-induced sepsis. Our findings reveal that TRAF1 V196A male mice are completely protected in the lethal model of LPS, and that this protection is less pronounced in female mice. However, the sublethal model does not show any differences in cytokine productions. Undoubtedly, this led us to explore the inflammatory responses in two different cell types, macrophages and T cells, to better understand the cell- and pathway- specific role that the TRAF1 V196A variant plays in regulating inflammation. Here, we discovered a significant reduction in LPS-induced inflammation in macrophages and a reduced response of TRAF1 V196A T cells to TNFα stimulation. The key to an effective therapeutic is a balanced immune response and by

understanding the protein-protein interactions in different immune cell types, TRAF1 can be selectively targeted. Cumulatively, these findings provide insights about the effects of selectively targeting TRAF1 to reduce inflammation which could lead to the development of future therapies to improve outcomes of abnormal inflammation that is driven by NF-κB activation.

Acknowledgements

First and foremost, I would like to express my sincerest gratitude and appreciation to my co-supervisors, Dr. Ali Abdul-Sater and Dr. Gary Sweeney, for their continuous guidance and support throughout the degree. I am very grateful to both of you for providing me with the opportunity to complete this project for my master's degree.

To Dr. Abdul-Sater, thank you for your unwavering support, motivation and guidance over the last two years and for providing me with the opportunity to learn lifelong skills that I will be able to take with me in my future academic endeavours. Sir, you truly went above and beyond as a mentor and supervisor, and I am very fortunate to have had the opportunity to be your student. You were always generous with your time in explaining ideas and protocols and I greatly appreciate your patience in answering my countless questions and text messages and for your advice and expertise every step of the way. Thank you for creating a lab environment that fostered competence, curiosity and empowerment. Sorry for all of the reference letter requests and sporadic timings of my messages!

I would also like to thank my committee member, Dr. Peter Backx, for providing valuable input, providing excellent feedback and thought-provoking questions to help direct this project. I would also like to thank Dr. Arthur Cheng for supporting the thesis examination and for our conversations about science and life which are always refreshing. I would also like to provide a special thanks to Dr. Nikolaus Troje (undergraduate supervisor), Dr. Adam Bebko (undergraduate mentor), Dr. Samuel Benchimol (undergraduate thesis supervisor), Dr. Robert Tsushima, and Dr. David Miller (undergraduate mentor and also a good friend, David) for sparking my interest in research and for always providing valuable support and guidance. David, our conversations about life and science are always refreshing and I truly appreciate you for providing advice whenever I needed. I would also like to recognize the valuable input that I received from the Vivaria team and express my gratitude for their support. Thank you Wendy, Roy and Melissa for your invaluable training and expertise, and Carly, Debra and the rest of the team for your support. Thank you Melissa for your time and help with managing our mice colony at UHN. I would also like to thank Dr. Amir Tehrani for his time in providing valuable insight on primer design and sharing the best practices for RT-qPCR.

I would also like to express my appreciation to alumni and current members of the Sater lab for their support and help throughout the project. A very special thank you to Alita, Saher,

Mayoorey, Yitian, Emily, Azin, Laura, Jasika and Ibrahim for making this an enriching, insightful and memorable experience. A special shoutout to all of the highlights in our group chat and our coffee runs, you have all made my experience unforgettable! Thank you to our post-docs, Ali A. and Ali M., for providing advice and for helping me learn some of the mice protocols. I would also like to thank Shahrzad, Arshdeep, Madison, Shivam, Luca, Aditya, Brooke, Andrew, Luke, Rohin, Mohamed, Parashar, Naz, Dana, Farnaz, Deysi, Sehaj and Hassan for always being there to share advice whenever I needed and for our interesting conversations about science and movies! I would like to thank everyone else who supported me in various ways throughout my degree. Among them, I would like to mention Puneet, Muskan, Richi, Shayan, Ramsha, Elana, Nour, Sukhi, Toby, Alita, Sarah, Saher, Jasika, Sejal, Gurnoor, Joel, Mihir and Karishma. I greatly appreciate your presence, comic relief and time for always providing encouragement and support.

Most importantly, I would like to share my deepest thanks and appreciation to my parents, Manjinder Kaur and Sarbjit Singh, for their constant love and support. Thank you mom and dad for always going above and beyond to support me in every aspect of my journey and to motivate me to pursue my dreams and aspirations. I am certain that I would not be on the path that I am on today without the support from both of you. I appreciate the sacrifices that both of you made, and I will always be thankful for the opportunities that you have provided me with. I truly hope I can express my gratitude and make both of you proud one day. Thank you to my sister, Avneet, for being there to support and for building Legos with me and to the rest of the family for always cheering me on.

The completion of this thesis marks the start of a new journey for me, and I will always be grateful for the wonderful experiences this degree has provided me with and the valuable connections that were made. It has been an honour and a pleasure to have had this experience.

Table of Contents

Abstract ii

Acknowledgements iv

Table of Contents vi

List of Tables ix

List of Figures x

List of Abbreviations xii

Chapter 1: Introduction 1

1.1 – Overview of Sepsis and Septic Shock 1

1.2 – Overview of Rheumatoid Arthritis 5

1.3 – Overview of the Immune System and NF-κB Activation 6

1.4 – Protein Regulation by Ubiquitination 10

1.5 – Toll-Like Receptors (TLRs) 12

1.6 – Tumour Necrosis Factor Receptors (TNFRs) 14

1.7 – TNFR-Associated Factor 1 (TRAF1) 15

1.8 – Multifaceted role of TRAF1 in TLR and TNFR Signalling 16

Chapter 2: Rationale and Hypothesis 19

2.1 – Rationale 19

2.2 – Objectives 20

2.3 – Hypothesis 20

Chapter 3: Materials and Methods 22

3.1 – Animal Care of C57BL/6 Mice 22

3.2 – Mice Genotyping 22

3.2.1 – DNA Extraction 22

3.2.2 – PCR Amplification and Gel Electrophoresis 22

3.2.3 – DNA Purification 24

3.2.4 – DNA Sequencing 24

3.3 – Cell Culture 26

3.3.1 – Culturing Primary and Immortalized Bone Marrow-Derived Macrophages 26

3.3.2 – Culturing T Cells 26

3.3.3 – Culturing HEK293T/17 Cells 26

3.3.4 – Culturing iMac Cells 27

3.3.5 – Cell Counting 28

3.3.6 – Freezing Cells 28

3.4 – Lethal and Sublethal Sepsis Models 28

3.4.1 – Lethal Model, Lethal Dose Determination and Murine Sepsis Scoring 28
3.4.2 – Sublethal Model 31
3.4.3 – LEGENDplex Bead-Based Flow Cytometry Assay 32
3.5 – In Vitro Lipopolysaccharide Experiments *34*
3.5.1 – Mouse Bone Marrow Extraction 34
3.5.2 – Immortalization of Primary Bone Marrow-Derived Macrophages 36
3.5.3 – Lipopolysaccharide (LPS) Stimulations 38
3.5.4 – RNA Extraction 38
3.5.5 – cDNA Synthesis through Reverse Transcription (RT) of RNA 40
3.5.6 - Real-Time Quantitative Polymerase Chain Reaction (RT-qPCR) 41
3.5.7 – Protein Lysate Preparation 43
3.5.8 –Bradford Protein Assay 44
3.5.9 – Western Blotting 45
3.5.10 – Detection of Phospho-Signalling by Flow Cytometry 47
3.5.11 – Inflammasome Activation 49
3.5.12 – IL-1β ELISA 49
3.6 – T Cell Isolation and Stimulation Assays *51*
3.6.1 – Collection of Splenocytes from the Spleen 51
3.6.2 – Negative Selection of T Cells from Splenic Suspension 52
3.6.3 – Carboxyfluorescein Succinimidyl Ester (CFSE) Staining 52
3.6.4 – Co-stimulation with CD3 and 3H3 53
3.6.5 – CD3 and TNFα Stimulations 54
3.6.6 – Proliferation Assay – Flow Cytometry 55
3.6.7 – Proliferation Assay – Trypan Blue 56
3.7 – Site-Directed Mutagenesis (SDM) for TRAF1 T268A and W271A Variants *56*
3.7.1 – Plasmid Design 56
3.7.2 – PCR Amplification 57
3.7.3 – Kinase, Ligase and Dpnl (KLD) Reaction, Ligation and Transformation 58
3.7.4 – Plasmid Isolation (Miniprep) 59
3.7.5 – Plasmid Isolation (Midiprep) 60
3.8 – Validation of Successful TRAF1 T268A SDM *61*
3.8.1 – Restriction Enzyme Digestion 61
3.8.2 – TRAF1 T268A SDM Sequencing 61
3.9 – Plasmid Transformation of DH5α E. coli Cells *61*
3.10 – DNA Plasmid Transfections and Lysate Preparation *62*
3.10.1 – Transfections 62
3.10.2 – Lysate Preparation 63
3.11 – Co-Immunoprecipitation *63*
3.11.1 Protein A/G Agarose Beads 63
3.11.2 – Protein G Dynabeads 65
3.12 – Immunoblotting *66*
3.13 – Statistical Analysis *67*
Chapter 4: Results **69**
4.1 – TRAF1 V196A/V196A can Protect Mice from LPS-Induced Sepsis *69*

4.2 – TRAF1 V196A/V196A Delays the Progression of Symptoms during LPS-Induced Sepsis *71*
4.3 – Effects of TRAF1 V196A/V196A on Cytokine Production in the Sublethal LPS Model *74*
4.4 – Effects of TRAF1 V196A on Gene Expression of Inflammatory Markers *76*
4.5 – Effects of TRAF1 V196A on Protein Expression of Inflammatory Markers *81*
4.6 – Effects of TRAF1 V196A on Phospho-Signalling *84*
4.7 – TRAF1 V196A Reduces Inflammasome-Driven IL-1β Secretion *86*
4.8 – TRAF1 V196A Reduces T Cell Proliferation in Response to TNFα *88*
4.9 – Successful Validation of the hTRAF1 T268A Mutant Plasmid *90*
4.10 – hTRAF1 T268A Maintains Interaction with cIAP2 ..... *92*
4.11 – hTRAF1 T268A Reduces Interaction with HOIL-1 ..... *95*

Chapter 5: Discussion **97**

Chapter 6: Conclusions and Future Directions **107**
6.1 – Future Directions *107*
6.2 – Conclusions *108*

References **110**

Appendix A **129**

List of Tables

Table 3.1: Primers for TRAF1 V196A genotyping PCR reaction.....23

Table 3.2: Thermocycler conditions for TRAF1 V196A genotyping PCR reaction. 23

Table 3.3: Thermocycler conditions for reverse transcription (RT) step 1. 40

Table 3.4: Thermocycler conditions for reverse transcription (RT) step 2. 40

Table 3.5: Thermocycler conditions for RT-qPCR. 42

Table 3.6: List of primers used to measure inflammatory gene expression by RT-qPCR. 42

Table 3.7: List of primary antibodies used to assess inflammatory signalling by western blotting. 46

Table 3.8: List of fluorescent antibodies used to measure inflammatory signalling by flow cytometry.....48

Table 3.9: Primer designs for hTRAF1 268A and W271A. 57

Table 3.10: Components of SDM PCR reaction. 57

Table 3.11: Thermocycler conditions for amplifying the SDM amplicon. 58

Table 3.12: List of primary antibodies used to assess protein interactions by immunoblotting. 67

List of Figures

Figure 1.1 The multifaceted role of TRAF1 in the immune system. 18

Figure 3.1: Genotyping strategy for TRAF1 V196A mice. 25

Figure 3.2: Kaplan-Meier survival curve of wildtype female C57BL/6 mice treated with various doses of LPS to establish the 35 mg/kg lethal dose. 30

Figure 3.4: Schematic representation of experiments employing the lethal and sublethal model of LPS. 32

Figure 3.5: Schematic representation of flushing mouse bone marrow to generate bone marrow-derived macrophages (BMDMs). 36

Figure 3.5: Gating strategy for phospho-flow in pBMDMs and iBMDMs. 48

Figure 3.6: Schematic representation of performing CFSE proliferation assay and ELISA of key activation cytokines following co-stimulation of T lymphocytes. 55

Figure 3.7: Gating strategy for measuring CFSE dilution. 56

Figure 4.1: Assessing the survival of TRAF1 wt/wt, TRAF1 V196A/wt and TRAF1 V196A/V196A mice challenged with a lethal dose of lipopolysaccharide (LPS). 70

Figure 4.2: Assessing the progression of symptoms by measuring the murine sepsis score of TRAF1 wt/wt, TRAF1 V196A/wt and TRAF1 V196A/V196A male mice challenged with a lethal dose of lipopolysaccharide (LPS) 72

Figure 4.3: Assessing the progression of symptoms by measuring the murine sepsis score of TRAF1 wt/wt, TRAF1 V196A/wt and TRAF1 V196A/V196A female mice challenged with a lethal dose of lipopolysaccharide (LPS) 73

Figure 4.4: Assessing the cytokine production in TRAF1 wt/wt and V196A/V196A female mice challenged with a sublethal dose of lipopolysaccharide (LPS). 75

Figure 4.5: Assessing the gene expression of IFN-β, IL-1β, IL-6, IL-10, IL-12, TGFβ and TNFα by RT-qPCR following LPS stimulation of immortalized bone marrow-derived macrophages (iBMDMs). 80

Figure 4.6: Assessing the protein expression of p-p65, p-SAPK/JNK and total IκBα by western blot following LPS stimulation of bone marrow-derived macrophages (BMDMs). 82

Figure 4.7: Assessing the protein expression of p-ERK, p-p65, and p-SAPK/JNK by flow cytometry following LPS stimulation of bone marrow-derived macrophages (BMDMs). 85

Figure 4.8: Assessing the levels of IL-1β secretion following inflammasome activation. 87

Figure 4.9: Assessing the proliferation levels of T Cells following co-stimulation with TNFα. 89

Figure 4.10: Assessing the formation of a successful site-directed mutagenesis of the human TRAF1 (hTRAF1) plasmid. 91

Figure 4.11: Assessing the effects of hTRAF1 T268A on the interaction with cIAP2 and HOIL-1. 93

Figure 4.12: Assessing the effects of hTRAF1 T268A on the interaction with HOIL-1. 96

Figure 5.1: An overview of the pathway-specific role of TRAF1 in regulating inflammation through NF-κB activation. 106

Supplementary Figure 1.0: RT-qPCR amplification curves for the no reverse transcriptase control corresponding to the genes of interest. 129

List of Abbreviations

AIM2	Absent in melanoma-2
ALRs	AIM2-like receptors
ASC	Apoptosis-associated speck-like protein containing a CARD
ATP	Adenosine triphosphate
BAFFR	B cell activating factor
BCR	B cell receptor
BIR domains	Baculoviral IAP repeating domains
BMDMs	Bone marrow-derived macrophages
CARD	Caspase recruitment domain
Cas12a	CRISPR-associated protein 12a
Cas9	CRISPR-associated protein 9
CC	Coiled-coil
CD3	Cluster of differentiation 3
CFSE	Carboxyfluorescein succinimidyl ester
cIAP1/2	Cellular inhibitor of apoptosis proteins 1 and 2
CLP	Cecal ligation and puncture
CLRs	C-type lectin receptors
Co-IP	Co-immunoprecipitation
CRD	Cysteine-rich domain
CRISPR	Clustered regularly interspaced short palindromic repeats
CRP	C-reactive protein
DAMPs	Damage-associated molecular patterns
DUBs	Deubiquitination enzymes
ERK1/2	Extracellular signal-regulated protein kinases 1 and 2
ESR	Erythrocyte sedimentation rate
Fn14	Fibroblast growth factor-inducible 14
HDR	Homology-directed repair
HLA	Human leukocyte antigen
HOIL-1/RBCK1	Heme-oxidized IRP2 ubiquitin ligase-1
HOIP/RNF31	HOIL-1 interacting protein
IAPs	Inhibitor of apoptosis proteins
iBMDMs	Immortalized bone marrow-derived macrophages
IFN-β	Interferon-beta
IFNs	Interferons
IFNγ	Interferon-gamma
IKK	Inhibitor of κB kinase
IL	Interleukin
IL-1	Interleukin-1

IL-10	Interleukin-10
IL-18	Interleukin-18
IL-1Rs	Interleukin-1 receptors
IL-1β	Interleukin-1-beta
IL-6	Interleukin-6
IRAK	IL-1 receptor-associated kinase
IκB	Inhibitor of κB
JNKs	c-Jun N-terminal kinases (JNKs)
LCM	L929 conditioned medium
LMICs	Low- and middle-income countries
LPS	Lipopolysaccharide
LRR motifs	Leucine-rich repeat motifs
LTβR	Lymphotoxin-beta receptor
LUBAC	Linear ubiquitin chain assembly complex
MAP	Mean arterial pressure
MAPK	Mitogen-activated protein kinase
MATH domain	Meprin and TRAF homology domain
MODS	Multiple organ dysfunction syndrome
MSS	Murine sepsis score
MyD88	Myeloid differentiation primary protein response 88
NEMO	NF-κB essential modulator
NF-κB	Nuclear factor kappa B
NIK	NF-κB inducing kinase
NLRP3	NLR family pyrin domain-containing 3
NLRs	NOD-like receptors
NOD	Nucleotide oligomerization domain
NZF	Np14 zinc finger
pBMDMs	Primary bone marrow-derived macrophages
PGNs	Peptidoglycan
PRMs	Pattern recognition molecules
PRRs	Pattern recognition receptors
PTM	Post-translational modification
RA	Rheumatoid arthritis
RANK	Receptor activator for nuclear factor κB
RIG-1	Retinoic acid-inducible gene-I
RIPK1	Receptor-interacting serine/threonine protein kinase 1
RLRs	RIG-1-like receptors
RPLP0	Ribosomal protein lateral stalk subunit P0
SAPK	Stress-activated protein kinase
SDM	Site-directed mutagenesis

SHARPIN	Shank-associated RH domain-interacting protein
SNP	Single nucleotide polymorphisms
TAB	TGF-b-activated kinase
TAK1	Transforming growth factor b-activated kinase
TCR	T cell receptor
TGFβ	Transforming growth factor beta
TIMs	TRAF-interacting motifs
TIR	Toll/IL-1 receptor (TIR) domain
TLRs	Toll-like receptors
TNF	Tumor necrosis factor
TNFα	Tumor necrosis factor alpha
TNFR	TNF receptor
TRADD	TNFR1-associated death domain protein
TRAF	Tumour necrosis factor receptor (TNFR)-associated factor
TRAF1	Tumour necrosis factor receptor (TNFR)-associated factor 1
Tregs	Regulatory T cells
TRIF	TIR-domain-containing-adapter-inducing interferon-β
κB	Kappa B

Chapter 1: Introduction

1.1 – Overview of Sepsis and Septic Shock

Sepsis, a life-threatening condition, is characterized by a dysregulated inflammatory response to an infection ultimately leading to severe organ dysfunction and progression to a stage of septic shock. This condition affects approximately 49 million people each year and there are 11 million sepsis-related deaths reported worldwide, a staggering number which accounts for 20% of all global deaths (Rudd et al., 2020). It is important to note that the aforementioned numbers are not representative of low- and middle-income countries (LMICs) due to a lack of research and accessibility to resources. The true incidence and prevalence of sepsis is estimated to be higher in LMICs due to several factors that contribute to an increased risk. These factors include poverty, overcrowding, health disparities, improper hygiene, high incidence of nosocomial infections, high prevalence of HIV infection, and under-resourced and low-resilience public health systems (Finfer & Machado, 2016; Kumar, 2020; Rosenthal et al., 2014; Rudd et al., 2020). In Canada, 1 in every 20 deaths is attributed to sepsis which poses a significant burden on the healthcare system; experts and healthcare organizations are advocating for the importance of developing a stringent action plan to reduce this burden (Sheikh et al., 2024).

One of the challenges to improving public awareness, identification, and treatment of sepsis is due to the heterogeneity in the clinical presentation (diverse and nonspecific symptoms) of patients (Cohen et al., 2015; Fohner et al., 2019; V. X. Liu et al., 2021). Clinical features of sepsis can range from a fever of >38°C, shortness of breath, pallor, malaise, diaphoresis, tachycardia, tachypnea, altered mental status and in cases of pneumonia-induced sepsis, hypothermia with a body temperature of <36°C (Basodan et al., 2022; Edman-Wallér et al., 2016;

Jacobi, 2002). Another challenge in identifying sepsis is that some of the common symptoms are similar to other conditions like heart failure and stroke; shortness of breath (dyspnea) and weakness are two examples of symptoms that commonly occur during sepsis and are also found in patients with other conditions such as heart failure and stroke as well (V. X. Liu et al., 2021).

There are a number of clinical interventions that are employed to manage sepsis in order to facilitate early detection and to initiate treatment in a timely manner (Barichello et al., 2022; D. Liu et al., 2022; Ma et al., 2024; Rudd et al., 2020; Vincent, 2022). One example of a sepsis management paradigm involves three components: infection control, haemodynamic stabilization and modulation of the host response. The first component involves the administration of antibiotics or surgical interventions to remove the infection. The second component involves administering fluids (to compensate fluid loss because of perspiration and dehydration) and in some cases a vasopressor, such as noradrenaline, or an inotropic, to restore the mean arterial pressure (MAP). The third component involves the administration of medicines that target the immune response as well as improve organ function, such as glucocorticoids and vasopressin (Vincent, 2022).

As of now, there are no approved treatments for sepsis patients and most clinical trials were unsuccessful in reducing mortality due to the complex and heterogeneous pathophysiology that underlies the dysregulation in both the innate and adaptive immune responses (M. Cao et al., 2023; Giamarellos-Bourboulis et al., 2024; Mithal et al., 2022). Current studies are shifting towards precision medicine and implementing a personalized therapy approach in order to identify reliable and accurate biomarkers as this could potentially improve sepsis diagnosis and lead to novel treatments that are effective and devoid of the challenges that are associated with patient heterogeneity (Barichello et al., 2022; Das et al., 2024; Giamarellos-Bourboulis et al., 2024; Poll et al., 2021; Takahama et al., 2024). The heterogeneity observed in sepsis can arise in numerous

ways. For example, in terms of immunological profile, a patient with sepsis can exhibit hyperinflammation or sepsis-induced immunoparalysis (immune suppression). Additionally, patients can be predisposed for a certain immune endotype. One patient may experience hyperinflammation due to aberrant activation of interleukin (IL)-1 or IL-6 pathways while another patient may experience it due to complement activation. Precision medicine-based approaches coupled with modern technologies such as machine-learning and artificial-intelligence algorithms have enabled clinicians to clinically stratify sepsis patients based on similarities in their pathophysiology (Giamarellos-Bourboulis et al., 2024). This approach is revolutionary as patients will now be treated with the most effective therapeutic that is specific to their unique manifestation of sepsis in an effort to ultimately improve the quality of their life with minimal complications.

Recently, a panel of pro- and anti-inflammatory biomarkers has been identified which include fluid phase pattern recognition molecules (PRMs), complement system, cytokines, chemokines, damage-associated molecular patterns (DAMPs), non-coding RNAs, miRNAs, cell membrane receptors, cell proteins, metabolites, and soluble receptors (Barichello et al., 2022). Interestingly, another study by Das et al. (2024) identified a blood immune signature of sepsis that characterizes sepsis at an early stage in preterm babies even when the conventional clinical marker of inflammation, C-reactive protein (CRP), was not elevated. This study also identified the upregulation of a plasma analyte, amphiregulin, in leukocyte populations during sepsis even when CRP levels were normal. The identification of easily measured novel candidate immune markers proves to be an innovative approach in improving the diagnostic accuracy of detecting inflammation that is associated with sepsis (Das et al., 2024). Similarly, Takahama et al. (2024) mapped the cellular effects of sepsis and identified causal linkages between specific cytokine pairs for 195 cell types across 9 organs which was validated through whole-mouse spatial profiling.

Intriguingly, they identified cytokine pairs between tumor necrosis factor (TNF) and IL-18, interferon-gamma (IFNγ) or IL-1-beta (IL-1β) to explain the effects of sepsis across tissues and to create a unifying mechanistic framework for sepsis and other cytokine storms (Fajgenbaum & June, 2020; Takahama et al., 2024). The proposed model aligns with several studies that report the interaction between TNF and IFNγ or IL-1β leads to poor outcomes of sepsis and other inflammatory diseases in vivo (Babaeijandaghi et al., 2022; Doherty et al., 1992; Karki et al., 2021; Russell et al., 1995; Takahama et al., 2024; Waage & Espevik, 1988).

Immune dysregulation culminates due to the simultaneous imbalance between inflammatory and anti-inflammatory responses which ultimately leads to the development of septic shock and multiple organ dysfunction syndrome (MODS) (M. Cao et al., 2023; Giamarellos-Bourboulis et al., 2024; S. F. Liu & Malik, 2006; Mithal et al., 2022; van der Poll et al., 2017). The role of nuclear factor kappa B (NF-κB) in the pathophysiology of sepsis has been extensively investigated (Kelly et al., 2003; S. F. Liu et al., 1999; S. F. Liu & Malik, 2006; Pocock et al., 2003; Pritts et al., 2000) Interestingly, genes associated with the NF-κB signalling pathway have higher levels of hypermethylation in sepsis patients, indicating the activation of this pathway (L. Cao et al., 2020). Consequently, inhibiting NF-κB activation, through inhibitors such as the anti-inflammatory cytokine IL-10, protects animals from septic shock in the lipopolysaccharide LPS (endotoxin model) or cecal ligation and puncture (CLP, polymicrobial model) models (Altavilla et al., 2002; Bernard et al., 2001; Howard et al., 1993; Ikezoe et al., 2003; Sheehan et al., 2003; Zhu et al., 2015). It is important to note that although this strategy can be beneficial in improving survival, numerous studies indicate that global inhibition of NF-κB signalling can be deleterious because of its essential role in regulating immune responses, maintaining tissue homeostasis, and cell survival (Bennett et al., 2018; J. Liu et al., 2017; S. F. Liu & Malik, 2006; T. Liu et al., 2017).

In the case of the bacterial challenge during sepsis, it is important to clear the bacterial burden in a timely and efficient manner, however, deactivation of NF-κB is associated with impaired antimicrobial activities (J. Liu et al., 2017; S. F. Liu & Malik, 2006). Therefore, it follows that a promising strategy to achieve immune homeostasis would be to inhibit NF-κB activation in a cell- and pathway-specific manner.

1.2 – Overview of Rheumatoid Arthritis

Rheumatoid arthritis (RA) is a chronic autoimmune disease characterized by persistent and abnormal inflammation leading to the destruction of cartilage and bone (Edilova et al., 2021). This disease affects approximately 1% of the world's population and 1.2% of Canadians aged 16 years and older (Public Health Agency of Canada, 2020). The prevalence in females and males is 1.7% and 0.8%, respectively, and the incidence is 1.0 per 1,000 persons per year and 0.5 per 1,000 persons per year, respectively. Løppenthin et al. (2019) conducted a longitudinal analysis and reported that the 5-year survival rate of RA patients was approximately 80%, compared to age- and sex- matched controls with a 5-year survival rate of 88%.

Historically, the first modern medicine description of RA was documented in 1800 by French physician Augustin Jacob Landré-Beauvais (Entezami et al., 2011). Patients with early-stage RA typically have a diverse range of non-specific symptoms such as fatigue, flu-like feeling, swollen and tender joints and morning stiffness. Elevated levels of CRP and increased erythrocyte sedimentation rate (ESR) are typically observed in these patients and exploited as potential disease biomarkers (Lin et al., 2020). Patients with later-stage RA present more complex symptoms such as pleural effusions, lymphomas, atherosclerosis, hematologic abnormalities, and joint malalignment.

Diagnosing RA at an early stage and ensuring the patient receives the appropriate treatment is crucial to slowing the progression and preventing the chronic symptoms of the disease. Despite the current advances in the understanding of RA, there is no cure; the treatment modalities available focus on alleviating the symptoms and slowing the progression of the disease (Bullock et al., 2018). There are several environmental and genetic factors that contribute to the development of RA. One of the main genetic factors of RA is a mutation in the human leukocyte antigen (HLA) DRB1 alleles, which belong to the HLA family (Deane et al., 2017; Silman & Pearson, 2002). Environmental factors such as exposure to air pollution, infectious agents, and smoking can also increase the risk of developing RA.

One intervention is the use of etanercept, the first approved anti-TNF agent, which delays the onset of RA and reduces the symptoms; hence, improving the quality of life of patients (Haraoui & Bykerk, 2007). Genome-wide association studies first identified single nucleotide polymorphisms (SNPs) at the TRAF1-C5 locus on chromosome 9 as risk factors for developing RA in human patients; SNPs in this locus are predictors of how patients would respond to anti-TNF therapy in a clinical setting (Lalani et al., 2018).

1.3 – Overview of the Immune System and NF-κB Activation

Ongoing research continues to uncover new information about the importance, function and complex regulatory mechanisms of the immune system. This system is comprised of a collection of cells, chemicals and processes that provide us with the structural and chemical barriers necessary to respond to invading pathogens (Marshall et al., 2018). The immune system is grouped into two branches, namely, the innate immunity and the adaptive immunity. The innate immune response is the first line of defence that is activated within hours or days of an intrusion and exerts an antigen-independent (non-specific) defence mechanism. However, the quick

response comes at a cost of having no immunological memory of the pathogen for future exposures. On the other hand, the adaptive immune response is activated 1-2 weeks following exposure to the foreign pathogen and generates a more robust, antigen-dependent, and antigen-specific response. The adaptive immune response has the capacity for immunological memory, thereby exerting a more rapid and efficient response for subsequent exposures to the same pathogen. Both innate and adaptive immunity are complementary host defenses and many of the cells in the innate immune system (such as basophils, dendritic cells, eosinophils, macrophages, mast cells and neutrophils) cultivate the activation of cells in the adaptive immune system through the production of cytokines or through cell-cell interactions. (Marshall et al., 2018).

NF-κB is a family of inducible transcription factors that are widely accepted as the master regulators of the immune system, specifically the innate and adaptive immune responses (T. Liu et al., 2017). This family is comprised of five members, namely, NF-κB1 (or p50), NF-κB2 (or p52), RelA (or p65), RelB and c-Rel (T. Liu et al., 2017; S.-C. Sun, 2011; S.-C. Sun et al., 2013; Zhang & Sun, 2015). The members of this family can act as a transcriptional factor by forming hetero- or homo-dimers with each other and binding to κB, a DNA element, to promote the activation of several target genes. In an inactivated state, NF-κB is sequestered in the cytoplasm by the Inhibitor of κB (IκB) family proteins and related proteins with ankyrin repeats. The best studied IκB family member is IκBα. Additionally, the precursor proteins of NF-κB1 and NF-κB2, namely, p105 and p100, have a similar structure as IκB and exhibit NF-κB inhibitory capabilities and thus, serve as IκB-like proteins. In order to relieve the inhibition on NF-κB from entering into the nucleus, activation occurs through either the canonical or non-canonical (alternative) pathway.

The canonical pathway is responsible for the rapid and transient nuclear translocation of the p50/RelA and p50/c-Rel heterodimers culminating in the activation of target genes (T. Liu et

al., 2017). This pathway is initiated in response to a wide range of stimuli including ligands of various cytokine receptors, pattern recognition receptors (PRRs), TNF receptor (TNFR) superfamily members, and T cell receptor (TCR) and B cell receptor (BCR). Here, NF-κB is activated through the inducible degradation of IκBα through its phosphorylation by a multi-subunit IκB kinase (IKK). The IKK complex is composed of two catalytic subunits, IKKα and IKKβ, and a regulatory subunit, NF-κB essential modulator (NEMO) or IKKγ. Once activated, the IKK complex phosphorylates IκBα at two N-terminal serines which results in its K48-linked polyubiquitination (K48-Ub) followed by subsequent degradation in the proteasome. As a result, IκBα dissociates from NF-κB, resulting in the nuclear translocation of NF-κB to activate target genes (T. Liu et al., 2017).

The noncanonical pathway is responsible for the slow and persistent nuclear translocation of the p52/RelB heterodimer culminating in the activation of target genes (T. Liu et al., 2017; S.-C. Sun, 2011). This pathway is initiated in response to specific stimuli that interact with a subset of TNFR superfamily members, including the B-cell-activating factor belong to the TNF family receptor (BAFFR), CD40, lymphotoxin-β receptor (LTβR), the receptor activator for nuclear factor κB (RANK), TNFR2, and fibroblast growth factor-inducible 14 (Fn14). Interestingly, the noncanonical pathway is activated through the phosphorylation, ubiquitination and processing of p100 by the interaction between NF-κB inducing kinase (NIK) and IKKα instead of IκBα degradation. p100 processing leads to the degradation of its c-terminal IκB-like structure to form mature NF-κB2 p52 and the subsequent nuclear translocation of the noncanonical NF-κB complex. It is important to note that the slow and persistent translocation occurs due to the extremely low steady level of the NIK protein. This is due to TRAF3-dependent ubiquitination of NIK resulting in its constitutive degradation. This process involves a multi-subunit ubiquitin ligase complex

consisting of TRAF3, TRAF2 and E3 ubiquitin ligases cIAP1/2 (named T3-T2-cIAP E3 complex) (S.-C. Sun, 2010, 2011; Vallabhapurapu et al., 2008; Zhang & Sun, 2015). Here, NIK directly interacts with TRAF3 and cIAP1/2 directly interacts with TRAF2. TRAF3 essentially dimerizes with TRAF2 to facilitate the recruitment of these ligases to NIK through the T3-T2-cIAP3 E3 complex and subsequently enable constant degradation of NIK.

Remarkably, the activation of non-canonical NF-κB can rescue NIK from TRAF3-mediated degradation (Liao et al., 2004; S.-C. Sun, 2011; Vallabhapurapu et al., 2008; Zhang & Sun, 2015). Structurally, non-canonical NF-κB receptors contain a TRAF-binding motif that is responsible for recruiting various TRAF1 members such as TRAF2 and TRAF3. Upon ligand binding, TRAF2 and TRAF3 are degraded through cIAP1/2-mediated ubiquitination, resulting in the stabilization and accumulation of newly synthesized NIK (Bishop & Xie, 2007; T. Liu et al., 2017; S.-C. Sun, 2010, 2011; Vallabhapurapu et al., 2008; Zhang & Sun, 2015). NIK then activates IKKα to collectively process p100 and facilitate downstream signalling. Intriguingly, activated IKKα in turn phosphorylates NIK to promote its degradation, hence, participating in a negative feedback mechanism to control the levels of NIK (S.-C. Sun, 2010, 2011).

Notably, the activation of NF-κB can lead to several activities such as the expression of pro-inflammatory genes for cytokines and chemokines, activation of inflammasomes, and regulation of immune cell activation, differentiation, proliferation and apoptosis (T. Liu et al., 2017). In addition to NF-κB's paradoxical roles of promoting autoimmunity and inflammation, it is also responsible for providing immune tolerance (S.-C. Sun et al., 2013). Immune tolerance is achieved through the deletion of self-reacting T cells in the thymus (central tolerance) and by cultivating the development and stability of regulatory T cells (Tregs) (peripheral tolerance).

Altogether, it is imperative to ensure a closely regulated NF-κB activation to ensure a healthy and balanced immune response, devoid of immune dysregulation.

1.4 – Protein Regulation by Ubiquitination

Ubiquitination has emerged as a key post-translational modification (PTM) implicated in numerous cellular processes including apoptosis, DNA repair, immune response, intracellular signaling, metabolic reprogramming in cancer cells, and protein degradation, processing and trafficking (Cockram et al., 2021; Kaiser & Huang, 2005; S. Liu & Chen, 2011; Nakamura, 2018; T. Sun et al., 2020). Ubiquitin is a small protein consisting of only 76 amino acids, with 7 lysine residues (K6, K11, K27, K29, K33, K48 and K63) that is highly conserved in all eukaryotes and has the ability to form a chain of ubiquitin molecules, termed polyubiquitin chains. Similar to other PTMs, such as phosphorylation and dephosphorylation, ubiquitination can also be reversed by a large family of proteins classified as deubiquitination enzymes (DUBs). Ubiquitin precursors, either a fusion between a ribosomal subunit and ubiquitin or a "head-to-tail" linear polyubiquitin, are encoded by four individual genes and the human genome altogether encodes 2 E1 enzymes, ~50 E2 enzymes and over 1000 E3 ligases (S. Liu & Chen, 2011; M. Sun & Zhang, 2022).

The PTM ubiquitination involves the transfer of ubiquitin to a substrate protein and this reaction requires three different enzymes, namely, ubiquitin-activating enzyme (E1), ubiquitin-conjugating enzyme (E2), and ubiquitin ligase (E3) (Cockram et al., 2021; S. Liu & Chen, 2011). The most abundant ubiquitin modification is the K48-linked ubiquitination which targets substrate proteins to the proteasome for degradation (M. Sun & Zhang, 2022). The next abundant ubiquitin modification is the K63-linked ubiquitination which facilitates DNA damage repair and regulates protein-protein interactions during cell signalling events like the activation of the NF-κB pathway and autophagy (Chen et al., 2019; P. Liu et al., 2018; M. Sun & Zhang, 2022). A less-well defined,

M1-linked linear ubiquitination occurs when ubiquitin molecules attach to the N-terminal Methionine of the next ubiquitin monomer (Emmerich et al., 2016; Iwai, 2021; Kirisako et al., 2006; M. Sun & Zhang, 2022).

Linear ubiquitination is mediated by the linear ubiquitin chain assembly complex (LUBAC) which is a key player in the regulation of innate and adaptive signalling pathways as well as cell death (Borghi et al., 2018; Fujita et al., 2014; Iwai, 2021; Tokunaga et al., 2009). The LUBAC complex is an E3 ligase that is comprised of three subunits, namely, heme-oxidized IRP2 ubiquitin ligase-1 (HOIL-1 or RBCK1), HOIL-1 interacting protein (HOIP or RNF31), and the Shank-associated RH domain-interacting protein (SHARPIN) (Kirisako et al., 2006; Tokunaga et al., 2009, 2011). Interestingly, alternate splicing of HOIL-1 produces two different transcripts; the longer mRNA was found to be more abundant than the shorter mRNA (lacking exon-2) and after further investigation, it was determined that most of the endogenous HOIL-1 is HOIL-1L. Notably, the activation of canonical NF-κB activation involves LUBAC-mediated linear polyubiquitination of the NF-κB essential modulator (NEMO or IKKγ) at specific lysine residues in the CC2-LZ domain of NEMO (Tokunaga et al., 2009).

The cellular inhibitor of apoptosis proteins 1 and 2 (cIAP1 and cIAP2) are members of a family of inhibitor of apoptosis proteins (IAPs) that have an important role of mitigating both intrinsic and extrinsic death signalling (Graber & Holcik, 2011; Vince et al., 2009). Proteins that belong to the IAP family possess baculoviral IAP repeating (BIR) domains which allow them to bind to and inhibit caspases (Eckelman & Salvesen, 2006; Graber & Holcik, 2011; Roy et al., 1997). Some members of IAPs, such as cIAP1/2, possess RING domains that act as ubiquitin E3 ligases (Graber & Holcik, 2011; Mahoney et al., 2008; Vince et al., 2009). As E3 ligases, cIAP1/2 have the potential of mediating both K48-ubiquitination, to target substrates for proteasomal

degradation, and K63-ubiquitination, to facilitate signaling events. cIAP1/2 has emerged as a key regulator of NF-κB signalling and programmed cell death due to its role of ubiquitylating members of the TNFR complexes. Interestingly, although cIAP1 and cIAP2 possess both specialized and redundant roles in different cellular processes, only cIAP1 can ubiquitinate cIAP2 to target it for degradation, thereby negatively regulating cIAP2 levels (Conze et al., 2005; Mahoney et al., 2008).

1.5 – Toll-Like Receptors (TLRs)

Toll-like receptors (TLRs), one of the first PRRs discovered, have an important role of activating the innate and adaptive immune responses (Fitzgerald & Kagan, 2020; Li & Wu, 2021; Yang et al., 2020). PRRs are germline-encoded sensors that are responsible for recognizing common molecular structures on the surface of pathogens, apoptotic cells and damaged senescent cells. Depending on the protein domain homology, PRRs can be characterized as TLRs, nucleotide oligomerization domain (NOD)-like receptors (NLRs), retinoic acid-inducible gene-I (RIG-I)-like receptors (RLRs), C-type lectin receptors (CLRs) and absent in melanoma-2 (AIM2)-like receptors (ALRs) (Kaur & Secord, 2019; Li & Wu, 2021; Yang et al., 2020). Currently, there are at least 10 members of the human TLR family and 13 members of the mouse TLR family (Li & Wu, 2021). Like PRRs, TLRs can recognize a diverse range of damage-associated molecular patterns (DAMPs) and pathogen-associated molecular patterns (PAMPs). DAMPs include high-mobility group box 1 protein, endogenous alarmins, heat-shock proteins and uric acid. PAMPs include LPS, peptidoglycan (PGNs), mannans, unmethylated microbial DNA, and viral RNA (Kaur & Secord, 2019). TLRs are found on different immune cells including macrophages, monocytes, dendritic cells, B lymphocytes, T lymphocytes, eosinophils, mast cells and neutrophils. TLRs are also found on non-immune cells such as fibroblast cells, endothelial cells, epithelial cells, and keratinocytes (Bhagwani et al., 2020; Kawai & Akira, 2007; G. Liu & Zhao, 2007). Interestingly, TLRs share

similar structural homology with interleukin-1 receptors (IL-1Rs) in the cytoplasmic portion, referred to as Toll/IL-1 receptor (TIR) domain (Akira & Takeda, 2004; Kawai & Akira, 2007; Takeda & Akira, 2005). Notably, the extracellular region of TLRs differ from IL-1Rs as they contain leucine-rich repeat (LRR) motifs. Upon stimulation, TLRs oligomerize to activate either a myeloid differentiation primary protein response 88 protein (MyD88)-dependent pathways or a TIR-domain-containing-adapter-inducing interferon-β (TRIF)-dependent pathways (Akira & Takeda, 2004; Dhillon et al., 2019; Kawai & Akira, 2007, 2010; Kawasaki & Kawai, 2014). Some TLRs, like TLR4, can activate MyD88-dependent pathways when they are found on the plasma membrane or TRIF-dependent pathways when they have translocated to the endosomal compartments. Interestingly, both MyD88 and TRIF are TIR domain-containing adaptor proteins that activate signalling cascades, resulting in the activation of NF-κB, interferon regulatory factors (IRFs), and mitogen-activated protein kinases (MAPKs) and subsequent expression of chemokines, cytokines and type 1 interferons (IFNs). Initiation of the MyD88-dependent pathway begins with the recruitment of the IL-1 receptor-associated kinase (IRAK) 4 which in turn activates IRAK1 and IRAK2 through phosphorylation. IRAK 1/2 subsequently recruits TRAF6 to promote K63-linked polyubiquitination of itself and other substrates including transforming growth factor β-activated kinase (TAK) 1, TGF-β-activated kinase (TAB) 1, TAB2 and NEMO (IKKγ) to activate the IKK complex. It is important to note that the activation of the IKK complex also requires LUBAC-mediated linear ubiquitination of NEMO. Following the activation, IκBα is phosphorylated and subsequently degraded, resulting in the activation of NF-κB. TAK1 facilitates the activation of MAPKs such as extracellular signal-regulated protein kinases 1 and 2 (ERK1/2), p38 and c-Jun N-terminal kinases (JNKs) through phosphorylation which in turn activates transcription factors like AP-1. Initiation of the TRIF-dependent pathway can begin with either the

recruitment of TRAF3 to activate IRF3 and IFN-β or TRAF6 to activate NF-κB and MAPK. When TRAF3 is recruited, it promotes K63-linked polyubiquitination of itself to activate the noncanonical IKKs, TANK-binding kinase 1 (TBK1) and IκB kinase epsilon (IKKε). This leads to the phosphorylation of interferon regulatory factor 3 (IRF3) and subsequent translocation and expression of type 1 IFNs. When TRIF recruits TRAF6, it also recruits receptor-interacting protein 1 (RIP1) to form a multiprotein signalling complex including TNFR1-associated death domain protein (TRADD) and Pellino-1. This signalling complex then activates the TAK1/IKK axis which in turn activates the NF-κB and MAPK signalling cascades (Akira & Takeda, 2004; Dhillon et al., 2019; Kawai & Akira, 2007, 2010; Kawasaki & Kawai, 2014).

1.6 – Tumour Necrosis Factor Receptors (TNFRs)

The tumour necrosis factor (TNF) and TNF receptor (TNFR) superfamilies consist of 19 ligands and 29 receptors that are involved in a variety of pathways related to cell survival and cell death (Brenner et al., 2015; Wajant & Siegmund, 2019). The well-characterized members of this superfamily, TNF, TNFR1 and TNFR2, culminate in the activation of NF-κB through the complex regulation of receptor-interacting serine/threonine protein kinase 1 (RIPK1) activation by linear and branched ubiquitination modulated by LUBAC and IAPs such as cIAP1 and cIAP2. TNF receptors including TNFR1 and TNFR2 have an extracellular cysteine-rich domain (CRD) and an intracellular domain that is unique to the receptor and downstream signalling events. TNFR1 contains of an 80 amino acid death domain which helps recruit the adaptor molecule TNFR1-associated death domain complex; the TNFR1-TRADD complex can either promote cell survival or cell death depending on the type of cell and downstream signalling events. TNFR2 does not have this cytoplasmic death domain and recruits TNFR-associated factor 1 (TRAF1) and TRAF2 which promotes cell survival by activating the NF-κB signalling cascade. It is important to note

that while transmembrane TNF activates both TNFR1 and TNFR2 with high efficacy, soluble TNF induces strong activation of TNFR1 signalling (Brenner et al., 2015; Siegmund et al., 2016; Wajant et al., 2003; Wajant & Siegmund, 2019). Furthermore, while TNFR1 is expressed in most tissues and is a key player in TNF signalling, TNFR2 expression is highly regulated and primarily found in immune cells (such as T and B cells, myeloid cells, and Tregs), indicating an important role in the lymphoid system. There are numerous studies highlighting the importance of a subset of TNFR molecules in facilitating costimulatory signals that promote activation, clonal expansion, differentiation and survival of antigen-primed CD4+ and CD8+ T cells (So & Ishii, 2019). This subset includes receptors such as 4-1BB, CD27, CD30, OX40 and TNFR2 (So & Ishii, 2019; Watts, 2005). Moreover, the cytoplasmic tails of a group of TNRs contain one or more TRAF-interacting motifs (TIMs) which facilitates the recruitment and binding of TRAF proteins in various triplet combinations; this leads to the activation of various pro- and anti-inflammatory signal transduction pathways such as NF-κB, JNK, p38, ERK, and PI3K (Dempsey et al., 2003).

1.7 – TNFR-Associated Factor 1 (TRAF1)

Tumor necrosis factor receptor (TNFR)-associated factor 1 (TRAF1) is one of six TRAF proteins belonging to a family of signalling adapter proteins that play an important role in IL-1R, IFN, NLR, TCR, TLR, and TNFR signalling cascades, culminating in the activation of NF-κB, MAPK and IRF3s (Bishop & Xie, 2007; Edilova et al., 2018; Lalani et al., 2018; Wajant et al., 2003). TRAF1, an NF-κB inducible protein, along with TRAF2 were first identified through the yeast two-hybrid assay for their ability to interact with TNFR2 (Rothe et al., 1994). The six members of the TRAF family (TRAF1-6), are characterized by their conserved TRAF domain composed of the N-terminal coiled-coil (CC) region (TRAF-N) and the C-terminal β-sandwich domain (TRAF-C), also known as the meprin and TRAF homology (MATH) domain (Abdul-Sater

et al., 2016; Edilova et al., 2018; Lalani et al., 2018; Xie, 2013). Interestingly, minor structural differences in the TRAF domain among TRAFs is what provides them the structural specificity required to bind to various signalling complexes. Notably, all of the TRAF proteins, except TRAF1, possess an N-terminal RING finger domain, required for NF-κB activation, followed by a variable number of zinc fingers. The aforementioned RING finger is also a structural feature of many E3 ubiquitin ligases endowing the core of the ubiquitin ligase catalytic domain. Collectively, these structural domains provide TRAFs the ability to function as adaptor proteins, by linking upstream signalling receptors to downstream effector molecules, and as E3 ubiquitin ligases to regulate signaling. Another important feature of TRAF1 is the capacity to protect TRAF2 during TNFR signalling from cIAP1/2-mediated ubiquitination and subsequent proteasome-dependent degradation (Edilova et al., 2018; Wicovsky et al., 2009; Zheng et al., 2010). Zheng et al. (2010) discovered that TRAF1 and TRAF2 preferentially form a 1:2 heterotrimer and that the formation of $(TRAF2)_2$:TRAF1 has a stronger affinity for cIAP2 than the TRAF2 homotrimer. Collectively, the formation of this heterotrimer and the subsequent protection of TRAF2 from degradation enhances proinflammatory NF-κB signalling to promote cell survival (Edilova et al., 2018; Wicovsky et al., 2009; Zheng et al., 2010).

1.8 – Multifaceted role of TRAF1 in TLR and TNFR Signalling

TRAF1 has a multifaceted role across different immune cell types (e.g., macrophages and T lymphocytes) and receptor signalling pathways. In innate immune cells, such as monocytes, TRAF1 serves as a negative regulator of NF-κB activation in the toll-like receptor (TLR) signalling pathway (Abdul-Sater et al., 2016). When this pathway is activated, TRAF1 binds to all three components of LUBAC through its MATH domain. Linear ubiquitination of NEMO by LUBAC is required for NF-κB activation. Abdul-Sater et al. (2016) reported that the MATH domain of

TRAF1 binds to the Np14 zinc finger (NZF) domains of HOIP and HOIL-1, thus hindering the interaction between NEMO and HOIP. This interaction of TRAF1 with LUBAC restrains linear ubiquitination of NEMO to inhibit NF-κB activation resulting in a dampened inflammatory response. However, in the absence of TRAF1, there is an increase in LUBAC-mediated ubiquitination of NEMO resulting in higher levels of NF-κB activation. Conversely, in adaptive immune cells, such as T lymphocytes, TRAF1 serves as a positive regulator of NF-κB activation downstream of specific TNFR signalling pathways such as 4-1BB and CD40 (McPherson et al., 2012). When this pathway is activated, TRAF1 forms a complex with TRAF2 and recruits cIAP2. cIAP2 is responsible for mediating K63 ubiquitination of other proteins in the signaling cascade, ultimately leading to the activation of NF-κB (Dhillon et al., 2019). In adaptive immune cells, TRAF1-mediated activation of NF-κB promotes the survival and proliferation of lymphocytes.

Although earlier studies showed that TRAF1-mediated activation of NF-κB promotes the survival and proliferation of lymphocytes, some studies have reported that TRAF1 negatively regulates TNFR2 signalling (Borghi et al., 2018; Edilova et al., 2018; Sabbagh et al., 2008; Speiser et al., 1997; Tsitsikov et al., 2001). The dichotomous role of TRAF1 is best exemplified in the TNFR2 signalling pathway where both cIAP2-mediated K63 ubiquitination and LUBAC-mediated linear ubiquitination are required for maximal TNFR2-induced NF-κB activation. When this pathway is activated, TRAF1 forms a complex with TRAF2 and recruits cIAP2 which is responsible for recruiting LUBAC to the complex. Similar to TRAF1's role in TLRs, TRAF1 interacts with LUBAC to restrain linear ubiquitination downstream of TNFR2. Therefore, it follows that alleviating the restraint on LUBAC by disrupting the interaction between TRAF1 and LUBAC would lead to an increase in T cell activation and proliferation. Interestingly, Tsitsikov et al. (2001) showed that activated TRAF1-deficient cells proliferate in response to TNFα mediated

through the TNFR2 signalling pathway. As shown in Figure 1.1, TRAF1 has a multifaceted role in the immune system to regulate NF-κB activation in innate and adaptive immune cells.

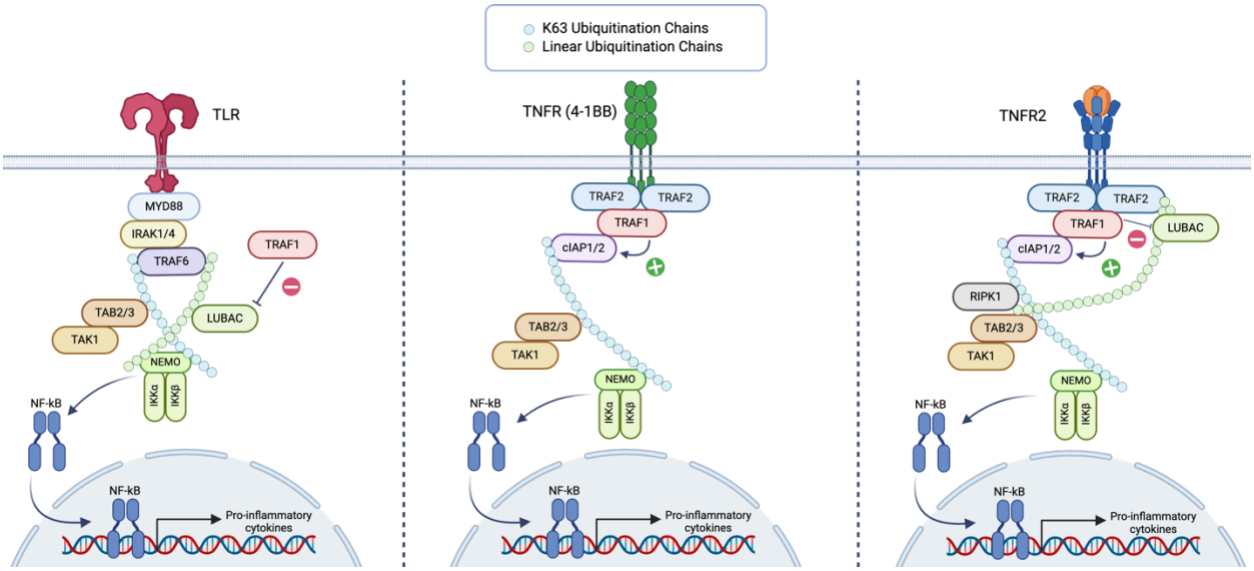

Figure 1.1 The multifaceted role of TRAF1 in the immune system.

TRAF1 is involved in the toll-like receptor (TLR) pathway in innate immune cells such as monocytes and the tumour necrosis factor receptor (TNFR) pathway in adaptive immune cells such as lymphocytes. Downstream of TLR, TRAF1 is a negative regulator of NF-κB activation. When this pathway is activated, TRAF1 binds to the linear ubiquitin assembly complex (LUBAC). Linear ubiquitination of NF-κB essential modulator (NEMO) by LUBAC is required for NF-κB activation. This interaction of TRAF1 with LUBAC restrains linear ubiquitination of NEMO to inhibit NF-κB activation resulting in a dampened inflammatory response. Downstream of 4-1BB, TRAF1 is a positive regulator of NF-κB activation. When this pathway is activated, TRAF1 forms a complex with TRAF2 and recruits the cellular inhibitor of apoptosis protein 2 (cIAP2). cIAP2 is responsible for mediating K63 ubiquitination of other proteins in the signaling cascade to activate NF-κB resulting in the survival and proliferation of lymphocytes. Downstream of TNFR2, TRAF1 forms a complex with TRAF2 and recruits cIAP2 which then recruits HOIL-1. cIAP2-mediated K63 ubiquitination and LUBAC-mediated linear ubiquitination are both required for TNFR2-induced canonical NF-κB activation. Figure adapted from Abdul-Sater et al. (2016), Borghi et al. (2018) and Edilova et al. (2018). Created with BioRender.com.

Chapter 2: Rationale and Hypothesis

2.1 – Rationale

Recently, Abdul-Sater et al. (2016) showed that a RA-associated SNP in the TRAF1 gene results in lower levels of TRAF1 protein but higher amounts of inflammatory cytokines. RA patients with this SNP were also at a higher risk of mortality from sepsis (Panoulas et al., 2009). Individuals with this genetic variant of TRAF1 had lower levels of TRAF1 protein in both macrophages and T lymphocytes. Consequently, these individuals had less activated T lymphocytes and produced lower levels of destructive cytokines. This SNP in TRAF1 disrupted the negative regulation of the proinflammatory axis of immune cells such as macrophages (TLR signaling), which contributed to the heightened immune response. As such, TRAF1 is characterized for its dichotomous role of positively and negatively regulating for NF-κB activation. This unexpected finding highlights the challenges of targeting TRAF1 indiscriminately and the importance of studying the mechanisms underlying the disparate roles.

Our lab has recently identified a mutation in the CC domain of TRAF1, V203A, that disrupts the interaction with cIAP2 in human monocyte cells which can reduce their inflammatory responses when stimulated with LPS. Interestingly, through co-immunoprecipitation (Co-IP) assays, the V203A mutation was identified as V196A in mouse TRAF1 (mTRAF1); TRAF1 V196A disrupted the interaction between mTRAF1 and cIAP2 while maintaining the interaction between mTRAF1 and LUBAC. Using clustered regularly interspaced short palindromic repeats/CRISPR-associated protein 12a (CRISPR/Cas12a) gene editing, we have genetically engineered a mouse model with this TRAF1 V196A mutation to evaluate cell- and pathway-specific responses. In this study, we will primarily investigate the TRAF1 V196A proof of concept to elucidate the role of this variant in regulating inflammatory responses. We will then characterize

the gene expression, protein expression, and changes in the phosphorylation status of key inflammatory signalling cascade proteins. We will also explore the effects that the TRAF1 V196A mutation has on inflammasome activation. We will then determine the cell- and pathway- specific response by measuring CFSE dye dilution, indicating proliferation, of anti-CD3 activated T cells co-stimulated with TNFα. Additionally, we will also characterize a potential site of interaction that disrupts the interaction between hTRAF1 and LUBAC while maintaining the interaction between hTRAF1 and cIAP2.

2.2 – Objectives

The main objectives of this scientific study are to:

1. Investigate the survival response and cytokine production of TRAF1 V196A mice by employing the lethal and sublethal LPS model, respectively.
2. Determine whether LPS-induced NF-κB activation is reduced in TRAF1 V196A mice.
3. Elucidate the role of TRAF1 V196A on T cell signalling to assess whether the signalling pathway is altered downstream of TNFRs (i.e., 4-1BB and TNFR2).
4. Identify the site of interaction where the interaction between hTRAF1 and LUBAC is disrupted while the interaction between hTRAF1 and cIAP2 is maintained.

2.3 – Hypothesis

We hypothesize that the TRAF1 V196A mice will be protected from LPS-induced sepsis, exhibit reduced levels of inflammation relative to wildtype TRAF1 mice and exhibit reduced T cell signalling downstream of TNFRs. By disrupting the TRAF1/cIAP2/NF-κB axis, this mutation prevents TRAF1-mediated activation of NF-κB in lymphocytes while enhancing TRAF1-mediated inhibition of NF-κB in monocytes. We also hypothesize that hTRAF1 T268A will disrupt the

interaction between hTRAF1 and LUBAC while maintaining the interaction between hTRAF1 and cIAP2. The mouse equivalent of this mutation was previously identified as mTRAF1 T261A and because these regions are highly conserved with humans, we identified T268A as a site of interest.

Chapter 3: Materials and Methods

3.1 – Animal Care of C57BL/6 Mice

Female and male C57BL/6 mice were housed in humidity and temperature control rooms (30-40%, 24 $\pm$ 3°C) with a daily 12:12 hour light-dark cycle. Mice were housed with a regular chow diet and water ad libitum in the Animal Care Facility at York University in adherence to the guidelines of the Canadian Council on Animal Care. All experimental protocols were approved by the Animal Care Committee of York University.

3.2 – Mice Genotyping

3.2.1 – DNA Extraction

C57BL/6 mice pups were weaned from their mothers approximately 21-28 days after their date of birth. Upon request, the Animal Care Facility provided small (~5 mm) tails clips or ear notches to determine the genotype of each mouse. Genomic DNA was extracted using the REDExtract-N-Amp Tissue PCR Kit (Sigma-Aldrich). Each tail was immersed in a 62.5 μL master mix containing 50 μL of extraction solution and 12.5 μL of tissue preparation solution in a 1.5 mL eppendorf tube. The tails were incubated at room temperature for 10 minutes, transferred to a 95°C heating block for 3 minutes, followed by an addition of 50 μL of neutralization solution and thorough mixing by vortexing.

3.2.2 – PCR Amplification and Gel Electrophoresis

The region around TRAF1 V196A was amplified using primers outlined in Table 3.1 and PCR conditions outlined in Table 3.2. The PCR reaction consisted of 4 μL of genomic DNA from each sample, 4 μL of molecular biology grade water, 1 μL of the forward primer (10 mM), 1 μL

of the reverse primer (10 mM), and 10 μL of KAPA2G Fast Genotyping Mix (Sigma-Aldrich). The reactions were prepared in duplicates (one set for gel electrophoresis and the other set for DNA purification) in 200 μL PCR tubes and the samples were centrifuged briefly to bring all the contents down to the bottom before placing in the thermocycler (Bio-Rad). Once the samples were amplified, they were frozen at -20°C and ready for downstream applications.

13 μL of sample was loaded into the wells of a 2% agarose gel and separated by gel electrophoresis at 120 V for 90 minutes. A single band with a size of 587 bp indicates successful amplification of the region flanking the mutation. The purpose of this gel was to assess purity of the amplification prior to purifying and sequencing the samples, as shown in Figure 3.1A.

Table 3.1: Primers for TRAF1 V196A genotyping PCR reaction.

Primer	**Sequence**
TRAF1 V196A F	CTTCGATGGCGCTTTCCTGTGGA
TRAF1 V196A R	GAGGCCTCCTCCATGAGG

Table 3.2: Thermocycler conditions for TRAF1 V196A genotyping PCR reaction.

Step	**Temperature**	**Time**
Initial Denaturation	95°C	3 minutes
35 cycles	95°C	15 seconds
	60°C	15 seconds
	72°C	20 seconds
Final Extension	72°C	1 minute
Hold	4°C	Infinite Hold

3.2.3 – DNA Purification

Purification of DNA from the PCR amplification was performed using the GeneJET PCR Purification Kit (ThermoFisher). 20 μL of PCR product was mixed with a 1:1 volume of binding buffer and transferred to the purification column. The column was centrifuged at 13,000 rpm for 1 minute, flow-through was discarded, and 700 μL of wash buffer was added to the column. The column was centrifuged at 13,000 rpm for 1 minute, flow-through was discarded, and the empty column was centrifuged again at 13,000 rpm for an additional 1 minute to remove any residual wash buffer. The column is then transferred to a clean 1.5 mL eppendorf tube and 30 μL of prewarmed elution buffer is added to the center of the column followed by centrifugation at 13,000 rpm for 2 minutes. The concentration and purity of the purified DNA was measured using a NanoDrop One spectrophotometer and then stored at -20°C.

3.2.4 – DNA Sequencing

Purified DNA was prepared for sequencing according to the protocol provided by The Centre for Applied Genomics (TCAG) operated by SickKids. For PCR products less than 1 kb in size, 50 ng of sample was prepared in a final volume of 7 uL in a PCR strip tube. In addition to this, 0.75 μL of forward primer was added to the PCR tube (Table 3.1); forward primer was recommended by The Centre for Phenogenomics (TCP) where the mice were generated. The chromatogram for each sample was aligned with the template using Benchling to determine the genotype, as shown in Figure 3.1B-D**.**

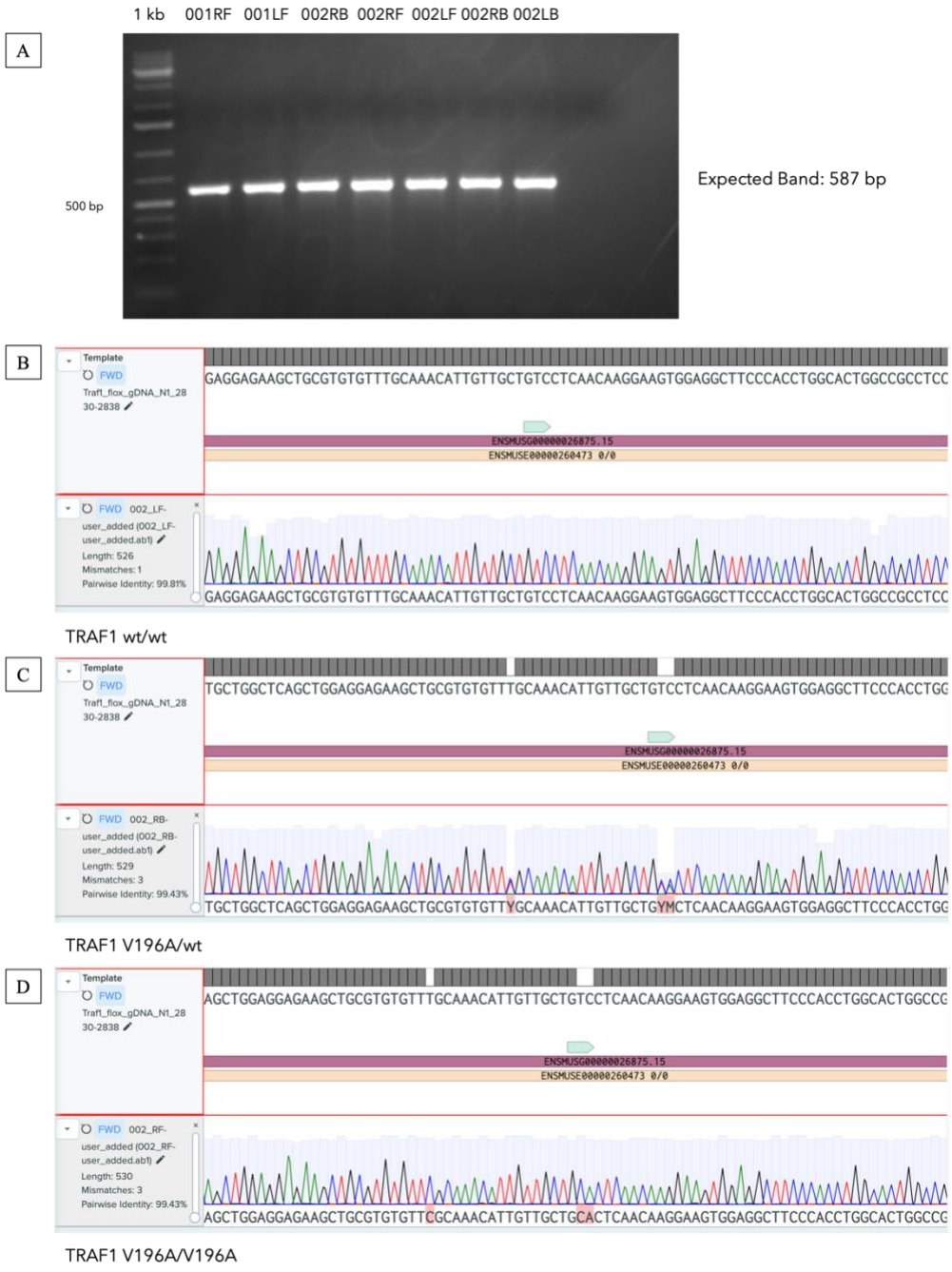

Figure 3.1: Genotyping strategy for TRAF1 V196A mice.

(A) The first step is to perform a PCR reaction to confirm that there is a band corresponding to the correct DNA size of 587 bp. Once this is done, the PCR product is cleaned up and prepared according to the instructions for sequencing samples at SickKids. **(B)** TRAF1 wildtype will possess the "GTC" sequence and have one clear peak in the chromatogram of the mutation site. **(C)** Mice heterozygous for the TRAF1 V196A mutation will show two peaks in the chromatogram

of the mutation site suggesting two distinct alleles. **(D)** Mice homozygous for the TRAF1 V196A mutation will possess the "GCA" sequence and have one clear peak in the chromatogram of the mutation site.

3.3 – Cell Culture

3.3.1 – Culturing Primary and Immortalized Bone Marrow-Derived Macrophages

Primary bone marrow-derived macrophages (pBMDMs) and immortalized bone marrow-derived macrophages (iBMDMs) were kept in a humidified incubator at 37°C with 20% O_2 and 5% CO_2 and cultured in RPMI-1640 media supplemented with 10% heat-inactivated Fetal Bovine Serum, 0.1% 2-Mercapthoethanol (2-ME), 1% L-Glutamine-Pyruvate-Penicillin-Streptomycin (GPPS), and non-essential amino acids (supplemented media referred to as S+ media). pBMDMs were also supplemented with 25% L929 conditioned medium (LCM). iBMDMs were only supplemented with LCM during the thawing process and weaned off gradually (20%, 10% and then 5%) each time they were passaged when they reached 80-90% confluency (for a minimum of 3 passages).

3.3.2 – Culturing T Cells

T cells were kept in a humidified incubator at 37°C with 20% O_2 and 5% CO_2 and cultured in RPMI-1640 media supplemented with 10% heat-inactivated fetal bovine serum, 0.1% 2-Mercapthoethanol (2-ME), 1% l-Glutamine-Pyruvate-Penicillin-Streptomycin (GPPS), and non-essential amino acids (supplemented media referred to as S+ media).

3.3.3 – Culturing HEK293T/17 Cells

Human embryonic kidney (HEK293T/17) cells were kept in a humidified incubator at 37°C with 20% O_2 and 5% CO_2 and cultured in Dulbecco's Modified Eagle Medium (DMEM)

supplemented with 10% heat inactivated Fetal Bovine Serum and 1% L-Glutamine-Penicillin-Streptomycin (GPS) (or 1% L-Glutamine-Pyruvate-Penicillin-Streptomycin (GPPS) if the DMEM media bottle does not contain sodium pyruvate). The cells were passaged once they reached 90-100% confluency using 4 ml of Trypsin followed by a 5-minute incubation at 37°C. An additional 8 mL of DMEM media was then added to inactivate the enzymatic activity of Trypsin followed by a centrifugation at 1300-1500 rpm for 5 minutes. The supernatant was then removed, and the pellet was resuspended in 10 mL of media. If the cells were being maintained, then 1 mL of this cell suspension was added to each T75 flasks along with DMEM media for a final volume of 10 mL. If the cells were going to be used for an experiment, then a cell count was performed, and cells were seeded depending on the experimental protocol.

3.3.4 – Culturing iMac Cells

The Cre-J2 virus producing cells, referred to as iMac, were kept in a humidified incubator at 37°C with 20% O_2 and 5% CO_2 and cultured in Dulbecco's Modified Eagle Medium (DMEM) supplemented with 10% heat inactivated Fetal Bovine Serum and 1% L-Glutamine-Penicillin-Streptomycin (GPS) (or 1% L-Glutamine-Pyruvate-Penicillin-Streptomycin (GPPS) if the DMEM media bottle does not contain sodium pyruvate). The cells were passaged once they reached 90-100% confluency using 4 ml of Trypsin followed by a 5-minute incubation at 37°C. An additional 8 mL of DMEM media was then added to inactivate the enzymatic activity of Trypsin followed by a centrifugation at 1300-1500 rpm for 5 minutes. The supernatant was then removed, and the pellet was resuspended in 10 mL of media. If the cells were being maintained, then they were passaged with a split ratio of 1:3. If the supernatant was going to be collected for a round of infection the following day, then 75% of the cells were reseeded.

3.3.5 – Cell Counting

Cells were visually inspected to estimate confluency or counted for experiments to ensure that there was an even seeding density across different conditions during plating. 10 μL of cell suspension was mixed with a 1:1 mixture of 0.4% Trypan Blue Stain. 10 μL was then added to a hemocytometer and then each 4x4 grid was viewed under 10x microscope magnification to count the number of viable cells (in some experiments, fewer grids were counted, and the formula was adjusted accordingly). The number of viable cells per mL was calculated by multiplying the average viable cell number by 10,000 and the dilution factor.

3.3.6 – Freezing Cells

To freeze BMDMs, cells were collected and resuspended in 5 mL of S+ media containing 10% DMSO. This mixture was then split 1:5 in cryovials and transferred to a Mr. Frosty (cryo-freezing container). To freeze HEK293/17 cells, cells were collected and resuspended in 10 mL of a freezing mixture containing 40% DMEM, 50% FBS and 10% DMSO. This mixture was then split 1:10 in cryovials and transferred to a Mr. Frosty (cryo-freezing container) to ensure that the temperature gradually decreases. The container was placed in the -80°C freezer before transferring the vials to a liquid nitrogen dewar.

3.4 – Lethal and Sublethal Sepsis Models

3.4.1 – Lethal Model, Lethal Dose Determination and Murine Sepsis Scoring

Male and female littermate mice between 6-8 weeks were used for the in vivo LPS lethal model. After measuring the body weight of the mice, LPS from *E. coli* (O55:B5) was diluted accordingly in sterile PBS and injected intraperitoneally (final volume 200 μL) into mice. To establish the lethal dose of 35 mg/kg LPS, defined as 75-80% of the mice achieving a moribund

state, various doses of LPS were tested (Figure 3.2). In collaboration with the Animal Care Facility, we adapted and revised a murine sepsis score (MSS) scoring sheet to assess for moribund state (Figure 3.3). All of the mice were genotyped prior to assigning the cages for the experiment. Due to the subjective nature of this experiment, the Animal Care Facility swapped the cage identification cards and reidentified them to ensure a double-blinded monitoring process. This experiment involves hourly monitoring until 50 hours post-injection or until the mice improve, generally 30 hours post-injection (Figure 3.4). Mice were euthanized once they had reached the threshold set for humane endpoint on the MSS or if they survived until the end of the experiment. When mice reached a moribund state, body weight was measured and then 5% isoflurane was administered. Under anesthesia, blood was collected in 1.5 mL eppendorf tubes using the cardiac puncture method. Next, several organs including the heart, lung, liver and spleen were collected, and stored in the -80°C after snap freezing. Of all the organs that were collected, only the weight of the spleen was measured. Once the experiment was complete, we received the cage identifiers from the Animal Care Facility to match with the original card cards.

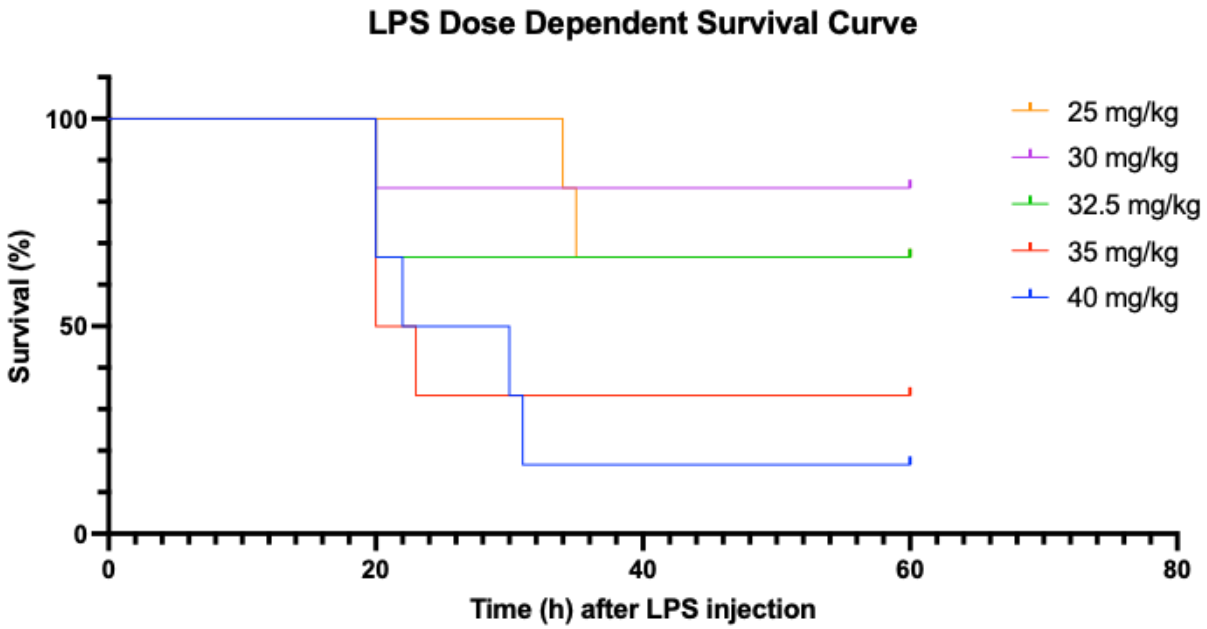

Figure 3.2: Kaplan-Meier survival curve of wildtype female C57BL/6 mice treated with various doses of LPS to establish the 35 mg/kg lethal dose.

TRAF1 wildtype littermates challenged with 25 mg/kg (n=6) in experiment one, 30 mg/kg (n=6) and 32.5 mg/kg (n=5) in experiment two, and 35 mg/kg (n=6) and 40 mg/kg (n=6) in experiment three. Mice were monitored for a total of 60 hours and assigned a murine sepsis score. Mice that met the criteria for moribund state or survived until the end of the experiment were euthanized.

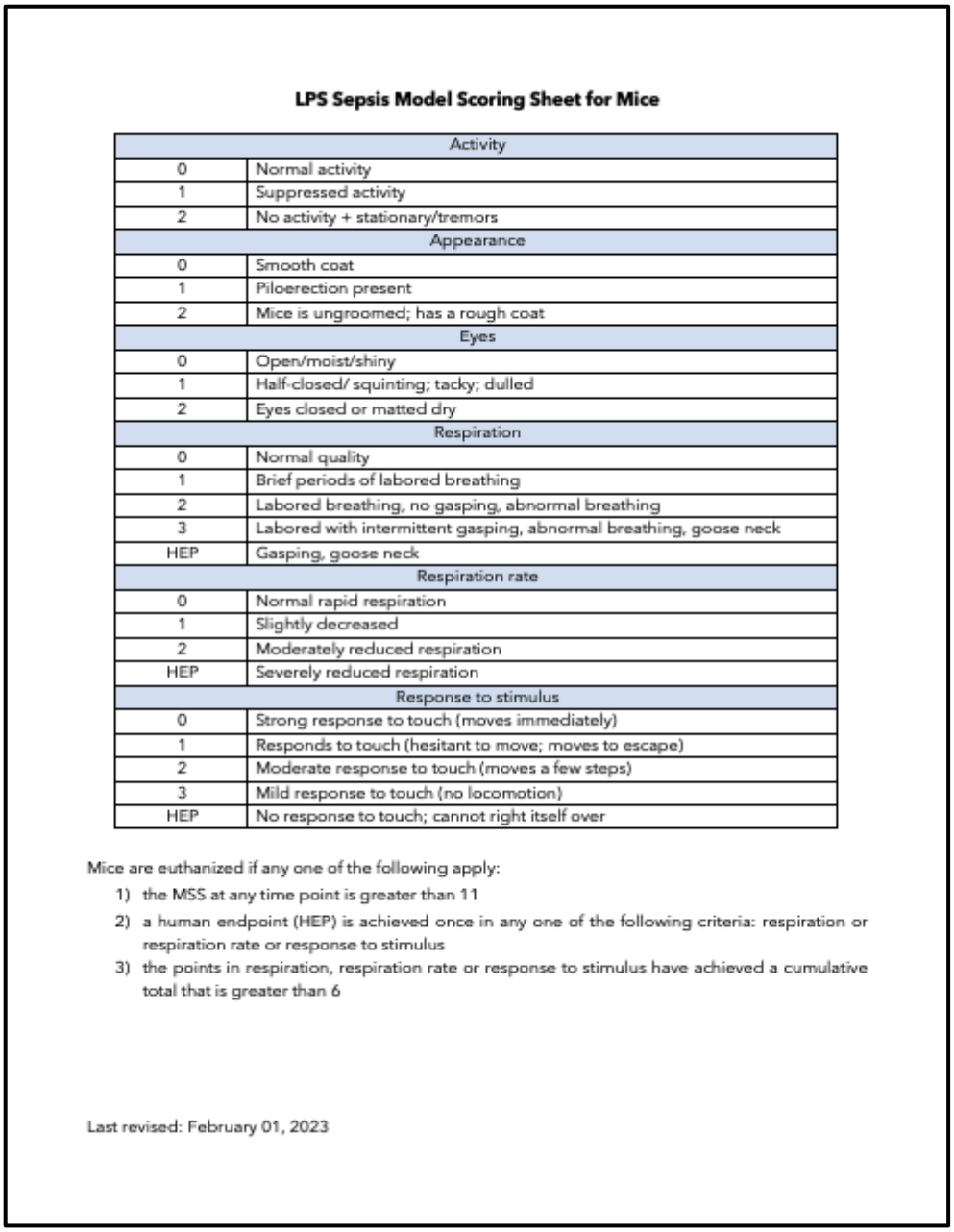

LPS Sepsis Model Scoring Sheet for Mice

Activity	
0	Normal activity
1	Suppressed activity
2	No activity + stationary/tremors
Appearance	
0	Smooth coat
1	Piloerection present
2	Mice is ungroomed; has a rough coat
Eyes	
0	Open/moist/shiny
1	Half-closed/ squinting; tacky; dulled
2	Eyes closed or matted dry
Respiration	
0	Normal quality
1	Brief periods of labored breathing
2	Labored breathing, no gasping, abnormal breathing
3	Labored with intermittent gasping, abnormal breathing, goose neck
HEP	Gasping, goose neck
Respiration rate	
0	Normal rapid respiration
1	Slightly decreased
2	Moderately reduced respiration
HEP	Severely reduced respiration
Response to stimulus	
0	Strong response to touch (moves immediately)
1	Responds to touch (hesitant to move; moves to escape)
2	Moderate response to touch (moves a few steps)
3	Mild response to touch (no locomotion)
HEP	No response to touch; cannot right itself over

Mice are euthanized if any one of the following apply:

1) the MSS at any time point is greater than 11
2) a human endpoint (HEP) is achieved once in any one of the following criteria: respiration or respiration rate or response to stimulus
3) the points in respiration, respiration rate or response to stimulus have achieved a cumulative total that is greater than 6

Last revised: February 01, 2023

Figure 3.3: Lipopolysaccharide (LPS) sepsis model scoring sheet for mice.

3.4.2 – Sublethal Model

Male and female littermate mice between 6-8 weeks were used for the in vivo LPS sublethal model. LPS from *E. coli* (O55:B5) was diluted in sterile PBS and injected intraperitoneally (final volume 200 μL) into mice according to the body weight for a sublethal dose of 10 mg/kg. In this model, blood was collected at 1-, 6- and 24-hour timepoints (Figure 3.4; future experiments will include the 3-hour timepoint; for some experiments, the 6-hour timepoint was the endpoint). Dr. Ali Abdul-Sater kindly trained and assisted me with collecting the blood at all non-endpoint timepoints by saphenous vein blood draw. At the endpoint, blood was collected in 1.5 mL eppendorf tubes using the cardiac puncture method. The blood was then placed at room temperature for 30 minutes or on ice for 60 minutes to allow the blood to clot. Next, the tube was centrifuged at 10,000 rpm for 5 minutes and the serum (corresponding to the supernatant) was transferred to a fresh tube and stored in the -80°C after snap freezing. The serum was then used to perform the LEGENDplex immunoassay (Bio-Legend) to measure cytokine production using flow cytometry.

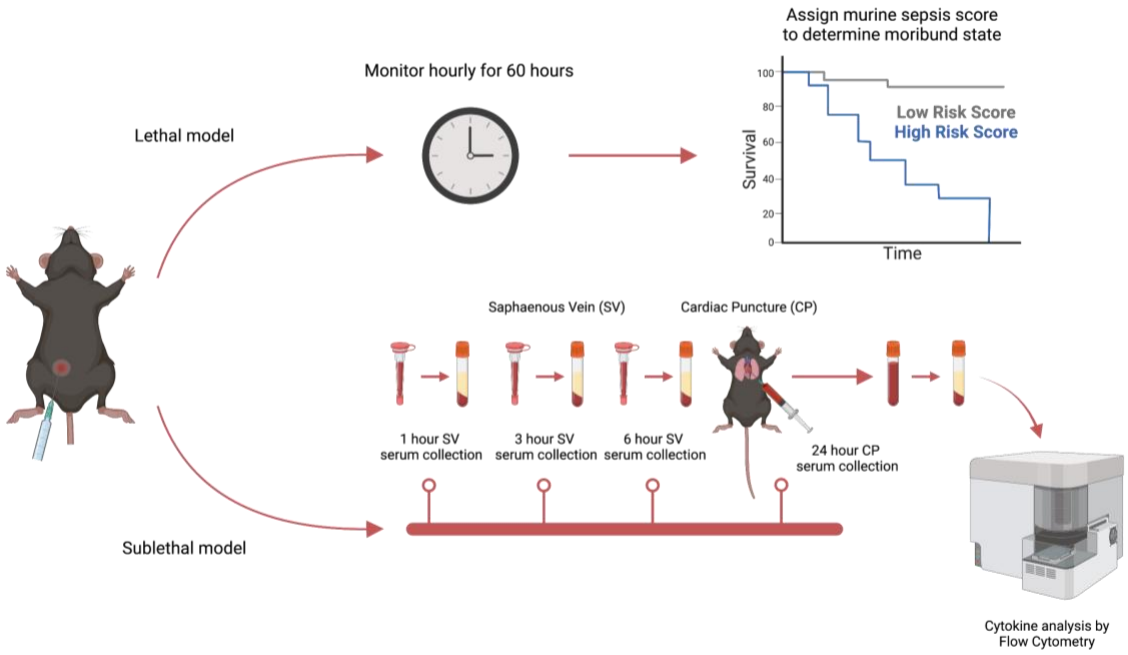

Figure 3.4: Schematic representation of experiments employing the lethal and sublethal model of LPS.

In the lethal model, mice will be intraperitoneally (IP) injected with 35 mg/kg LPS and monitored hourly for 60 hours. Each mouse will be assigned a moribund sepsis score to determine moribund state. Mice that achieve a score greater than the threshold are euthanized. In the sublethal model, mice will be IP injected with 10 mg/kg LPS, and blood will be collected at 1-, 3-, 6- and 24-hour timepoints to measure cytokine production from the serum using the LEGENDplex immunoassay. Created with BioRender.com.

3.4.3 – LEGENDplex Bead-Based Flow Cytometry Assay

Cytokine levels were assessed using the LEGENDplex bead-based flow cytometry immunoassay (Bio-Legend). The reagents were prepared and diluted according to the manufacturer's protocol. First, the lyophilized standard was reconstituted with 250 µL of assay buffer and transferred to a 1.5 mL eppendorf tube labelled top standard C7 following a 10-minute room temperature incubation. 75 µL of assay buffer was added to six 1.5 mL centrifuge tubes

labelled C6, C5, C4, C3, C2, and C0 (in order of decreasing concentration). The top standard was then used to perform 1:4 serial dilutions until C1. Another tube was labelled C0 containing only 75 μL which was used as the 0 pg/mL blank standard. Next, the serum samples were diluted 1:10 and 1:5 for the 1-hour and 6-hour timepoints, respectively. 25 μL matrix A was added to the standard wells and 25 μL of assay buffer was added to the sample wells. The samples and standards were prepared in duplicates and 25 μL per well was loaded in a vertical configuration. Pre-mixed beads were vortexed for 1 minute and 25 μL was added to each well followed by gentle mixing with a pipette (total volume should be 75 μL in each well after adding the beads). The plate was then covered with a plate sealer and aluminum foil to protect from light (plate is sealed and protected from light during all incubation steps) and placed on a plate shaker at 250 rpm for 2-hours at room temperature. Next, the plate was centrifuged at 1000 rpm for 5 minutes and the supernatant was decanted using the plate flip method (tap the plate very gently on paper towel to remove excess supernatant and keep an eye in the pellet to ensure that the pellet does not dissociate). 200 μL of 1x was buffer was then added on top of each well (without disturbing the pellet) and incubated for 1 minute at room temperate followed by a second wash. Then, 25 μL of detection antibodies were added followed by gentle mixing by pipette 3-5 times to resuspend the pellet. The plate was than sealed and placed on a plate shaker at 250 rpm for 1 hour. Once the incubation is finished, 25 μL of SA-PE is added directly to each well and placed on the shaker at 250 rpm for another hour. The plate was then centrifuged at 1000 rpm for 5 minutes and the pellet was resuspended with 150 μL of 1x wash buffer with a pipette. The assay was then performed using a template created beforehand on the Cytek Aurora flow cytometer.

3.5 – In Vitro Lipopolysaccharide Experiments

3.5.1 – Mouse Bone Marrow Extraction

The mice used in this study were euthanized with 5% isoflurane followed by removal of the heart. The mice were then clipped facing upward on a Styrofoam board using needles and 70% ethanol was sprayed on the lower abdominal and hind leg regions of the mouse. The first incision was made in the lower abdomen towards the bottom of the hind legs. Next, the muscle around the bones and the tissue around the pelvis was removed. After having a better view of the attachment between the hind legs and the pelvis, both legs were carefully removed by cutting after the joint in the pelvis (it is important to ensure that the bone marrow is not exposed to the air and that the femur and tibia bones were not broken). The bones were then stored in a 15 mL falcon tube containing S+ media which was placed in ice until all samples were collected. In the biosafety cabinet, the extra muscle was removed, the tibia and femur were separated at the knee joint, and the tips of the bones were cut to expose the bone marrow. Each bone (total of 4) was flushed with roughly 2.5 mL of S+ media (prewarmed to 37°C) from both sides for a total of 10 mL per mouse, collected in a 50 mL falcon tube. The solution was then filtered using a sterile 70 μm filter and then centrifuged at 1300 rpm for 5 minutes. The supernatant was decanted, and the pellet was resuspended with 2 mL of red blood cell lysing buffer (Sigma) followed by a 5-minute incubation at room temperature. Next, 6 mL of S+ media was added to each tube and the mixture was centrifuged at 1300 rpm for 5 minutes. The cell pellet was then resuspended with 40 mL of S+ media with 25% LCM. L929 cells secrete macrophage colony stimulating factors (M-CSF) which was then collected and filtered to supplement S+ media; LCM essentially helps cells differentiate into bone marrow-derived macrophages. The 40 mL cell suspension was then divided evenly across 8 bacterial petri dishes (5 mL of media each; volume and number of plates can differ

depending on the experiment) and incubated for 3 days in a humidified incubator at 37°C with 20% O_2 and 5% CO_2.

On day 3, media from all of the dishes was aspirated to remove all of the cells that had not adhered to the plate (carefully to not disrupt the cells that had adhered). Next 3 mL of S+ media was added to each dish and cells were carefully scraped to bring them into suspension and transferred to a 50 mL falcon tube, for a total of 24 mL per mouse. The cells were then counted using the hemocytometer and seeded at a concentration of 0.75-1.0 x 10^6 cells per mL of S+ media supplemented with 25% LCM. 1 mL was then added to each well of a 6-well tissue culture plate and incubated for another 48-60 hours (media may be replenished around 48 hours depending on the colour) to allow the cells to proliferate to confluency and differentiate into M0 (non-activated) bone marrow-derived macrophages. The cells are now ready for experimental treatments. An overview of this process is depicted in Figure 3.5.

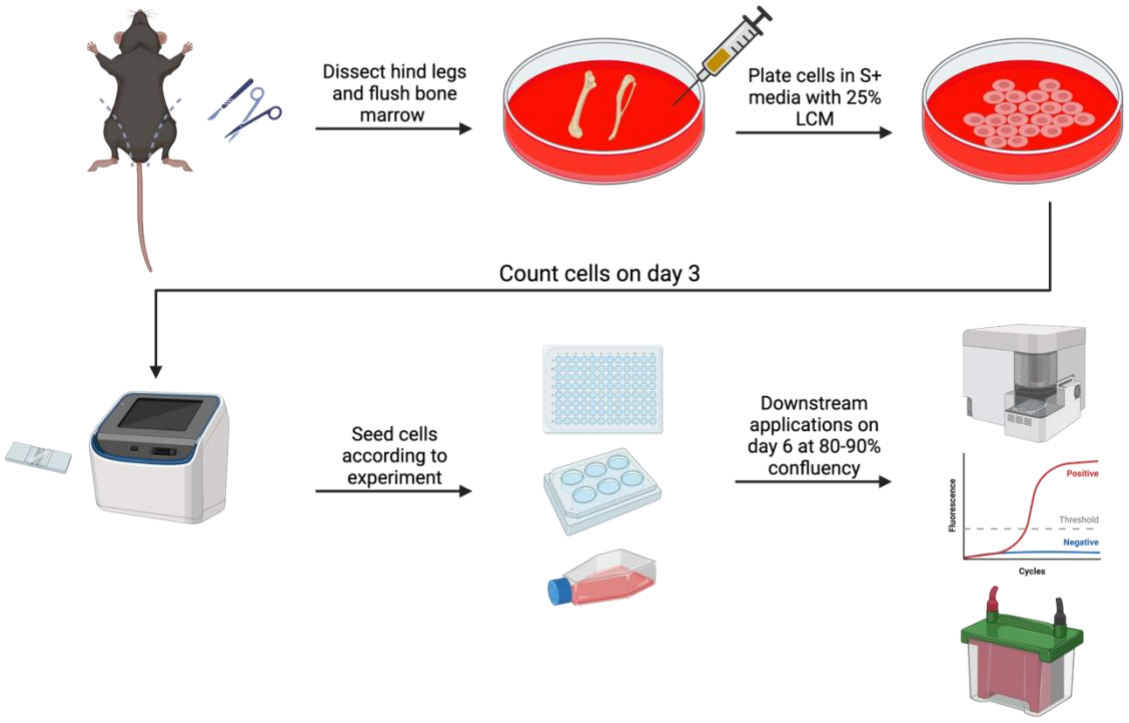

Figure 3.5: Schematic representation of flushing mouse bone marrow to generate bone marrow-derived macrophages (BMDMs).

Hind legs are dissected, and the bone marrow is flushed with S+ media. Cells are then cultured for 3 days in S+ media containing 25% L929 culture media (LCM). LCM contains macrophage colony stimulating factors (M-CSF). On day 3, cells are counted and seeded depending on the experiment which can begin on day 6 once the cells are 80-90% confluent. These experiments will include techniques such as real-time quantitative polymerase chain reaction (RT-qPCR), western blot and flow cytometry. Created with BioRender.com.

3.5.2 – Immortalization of Primary Bone Marrow-Derived Macrophages

pBMDMs from female littermate mice with TRAF1 wt/wt, TRAF1 V196A/wt, TRAF1 V196A/V196A genotypes were immortalized following the Cre-J2 retroviral infection method (Blasi et al., 1985; De Nardo et al., 2018). This method involves infecting cells with the J2 recombinant retrovirus (derived from a replication-defective 3611-Moloney sarcoma virus (MSV)) carrying the v-raf and v-myc oncogenes. I worked closely with Dr. Mayoorey Murugathasan to learn and employ the protocol described below.

First, we thawed and propagated the Cre-J2 virus producing iMac cells as described in section 3.3.4 to harvest the supernatant on the day of the infection. Once the supernatant was collected in a 50 mL falcon tube, it was filtered through a 0.2 μm syringe filter (Fisher Scientific) into a new 50 mL falcon tube. Bone marrow cells were also extracted as described in section 3.5.1 for the first round of infection. The entire bone marrow for one mouse was resuspended in 5 mL of S+ media supplemented with 50% LCM (will be diluted to 25% LCM in the following step). Next, two 10 cm dishes were labelled according to the two conditions of Cre-J2 virus and no-Cre-J2 virus negative control. For the Cre-J2 virus labelled plate, 2.5 mL of the bone marrow suspension was mixed with 2.5 mL of the Cre-J2 virus. For the no-Cre-J2 virus negative control, 2.5 mL of the bone marrow suspension was mixed with 2.5 mL of DMEM media. The plates were

then incubated for 16-24 hours in a humidified incubator at 37°C with 20% O_2 and 5% CO_2. The following day, the supernatant and the remaining cells were collected into a 50 mL falcon tube, centrifuged at 1300 rpm followed by removal of supernatant, resuspended in 10 mL of S+ media supplemented with 25% LCM and reseeded in 10 cm plates. The plates were then placed back in the incubator and maintained until the second round of infection. The second round of infection normally takes place on the third day but in our case, we performed the second round of infection on the fifth day. We had to thaw a new vial of iMac cells to collect the virus for the second infection since our original iMac cells that were in culture stopped proliferating. On day five, the supernatant and the remaining cells were collected into a 50 mL falcon tube, centrifuged at 1300 rpm followed by removal of supernatant, resuspended in 5 mL of S+ media supplemented with 50% LCM. The cells were then infected with the virus following the same steps and conditions as the first round. On day six the supernatant and the remaining cells were collected into a 50 mL falcon tube, centrifuged at 1300 rpm followed by removal of supernatant, resuspended in 10 mL of S+ media supplemented with 25% LCM and reseeded in 10 cm plates. The cells were then maintained for 2-3 weeks and replated at a split ratio ranging from 1:3 to 1:10. Cells were also frozen after several passages as described in section 3.3.6 to thaw in the future, if needed. During this period, the infected plate was observed under a microscope and compared to the control plate. Here, we observed that the infected plate had more cells than the control plate. After 3 weeks, we gradually decreased the concentration of LCM after each passage. To do this, we would seed cells supplemented with the same LCM concentration in one plate and cells supplemented with a lower LCM concentration in a second plate. As the weaning progressed, we noticed that the infected plate formed colonies compared to the control plate. This is a promising indication that the

immortalization worked as the cells were surviving and proliferating independent of LCM. Once we reached an LCM concentration between 0-5%, we consider the BMDMs to be immortalized.

3.5.3 – Lipopolysaccharide (LPS) Stimulations

Lipopolysaccharide (LPS) from *E. coli* O55:B5 (Sigma-Aldrich) was used for all in vivo and in vitro experiments. The lyophilized LPS powder was reconstituted in phosphate buffered saline (PBS) without calcium and magnesium at a stock concentration of 5 mg/mL, filtered, aliquoted in eppendorf tubes, and stored in the -80°C for long-term storage. The concentration of LPS used in this scientific study was 100 ng/mL (indicated in the figure caption). Sterile PBS served as the vehicle control. The stock concentration was diluted to 1 mg/mL and stored at 4°C for up to one month. From this stock concentration, a 0.1 mg/mL aliquot of LPS was prepared for the duration of the experiment. From this 0.1 mg/mL aliquot, a 0.01 mg/mL aliquot of LPS was prepared at each timepoint and 10 μL from this new stock was added per mL of media. The 0.01 mg/mL stock LPS was discarded after each timepoint and made fresh due to stability recommendations indicated on the product sheet.

3.5.4 – RNA Extraction

pBMDMs and iBMDMs were harvested for total RNA on ice. 500 μL of TRIzol was added to each well of a 6-well plate and the surface was scraped (with a p20-200 tip using the opening that attaches to the micropipette). At this point, samples were transferred to eppendorf tubes and stored at -80°C (stable for up to a year at -20°C). On the day of the extraction, the samples were thawed for 30 minutes at room temperature (allows for more yield and better extraction). Next, 100 μL of chloroform was added to the samples and incubated for 15 minutes at room temperature. The samples were then vortexed (resulting in a milky pink colour) and centrifuged at 12,000 g for

15 minutes (all centrifugation steps during the extraction were done either in the 4°C cold room or in a centrifuge with the internal temperature set to 4°C). The aqueous phase (containing the RNA) was carefully transferred to a new tube (it is important to avoid collecting the interphase and organic layer). A second extraction was performed by adding 100 μL of acid phenol chloroform, incubation for 5 minutes at room temperature, followed by centrifugation at 12,000 g for 10 minutes (due to the acidic nature of this extraction, the DNA is protonated thereby precipitating in the lower phase which helps minimize DNA contamination; Supplementary Figure 1.0). The aqueous phase was transferred to a new tube and mixed with 250 μL of isopropanol. After a 10-minute room temperature incubation, the sample was vortexed and centrifuged at 12,000 g for 10 minutes resulting in a white pellet at the bottom of the tube. The supernatant for this step was removed by emptying the tube. Next, 1000 μL of 75% ethanol was added followed by centrifugation at 10,000 for 10 minutes. Here, the supernatant was removed by pipetting. The tube was then filled with 200 μL of molecular biology grade water, 20 μL of 3M sodium acetate (NaOAC), 2 μL of 20 mg/ml glycogen, and 600 μL of 100% ethanol. The samples were then mixed and precipitated at -80°C for at least 1 hour (overnight precipitation can help increase the overall yield). Then next day, the samples were centrifuged at 10,000 for 5 minutes and a larger pellet usually appears. The supernatant was removed with a pipette, 100 μL of 75% ethanol was added to wash the pellet followed by centrifugation at 10,000 g for 5 minutes. Here, the ethanol was removed as much as possible without disturbing the pellet followed by another centrifugation at 10,000 g for 5 minutes. Residual ethanol was then carefully removed by a p20 pipette followed by a 10-minute incubation at room temperature with the eppendorf caps open to air dry the RNA pellet. After this, the RNA pellet was solubilized in 30-50 μL of molecular biology grade water (volume depends on the size of pellet after the overnight precipitation) and placed on the heating

block preset to 55-60°C for 10-15 minutes. The RNA concentration and absorbance values (A260/A280 and A260/230) was measured using a NanoDrop One spectrophotometer and then either converted to cDNA immediately or stored at -80°C.

3.5.5 – cDNA Synthesis through Reverse Transcription (RT) of RNA

Once all of the total RNA samples were quantified, each sample was normalized to have between 800-1000 ug of RNA (within an experiment, the ug of RNA used in the RT reaction is constant but can vary between experiments) in a final volume of 14.8 μL. Next, 1 μL of Oligo dT and 1 μL of 10 mM dNTP was added to the RNA mixture (final volume now 16.8 μL) and placed in a thermocycler (Bio-Rad) according to the conditions outlined below in Table 3.3. Once step one was complete, step two involves adding 2 μL of 10x reverse transcriptase buffer, 0.2 μL RNase inhibitor, 1 μL of M-MuLV Reverse Transcriptase (final volume now 20 μL) and placed back in the thermocycler (Bio-Rad) according to the conditions outlined below in Table 3.4. Once the reaction for step two was complete, 20 μL of cDNA was diluted 1:10 with molecular biology grade water. The resulting 200 μL of diluted cDNA was stored at -20°C until further downstream applications such as real-time quantitative PCR were to be performed.

Table 3.3: Thermocycler conditions for reverse transcription (RT) step 1.

Step	Temperature	Time
1	65°C	5 minutes

Table 3.4: Thermocycler conditions for reverse transcription (RT) step 2.

Step	Temperature	Time
1	37°C	50 minutes

2	72°C	15 minutes
3	4°C	Infinite Hold

3.5.6 - Real-Time Quantitative Polymerase Chain Reaction (RT-qPCR)

The 1:10 diluted cDNA was thawed and amplified in either a CFX384 Touch Real-Time PCR Detection System (BioRad) or CFX Opus 384 Real-Time PCR Detection System (Bio-Rad) according to the conditions outlined below in Table 3.5. A master mix for each gene of interest was prepared depending on the number of reactions. For each reaction, 5 μL of 2x SYBR Green PCR Master Mix (Bio-Rad) was mixed with 0.5 μL of the forward and reverse primer (10 mM concentration) corresponding to the gene of interest, outlined in Table 3.6, for a total volume of 6 μL. The master mix for each gene of interest was loaded separately into a 384-well plate followed by 4 μL of diluted cDNA. Each sample was run in technical triplicates. The primers used in this thesis were either validated previously by lab alumni or by myself to ensure efficient and site-specific amplification of the target gene. Early experiments consisted of thorough optimizations to ensure minimal or insignificant genomic DNA amplification, outlined in Supplementary Figure 1.0, and the identification of a reliable housekeeping gene for our model.

After performing the RT-qPCR, relative gene expression analysis was calculated using the $2^{-\Delta\Delta CT}$ method; CT values were normalized to the mouse RPLP0 housekeeping gene. In order to normalize, the housekeeping CT value for each sample was subtracted from the gene of interest CT value for the same sample. From here, two different approaches were employed to calculate the fold change. In the first approach, the average delta CT of the unstimulated timepoint for a particular genotype was subtracted from the delta CT of the stimulated timepoints for the same genotype. In the second approach, the average delta CT of the wildtype condition for a particular

timepoint was subtracted from the delta CT of the other genotypes for the same timepoint. The resulting value from both approaches is the delta delta CT value, which is then used to determine the fold change, calculated as $2^{-\Delta\Delta CT}$. Statistical analysis was performed on the fold change values.

Table 3.5: Thermocycler conditions for RT-qPCR.

Step	**Temperature**	**Time**
Initial Denaturation	95°C	3 minutes
40 cycles	95°C	15 seconds
	60°C	30 seconds
	Plate Read	
Melt Curve Plate Read	65°C to 95°C	0.5°C/0.05sec
Hold	4°C	Infinite Hold

Table 3.6: List of primers used to measure inflammatory gene expression by RT-qPCR.

Primer	**Sequence**
m-IFNbeta For	TCCAAGAAAGGACGAACATTCG
m-IFNbeta Rev	TGAGGACATCTCCCACGTCAA
m-IL-1beta For	GCAGCACATCAACAAGAG
m-IL-1beta Rev	CAGCAGGTTATCATCATCATC
m-IL6 For	ACAGAAGGAGTGGCTAAG
m-IL6 Rev	AGAGAACAACATAAGTCAGATAC
mIL-10 For	ATAACTGCACCCACTTCCCA
mIL-10 Rev	GGGCATCACTTCTACCAGGT
m-IL12 For	GATGACATGGTGAAGACGGC
m-IL12 Rev	AGGCACAGGGTCATCATCAA
mRPLP0 For	TTGGAGTGACATCGTCTT
mRPLP0 Rev	ATCTTGAGGAAGTAGTTGGA
m-TGFbeta For	CCTGCAAGACCATCGACATG

m-TGFbeta Rev	TGTTGTACAAAGCGAGCACC
m-TNFalpha For	AGAATGAGGCTGGATAAGAT
m-TNFalpha Rev	GAGGCAACAAGGTAGAGA
mTRAF1 For	GACTGTCAGCCTCTTCTC
mTRAF1 Rev	GCATCGTATTCTCCTCTCA

3.5.7 – Protein Lysate Preparation

Once LPS stimulations were completed, the media was aspirated, and each well was then washed with 1 mL of ice-cold PBS with magnesium and calcium (both magnesium and calcium ensure that the macrophages remain bound to the plate). Depending on the number of cells and experiment, 100-200 μL of freshly prepared 1x lysis buffer was added to each well. This lysis buffer was prepared with 0.5% NP-40, 50 mM Tris pH 8.0, 10% glycerol, 0.1 mM EDTA, 150 mM NaCl, 1x protease inhibitor cocktail (Sigma-Aldrich), 1x phosphatase inhibitor cocktail 3 (Sigma-Aldrich), 1 mM DTT (Sigma-Aldrich) and deionized water. The plate was then incubated on ice for a minimum of 10 minutes and then the surface of each well was scraped (with a p20-200 tip using the opening that attaches to the micropipette). The cells from each well were transferred to corresponding pre-chilled 1.5 mL eppendorf tubes and incubated on ice for 15 minutes; during this period, the tubes were vortexed every 5 minutes to facilitate cell lysis. Next, the lysates were centrifuged at 13,300 rpm for 15 minutes. The supernatant was then transferred to new pre-chilled 1.5 mL eppendorf tubes (in order to remove cell debris) and stored in the -80°C after snap freezing.

3.5.8 –Bradford Protein Assay

The Bradford protein assay was performed to measure the protein concentration of the samples. This protein assay was performed in a 96-well flat bottom plate using the Bradford Reagent (Bio-Rad or BioShop). 1 mg/mL bovine serum albumin (BSA) was used as the protein standard. The standard was prepared through a series of two-fold serial dilutions beginning with 128 μg/mL and subsequent dilutions of 64 μg/mL, 32 μg/mL, 16 μg/mL, 8 μg/mL, and 4 μg/mL. The first 128 μg/mL standard was prepared by mixing 128 μL of the 1 mg/mL BSA with 872 μL of the Bradford reagent. For the subsequent five dilutions, 500 μL of Bradford reagent was added to five eppendorf tubes. The 128 μg/mL standard was mixed thoroughly and then 500 μL was transferred into the next eppendorf tube containing, which already has 500 μL of Bradford reagent, resulting in a two-fold dilution to achieve a concentration of 64 μg/mL. The serial dilution then continued until the lowest concentration of 4 μg/mL. The blank for this protein assay was the Bradford reagent alone; this absorbance value allows background subtraction from all of the standard and sample absorbance values. Next, 500 μL of Bradford reagent to eppendorf tubes corresponding to the number of samples. 5 μL of sample was then added to corresponding eppendorf tubes resulting in a 1:100 dilution of the protein samples (the dilution of the samples can vary depending on the absorbance readings). The standards and samples were then vortexed and transferred into a 96-well flat bottom plate in duplicates (oriented horizontally). The absorbance was then measured at 595 nm using a plate reader (Verioskan). The absorbance values were then exported to an Excel template and a standard curve was created for the BSA. Using the line of best fit and the equation for the standard curve, the concentrations of the unknown protein samples were calculated to ensure equal protein loading for the western blot. After quantification, all of the protein lysates were brought to the same working concentration, usually 0.66 μg/μL, by

diluting with either water or lysis buffer. The protein samples were also mixed with 5x Laemmeli Sample Buffer prepared with 2-ME (final working concentration of Laemmeli was 1x). The protein samples were then placed on a heating block set to 100°C for 5 minutes followed by a quick spin. At this point, the samples were either stored in the -20°C or a western blot was performed.

3.5.9 – Western Blotting

Protein samples that were stored in the -20°C were placed on a heating block set to 100°C for 5 minutes followed by a quick spin. Equal amount of protein, usually between 10-20 μg, was loaded in each well and separated by a 10% SDS-polyacrylamide gel electrophoresis at 80 V for 30 minutes followed by 120 V for 60 minutes. The protein samples were then transferred using the Trans-Blot Turbo Transfer System (Bio-Rad) for 7 minutes onto a polyvinylidene difluoride (PVDF) membrane (Bio-Rad). The PVDF membrane was activated in 100% methanol prior to forming the transfer sandwich. After the transfer, the membrane was rinsed with water three times and then 10 mL of Ponceau stain was added (helpful to determine equal loading and successful transfer). The membrane was then placed on the rocker and incubated for 10-15 minutes at room temperature. The membrane was then placed in water to remove excess Ponceau stain and then an image was captured using the ChemiDoc MP Imaging System (Bio-Rad). The membrane was washed three times with 1x TBS with 0.1% Tween-20 (TBST) washing buffer and then blocked with 5% skim milk in TBST for a minimum of 1 hour at room temperature. Next, the membranes were incubated with primary antibodies, diluted in 5% BSA containing 0.02% sodium azide, overnight at 4°C. The primary antibodies that were used to assess protein expression are outlined in Table 3.7. Following the incubation with the primary antibodies, the membranes were washed three times (15 minutes, 10 minutes, and 5 minutes) with TBST. The membranes were then

incubated for 1 hour at room temperature with peroxidase-conjugated secondary antibodies (1:5000 dilution for phospho-antibodies; 1:10000 dilution for housekeeping gene) diluted in 5% skim milk in TBST. Following the incubation with the secondary antibodies, the membranes were washed again three times (15 minutes, 10 minutes, and 5 minutes) with TBST. Proteins of interest and housekeeping protein were detected with Immobilon Forte (Millipore) and Clarity (ThermoFisher Scientific) western blotting ECL detection reagents, respectively. The image was captured using the chemiluminescence feature on the ChemiDoc MP Imaging System (Bio-Rad). The results were then qualitatively assessed by normalizing the target genes to the Ponceau stain instead of a housekeeping gene because the proteins of interest overlapped with three housekeeping genes that were tested, β-Actin, GAPDH and α-Tubulin.

Table 3.7: List of primary antibodies used to assess inflammatory signalling by western blotting.

Primary Antibody	**Dilution**	**Company**	**Catalog Number**
p-p65 (93H1)	1:1000	Cell Signaling Technology	3033T
p-SAPK/JNK (81E11)	1:1000	Cell Signaling Technology	4668S
Total IκBα (L35A5)	1:1000	Cell Signaling Technology	4814S
Beta (β)-Actin (BA3R)	1:5000	Thermo Scientific	MA5-15739
GAPDH (14C10)	1:1000	Cell Signaling Technology	2118S
α-Tubulin	1:1000	Cell Signaling Technology	3873S

3.5.10 – Detection of Phospho-Signalling by Flow Cytometry

Once all of the timepoints were completed for the LPS experiment, the media was quickly aspirated and discarded from each well of a 6-well plate (time-sensitive experiment). Next, 500 μL of the intracellular IC fixation buffer was added to each well followed by a 30-minute incubation at room temperature. During this incubation, each well was scraped with a scraper gently and the cells were transferred to 1.5 mL eppendorf tubes. The samples were then centrifuged at 1300 rpm for 2 minutes followed by the removal of the supernatant with a pipette (ensure that the cell pellet was not removed). The cell pellet was then resuspended with 200 μL of ice-cold methanol and incubated overnight at 4°C or incubated at -20°C for a few days. Following the incubation, 230 μL of 2% FACS (2% in PBS without calcium and magnesium) was mixed with the contents of each tube resulting in a final volume of 430 μL. From here, 100 μL of cell suspension was transferred to four different 96-well U-bottom plates. 100 μL of FACS buffer was added on top (half-wash) followed by centrifugation at 1300 rpm for 3 minutes. The plate was then decanted and washed two more times with 200 μL FACS buffer (full-wash) followed by centrifugation at 1300 rpm for 3 minutes. Next, fluorescently conjugated antibodies were diluted in FACS buffer and added to the samples as single-stains. The fluorescently conjugated antibodies that were used to measure inflammatory signalling are outlined in Table 3.8. For the unstained wells, 50 μL of FACS buffer was added to the samples accordingly. The plates were then incubated for 1 hour at room temperature. Following the incubation, 150 μL of FACS buffer was added on top (half-wash) followed by centrifugation at 1300 rpm for 3 minutes. The plate was then decanted and washed two more times with 200 μL FACS buffer (full-wash) followed by centrifugation at 1300 rpm for 3 minutes. The cells were then resuspended in 150-200 uL of FACS buffer and flow

cytometry was performed. Figure 3.5 is a representative example of the gating strategy used to measure phospho-signalling in pBMDMs (Figure 3.5A) and iBMDMs (Figure 3.5B).

Table 3.8: List of fluorescent antibodies used to measure inflammatory signalling by flow cytometry.

Antibody	Fluorophore	Dilution	Company	Catalog Number
p-ERK1/2 (MILAN8R)	Alexa Fluor 488	1:50	Thermo Scientific	53-9109-42
p-p65 (93H1)	Alexa Fluor 647	1:50	Cell Signalling Technology	4887S
p-SAPK/JNK (G9)	Alexa Fluor 647	1:50	Cell Signalling Technology	9257S

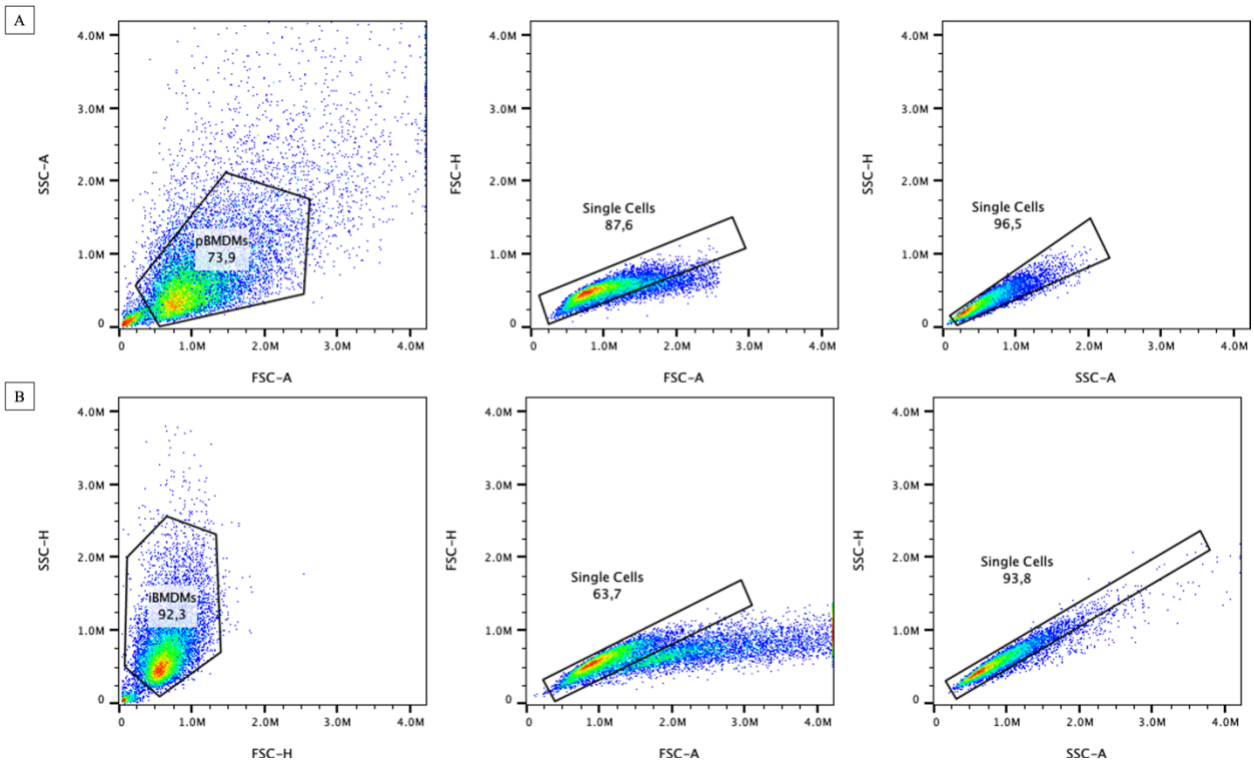

Figure 3.5: Gating strategy for phospho-flow in pBMDMs and iBMDMs.

The gating strategy was created on FlowJo (Version 10.8.2). A representative gating strategy is shown for both pBMDMs (Figure 3.5A) and iBMDMs (Figure 3.5B). Cells were single-stained, washed and then resuspended in FACS buffer before being loaded into the flow cytometer. The

gating strategy shown above was optimized to exclude debris and doublets from the analysis. The second single stain gate was then used to determine the MFI values for each antibody stain.

3.5.11 – Inflammasome Activation

To assess the levels of IL-1β following inflammasome activation, BMDMs were first primed with 100 ng/mL LPS for 3 hours in 1 mL S+ media (signal 1). At the end of the 3-hour treatment, S+ media was replaced with 1 mL of Opti-MEM reduced serum media. Next, the cells were treated for 1 and 3 hours with either 5 mM ATP or 10 μM Nigericin (signal 2). The samples were treated so that they could all be harvested at the same endpoint. At the end of the 6-hour endpoint, 1 mL of the supernatant was collected of which 800 μL was allocated for TCA precipitation, 100 μL for ELISA and the remaining 100 μL for the LDH assay. Additionally, the cells were also lysed according to the protocol described in section 3.5.7 for western blot analysis.

3.5.12 – IL-1β ELISA

The mouse IL-1β uncoated ELISA kit (ThermoFisher Scientific) was used to perform quantitative analysis on the amount of IL-1β secreted (present in the supernatant) from the BMDMs that were treated during the inflammasome experiment. First, 100 μL/well of the anti-mouse IL-1β capture antibody (1:250) was immobilized in high protein-binding 96-well plates (Greiner Bio-One), optimal for performing ELISA, and incubated overnight at 4°C. The next day, the supernatant was decanted using the plate flip method and the wells were washed four times with 200 μL of 0.05% Tween-20 (wash buffer). For all of the washes in this protocol, the wash buffer was soaked for approximately 1-2 minutes before being decanted. The plate was then blocked with 200 μl of ELISA/ELISPOT diluent to minimize nonspecific binding and incubated for 1-3 hours at room temperature. During this incubation, the standards and samples were

prepared according to the manufacturer's protocol. The protein standard provided in the kit was reconstituted to make a standard curve ranging between 7.8-1000 ρg/mL through a series of two-fold dilutions. The supernatants were diluted at 1:5 and 1:10 for Nigericin and ATP, respectively, in 1X ELISA/ELISPOT diluent. At the end of the incubation, the plate was washed again four times with the wash buffer. The standards and samples were then added to the plate in duplicates (oriented horizontally) and incubated for 2 hours at room temperature. Following the incubation, the plate was washed five times and incubated with 100 μl of biotin-conjugated anti mouse IL-1β antibody (detection antibody; 1:250) for 1 hour at room temperature. The plate was then washed five times and incubated with 100 μl of streptavidin-horseradish peroxidase (HRP; 1:100) for 30 minutes at room temperature. The plate was then washed seven times followed by the addition of 100 μl of tetramethylbenzidine (TMB substrate solution), the substrate for HRP, followed by a 13-minute incubation. Once the colour change was observed in the lowest standard well, 100 μl of 1 M phosphoric acid was added to each well to stop the reaction and absorbance was measured at 450 nm and 570 nm. The 570 nm values were subtracted from the 450 nm values prior to analyzing the data. To analyze the data, the subtracted absorbance values for each sample was averaged between the two duplicate wells. Next, these values were subtracted by the absorbance value of the blank sample. The plate reader and Excel template generated a standard curve based on the results of the two-fold dilutions of the standard. The standard curve was then used to determine the IL-1β concentrations of all of the samples. These concentrations were also multiplied by their respective dilution factors to calculate the undiluted IL-1β concentrations.

3.6 – T Cell Isolation and Stimulation Assays

3.6.1 – Collection of Splenocytes from the Spleen

The mice used in this study were euthanized with 5% isoflurane followed by removal of the heart. The mice were then clipped facing upward on a Styrofoam board using needles and 70% ethanol was sprayed to sterilize the abdominal skin. The first incision was made on the left side of the mouse and the spleen was removed. In a 60 mm dish, the spleen was rinsed with PBS and removed of any excess tissue before being transferred to a 15 mL falcon tube with S+ media on ice. The spleen was then brought to the biosafety cabinet for the rest of the protocol. To create a splenic suspension, the spleen was crushed between two frosted microscope slides. Before starting, the premium frosted microscope slides (Fisherbrand) were sterilized with ethanol and washed in sterile PBS under the biosafety cabinet. Next, the splenic suspension was then filtered through a 70 μM cell strainer placed on top of a 50 mL falcon tube. The cell strainer was also washed with extra S+ media to improve the collection efficiency. The sample was then centrifuged at 500 g for 5 minutes followed by decanting of the supernatant. 5 mL of 1x RBC lysis buffer was then added to the sample followed by a 5-minute incubation at room temperature (ThermoFisher Scientific). To stop the lysis reaction, 20 mL of sterile PBS without calcium and magnesium was added to the sample before being centrifuged at 500 g for 5 minutes. The supernatant was decanted, the cell pellet was resuspended in 25 mL of FACS buffer, and a cell count was performed using a hemocytometer (generally around $1.0x10^8$ cells). Using the total cell count, the cell suspension was adjusted to a final concentration of $1.0x10^8$ cells/mL (i.e., 80 million cells were resuspended in 800 μL of S+ media). This concentration was recommended in the manufacturer's protocol for negatively selecting T cells.

3.6.2 – Negative Selection of T Cells from Splenic Suspension

T lymphocytes were negatively selected from the splenic suspension using the EasySep™ Mouse T Cell Isolation Kit (STEMCELL Technologies). The first step was to bring the samples to a concentration of $1.0x10^8$ cells/mL in FACS buffer, as previously mentioned. Depending on the experiment, the number of purified cells required varied, and therefore the volumes used during each step were adjusted accordingly. In order to isolate T cells from a suspension of 50,000 cells, 500 μL of sample was added to a sterile polystyrene round-bottom tube (can also be Röhren tubes). The first component added to the sample was either 25 μL of rat serum (50 μL/mL of sample) or in the newer model of the kit, 10 μL of FcR blocker (20 μL/mL of sample). Then 25 μL of isolation cocktail (50 μL/mL of sample) was mixed with the sample followed by a 10-minute incubation at room temperature. Next, RapidSpheres™ were vortexed for 30 seconds followed by the addition of 37.5 μL of this component to each sample (75 μL/mL of sample). This mixture was left to incubate for 2.5 minutes at room temperature followed by a top up of media to 2.5 mL. The tube was then placed into the magnet and incubated for 2.5 minutes at room temperature. Lastly, the enriched cell suspension was carefully pipetted into a sterile 15 mL falcon tube and another cell count was performed. Based on a few optimization experiments, the purity of the sample is between 80-90%, based on the percentage of cells that are CD3 positive.

3.6.3 – Carboxyfluorescein Succinimidyl Ester (CFSE) Staining

Cells were stained with carboxyfluorescein succinimidyl ester (CFSE) to monitor cell proliferation; essentially, as the cells divide, the stain becomes diluted and can be measured by a flow cytometer. Enriched T cells described in section 3.6.2 were washed with PBS twice to remove serum (centrifuged at 1300 rpm for 5 minutes between washes) and resuspended in prewarmed

PBS without magnesium and calcium at a concentration of $5x10^6$ cells/mL. The cell suspension was split into two tubes, one labelled unstained and the other labelled stained. In the stained tube, cells were stained with 0.1 μM CFSE and placed in the incubator at 37°C, protected from light, for 15 minutes. The CFSE working concentration was optimized through a series of experiments to ensure that the intensity was within the detection range of the flow cytometer. Following the incubation, the labelling was stopped by adding 4-5 volumes of cold S+ media and incubated on ice for 5 minutes to bind excess CFSE. The cells were then washed in S+ media once before being resuspended at a concentration of $1x10^6$ cells/mL (1:5 dilution of the concentration during the staining step). For this step, the total number of cells were calculated by multiplying the volume used during the staining step with the concentration of $5x10^6$ cells/mL. The resuspension volume was then calculated by dividing the total number of cells by the desired seeding density of $1x10^6$ cells/mL.

3.6.4 – Co-stimulation with CD3 and 3H3

A sterile 96-well flat-bottom plate was pre-coated with anti-CD3 and 3H3 (4-1BB agonist) antibodies a day before the T cells were enriched to allow sufficient time for the immobilization to take place. The plate was labelled according to three conditions consisting of no CD3 nor 3H3, CD3 only, and CD3 plus 3H3. Anti-CD3 (1.35 mg/mL) and 3H3 (1.38 mg/mL) antibodies were diluted in PBS (without magnesium and calcium) at a final concentration of 1 μg/mL and 10 μg/mL. 200 μL of this solution was added to the corresponding wells. The wells corresponding to the no CD3 nor 3H3 condition were left empty or loaded with 200 μL of PBS alone. Prior to seeding the cells the next day, the plate is washed 3 times with 200 μL of sterile PBS (aspirate

with a multi-channel between washes). 200 μL from the $1x10^6$ cells/mL cell suspension was added to each pre-coated well and placed in the incubator at 37°C for 48-60 hours.

3.6.5 – CD3 and TNFα Stimulations

A sterile 96-well flat-bottom plate was pre-coated with the anti-CD3 antibody a day before the T cells were enriched to allow sufficient time for the immobilization to take place. The plate was labelled according to two conditions consisting of no CD3 and CD3. Anti-CD3 (1.35 mg/mL) antibody was diluted in PBS (without magnesium and calcium) at a concentration of 0.5 μg/mL and 1 μg/mL. 200 μL of this solution was added to the corresponding wells in triplicates. The wells corresponding to the no CD3 condition were left empty or loaded with 200 μL of PBS alone. Prior to seeding the cells the next day, the plate is washed 3 times with 200 μL of sterile PBS (aspirate with a multi-channel between washes). 200 μL from the $1x10^6$ cells/mL cell suspension was added to each pre-coated well and placed in the incubator at 37°C for 72 hours. On the third day, the cells were transferred to a sterile 96-well U-bottom plate, centrifuged at 1300 rpm for 5 minutes and resuspended with 80 μL of S+ media. The triplicate wells were then pooled together, and a cell count was performed. A new sterile 96-well flat-bottom plate was labelled according to five conditions consisting of unstimulated cells, stimulated cells, and stimulated cells treated with 10-, 25-, 100 ng/mL TNFα. The number of unstimulated cells added to each well depended on which genotype had the fewest cells; usually $4\text{-}6x10^4$ cells were added to ensure some cells survived until the end of the experiment (these cells will continue to do because they were not activated). Meanwhile, $2x10^4$ stimulated cells were seeded in a final volume of 100 μL. Next, 100 μL of S+ media mixed with the three different concentrations of TNFα was added on top (to ensure

consistency between wells) and placed in the incubator at 37°C for an additional 72 hours. An overview of this process is depicted in Figure 3.6.

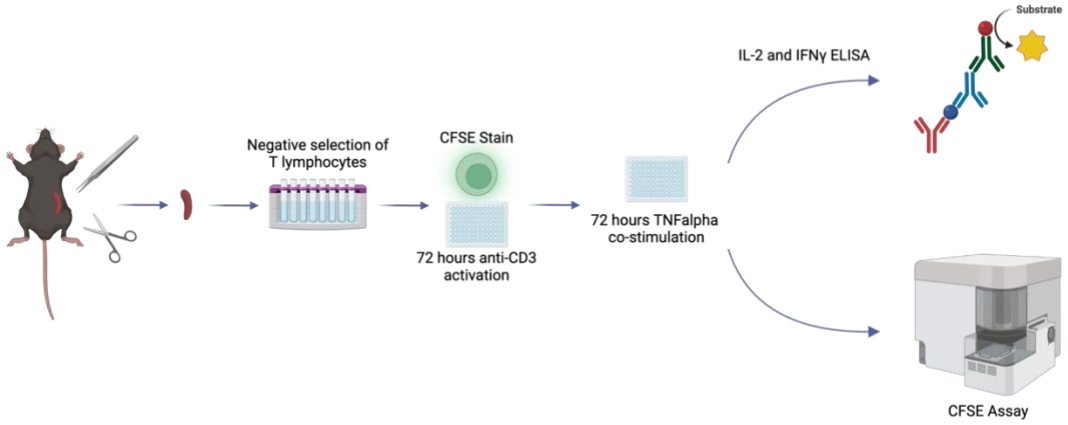

Figure 3.6: Schematic representation of performing CFSE proliferation assay and ELISA of key activation cytokines following co-stimulation of T lymphocytes.
T lymphocytes are isolated from the spleen through negative selection, stained with CFSE and activated with 1 μg/mL CD3 for 72 hours followed by 100 ng/mL TNFα co-stimulation for an additional 72 hours. Cells were cultured for 6 days in S+ media, with a media change on day 3, before CFSE and IL-2 ELISA protocols were employed. Created with BioRender.com.

3.6.6 – Proliferation Assay – Flow Cytometry

Once the endpoint was reached for the two different CFSE experiments described in sections 3.6.4 and 3.6.5, the cells were transferred to a new 96-well U-bottom plate and centrifuged at 1300 rpm for 5 minutes. The supernatant was then collected, transferred to a new 96-well flat-bottom plate, and stored in the -80°C freezer for ELISA. The cells were then washed with FACS buffer 3 times, with 1300 rpm centrifugations for 3 minutes between washes followed by decanting of the FACS buffer. Cells were then resuspended in 150-200 μL of FACS buffer prior to

performing flow cytometry. Figure 3.7 is a representative example of the gating strategy used to measure proliferation through the dilution levels of CFSE.

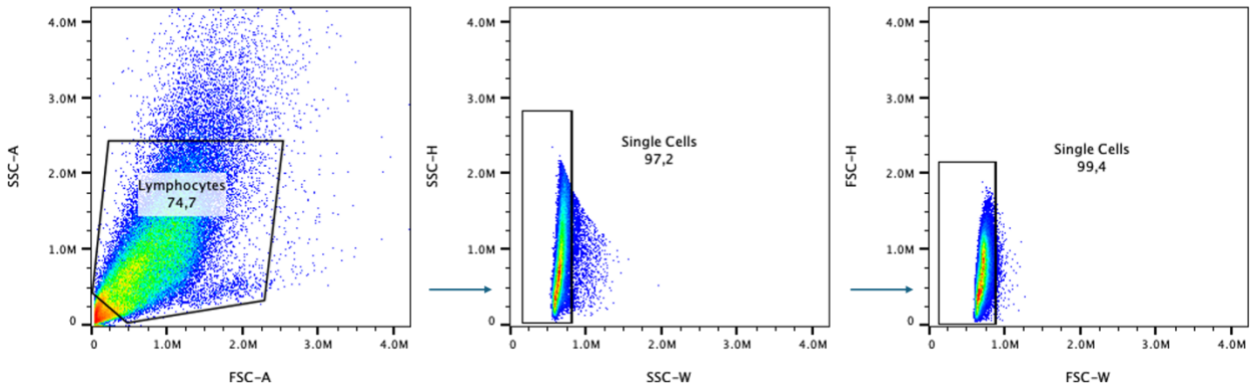

Figure 3.7: Gating strategy for measuring CFSE dilution.

The gating strategy was created on FlowJo (Version 10.8.2). A representative gating strategy is shown. Cells were single-stained, washed and then resuspended in FACS buffer before being loaded into the flow cytometer. The gating strategy shown above was optimized to exclude debris and doublets from the analysis. The second single stain gate was then used to determine the MFI value of CFSE for each sample.

3.6.7 – Proliferation Assay – Trypan Blue

Once the endpoint was reached for the two different CFSE experiments described in sections 3.6.4 and 3.6.5, 10 μL of sample from each condition was used to perform a cell count as described in section 3.3.5. The number of viable cells coincided with how much the population had expanded and thus provided additional insight into the proliferative capacity between the genotypes across different conditions.

3.7 – Site-Directed Mutagenesis (SDM) for TRAF1 T268A and W271A Variants

3.7.1 – Plasmid Design

The TRAF1 T268A and W271A variants were designed using NEB Base Changer, ordered through Integrated DNA Technologies (IDT) and validated through Benchling (Table 3.9). The

human TRAF1 full length (hTRAF1 FL) sequence was previously cloned into c-Flag pcDNA3 and was used as the template for the substitution reaction. The manufacturer's protocol included in the Q5 Site-directed Mutagenesis (SDM) Kit (NEB) was used to create the T268A and W271A substitutions in human TRAF1. In our study, we focused on TRAF1 T268A because we were unable to grow bacteria that were transformed with the hTRAF1 W271A plasmid.

Table 3.9: Primer designs for hTRAF1 268A and W271A.

Primer	**Sequence**
T268A F	CTTCGATGGCGCTTTCCTGTGGA
T268A R	GAGGCCTCCTCCATGAGG
W271A F	CACTTTCCTGGCGAAGATCACCAATGTCACC
W271A R	CCATCGAAGGAGGCCTCC

3.7.2 – PCR Amplification

To create the TRAF1 substitutions, the PCR product was amplified using the hTRAF1 FL as the template along with modified primers that were responsible for introducing the point-mutation. The components of the PCR reaction are outlined in Table 3.10 and the amplification protocol for the SDM amplicon is outlined in Table 3.11. The annealing temperatures used in the reaction for hTRAF1 T268A and W271A were 68°C and 65°C, respectively.

Table 3.10: Components of SDM PCR reaction.

Component	**25 µL Reaction**	**Final Concentration**
10 µM Forward primer	1.25 µL	0.5 µM
10 µM Reverse primer	1.25 µL	0.5 µM
Template DNA	1 µL	10 ng

Q5 Hot start high fidelity 2X Master mix	12.5 μL	1X
Nuclease-free water	9 μL	

Table 3.11: Thermocycler conditions for amplifying the SDM amplicon.

Step	**Temperature**	**Time**
Initial Denaturation	98°C	30 seconds
25 cycles	98°C	10 seconds
	Ta	30 seconds
	72°C	90 seconds
Final Extension	72°C	2 minutes
Hold	4°C	Infinite Hold

3.7.3 – Kinase, Ligase and Dpnl (KLD) Reaction, Ligation and Transformation

Upon successful amplification of the SDM amplicon, 1 μL of the PCR product was combined with 5 μL if the 2x KLD reaction buffer (NEB), 1 μL of the KLD enzyme mix, and 3 μL of molecular biology grade water for a total volume of 10 μL. This reaction was then incubated for 45 minutes at room temperature. Next, 5 μL of the reaction mixture was combined with 50 μL of the competent bacteria (provided in the SDM kit) and incubated on ice for 30 minutes. The mixture was heat shocked at 42°C for 30 seconds and then placed back on ice for another 5 minutes. Following this, 950 μL of SOC broth (provided in the SDM kit) was added to the bacteria and placed in an orbital shaker set to 37°C and 250 rpm for 1 hour. After this, 100 μL of the mixture was spread onto agar plates with the appropriate antibiotic (in this case, ampicillin) and placed in an incubator upside-down overnight (16-20 hours) at 37°C.

3.7.4 – Plasmid Isolation (Miniprep)

Following the overnight incubation of the agar plates after SDM transformation, 4-6 colonies per condition were picked and incubated individually in snap-capped tubes containing 3 mL of LB broth and the appropriate antibiotic, ampicillin. The culture was then incubated overnight at 37°C with the shaking set to 250 rpm. The next day, 850 μL of the overnight culture was mixed with 150 μL of glycerol and stored in -80°C as glycerol stocks. The remaining culture was used to extract the plasmid using the GeneJET Plasmid Miniprep Kit (ThermoFisher Scientific). The first step was to centrifuge the culture at 3000 g for 15 minutes at 4°C to pellet the bacteria cells. The pellet was then mixed with 250 μL of resuspension buffer and vortexed until complete resuspension occurred. 250 μL of lysis solution was then added, and the contents were mixed thoroughly by inverting the tube 4-6 times followed by a 3-5-minute incubation. Next, 350 μL of neutralization solution was added, mixed thoroughly by inverting the tube, and then centrifuged at 15000 g for 5 minutes. The supernatant was transferred to a GeneJET spin column by decanting and connected to the vacuum manifold system. The column was washed twice with 500 μL of wash solution, transferred to a collection tube and centrifuged at room temperature for 1 minute. Before eluting the plasmid DNA, the column was transferred to a fresh 1.5 mL eppendorf tube, 30-50 μL of elution buffer was added to the center of the column, incubated at room temperature for 2 minutes and centrifuged for another 2 minutes. The plasmid DNA concentration and absorbance values (A260/A280 and A260/230) was measured using a NanoDrop One spectrophotometer and then stored at -80°C.

3.7.5 – Plasmid Isolation (Midiprep)

Once the miniprep was validated to have the correct substitution, described in section 3.8, a midiprep was performed to create a more concentrated plasmid stock. Glycerol stocks, described in section 3.7.4, were used to create the starter culture in 3 mL of LB broth and 3 μL of ampicillin in snap-capped tubes. A sterile p20-p200 tip was used to scratch the glycerol stock and then placed in the snap-capped tube at 37°C for 6-8 hours with the shaking set to 250 rpm. Following the incubation, 120 μL of the day culture was added to 100 mL of LB broth and incubated overnight at 37°C with the shaking set to 250 rpm. The next day, the PureLink Fast Low-Endotoxin Midi Plasmid Purification Kit (ThermoFisher Scientific) was employed to purify the plasmids from the culture. The overnight culture was first collected in two 50 mL falcon tubes and centrifuged at 3000 g for 15 minutes at 4°C to pellet the bacteria cells. Following the removal of the supernatant, 8 mL of resuspension buffer was added to the cell pellet to allow for complete resuspension. Next, 8 mL of lysis solution was added, and the contents were mixed thoroughly by inverting the tube 4-6 times followed by a 3-5-minute incubation. Then, 8 mL of precipitation buffer was added followed by gently inverting the tube. The lysate was filtered using the syringe filter and 8 mL of binding buffer was then added to this filtered lysate. The lysate was then added to a column and filtered through the vacuum manifold system. After this, the plasmid DNA was washed first with 800 μL of wash buffer 1 and then 800 μL of wash buffer 2. Before eluting the plasmid DNA, the column was transferred to a fresh 1.5 mL eppendorf tube, 130-200 μL of elution buffer was added to the center of the column, incubated at room temperature for 2 minutes and then centrifuged at 10000 g for 1 minute at room temperature. The plasmid DNA concentration and absorbance values (A260/A280 and A260/230) was measured using a NanoDrop One spectrophotometer and then stored at -80°C.

3.8 – Validation of Successful TRAF1 T268A SDM

3.8.1 – Restriction Enzyme Digestion

In order to ensure that the TRAF1 T268A SDM was successful, the plasmid was digested with restriction enzymes Xbal1 (NEB) and BamH1 (NEB) for 1 hour at 37°C. The restriction enzyme (RE) digestion reaction consisted of 5 μL of the PCR product, 1 μL of each restriction enzyme (Xbal1 and BamH1), 5 μL of 10x Cutsmart Buffer (NEB) and 38 μL of molecular biology grade water. Following the RE digestion reaction, the samples were separated by DNA gel electrophoresis in a 1-2% gel.

3.8.2 – TRAF1 T268A SDM Sequencing

In order to ensure that the T268A substitution was in the correct region, the plasmid was prepared for sequencing according to the protocol provided by The Centre for Applied Genomics (TCAG) operated by SickKids. The facility performed two sequencing reactions; the first sequencing reaction used the CMV forward primer, and the second sequencing reaction used the BGH reverse primer.

3.9 – Plasmid Transformation of DH5α *E. coli* Cells

DH5α bacteria cells were used to replenish and create a more concentrated plasmid stock for a wide variety of plasmids such as c-Flag, HOIL-1, cIAP2, TRAF1 FL and TRAF1 T268A. These cells were thawed from the -80°C freezer to thaw and then 100 μL of bacteria was combined with 100 ng of plasmid DNA. This mixture was incubated for 30 minutes, followed by heat shock of bacteria at 42°C for 45 seconds and the samples were then placed back on ice for 3 minutes. Following this incubation, 1 mL of LB broth was added to the tubes under a flame and incubated

at 37°C for 1 hour with the shaking set to 250 rpm. Agar plates stored at 4°C were also brought to room temperature during this time. After the incubation, the eppendorf tube was centrifuged for 5 minutes at 10000 rpm with the temperature set to 4°C. Following the removal of 600 μL from the supernatant, the bacteria pellet was resuspended in the remaining volume. From this mixture, 120 μL of the bacterial culture was spread onto agar plates and placed in an incubator upside-down overnight (16-20 hours) at 37°C. The next day, a few colonies per condition were picked and streaked onto agar plates and placed in an incubator upside-down overnight (16-20 hours) at 37°C. The following day, glycerol stocks were made and either a miniprep or midiprep were performed, as described in section 3.7.4 and 3.7.5.

3.10 – DNA Plasmid Transfections and Lysate Preparation

3.10.1 – Transfections

A day before the transfection, HEK293T/17 cells were plated in 60 mm dishes at a seeding density of $1.35x10^6$ cells/mL which ensured that there was an optimal cell confluency between 80-90% which would consequently increase the transfection efficiency. First, the media was removed from the cells and replaced with 5 mL of pre-warmed Opti-MEM (Gibco), and placed in the 37°C incubator. The plasmids of interest were transfected into the cells following the manufacturer's protocol for the Lipofectamine 3000 (Invitrogen) reagent. Initial experiments used 3 μg of plasmid DNA but after a series of optimizations, we lowered the quantity to 2 μg instead. A master-mix was prepared where 600 μL of Opti-MEM per condition was added to a 15 mL falcon tube along with the appropriate amount of lipofectamine 3000 (the DNA to lipofectamine 3000 ratio is 1:2). A second master-mix comprised of 600 μL of Opti-MEM along with the appropriate amount of P3000 (the DNA to P3000 ratio is 1:2). For each condition, separate plasmid DNA mixes (4 μg

per mix) were prepared. The lipofectamine mix was combined with the DNA mix for a total of 1.2 mL and incubated for 15-20 minutes at room temperature. The mix was carefully added to the cells which were then incubated overnight in a humidified incubator at 37°C. The next day, cells were either harvested or cultured for an additional day after replacing Opti-MEM with normal DMEM media described in section 3.3.3; validated that there were no noticeable differences with the extra overnight and the decision was driven by feasibility.

3.10.2 – Lysate Preparation

Once the incubation for the transfection was complete, transfected HEK293T/17 cells in 60 mm plates were removed from the incubator and placed on ice. The media was aspirated, and the cells were washed with 3 mL of 1x PBS with magnesium and calcium. The lysis buffer was then subsequently replaced with 1 mL of freshly prepared Co-IP lysis buffer and incubated on ice for 10 minutes. The Co-IP lysis buffer consisted of 20 mM Tris-HCl pH 8, 137 mM NaCl, 10% glycerol, 1% NP40, 2 mM EDTA, complete protease inhibitor cocktail (Roche), PhosSTOP phosphatase inhibitor (Sigma), 1 mM DTT, and double-distilled water (ddH_2O). Following the incubation, the cells were scrapped and added to corresponding eppendorf tubes. The cells were incubated on ice for an additional 20 minutes while vortexing every 5 minutes. After 20 minutes, the cells were centrifuges at 13,300 rpm at 4°C for 15 minutes. The supernatant was then transferred to fresh eppendorf tubes and placed back on ice to prepare the lysate for the Co-IP.

3.11 – Co-Immunoprecipitation

3.11.1 Protein A/G Agarose Beads

After collecting the lysates as described in section 3.10.2, 15 μL was removed and added to separate eppendorf tubes to be used as the input. From the remaining volume, 250 μL of lysate

was used to perform the Co-IP using protein A/G agarose beads (ThermoFisher Scientific) and the remainder of the lysate was stored at -80°C. Since 20 μL of beads were required for each condition, the total volume required was added to a centrifuge tube. The protein beads slurry was then washed with 600 μL of 1x ice cold PBS 3 times and centrifuged between each wash at room temperature for 2 minutes at 1200 rpm. In some experiments, the beads were also blocked with 5% BSA at room temperature for 1 hour. Following the blocking, the protein beads slurry was washed again with 600 μL of 1x ice cold PBS 3 times and centrifuged between each wash at room temperature for 2 minutes at 1200 rpm. The beads were then washed with 1x Co-IP lysis buffer, centrifuged for 2 minutes at 1200 rpm, and resuspended in the final desired volume (account for bead volume as well and divide total volume by the number of conditions and extra samples). Once this was done, the beads were mixed with 0.8 μg/condition of the TRAF1 1F3 antibody and equal volume of beads were transferred into new centrifuge tubes corresponding to each condition. 250 μL of sample was added and mixed as well and incubated on the rotator at room temperature for 2 hours. Following the incubation, the beads were washed 3 times with 1x Co-IP wash buffer (1:1 ratio between 2x Co-IP lysis buffer and double-distilled water (ddH_2O)) while centrifuging between washes for 2 minutes at 1200 rpm. The beads were then washed 2-3 times with 1x ice cold PBS without magnesium and calcium and centrifuged between washes for 2 minutes. Lastly, the input was mixed with 15 μL of 2x Laemmeli and the beads were eluted using 20 μL of 2x Laemmeli, placed on a heat block set to 100°C for 5 minutes followed by a quick spin. At this point, the samples were either stored in the -20°C or a western blot was performed.

3.11.2 – Protein G Dynabeads

The magnetic beads approach was also employed for the Co-IP and resulted in similar results. After collecting the lysates as described in section 3.10.2, 15 μL was removed and added to separate eppendorf tubes to be used as the input. The Protein G Dynabeads (Invitrogen) were first resuspended in solution by vortexing for ~30 seconds. The desired volume of Dynabeads (25 μL per sample) was then transferred to a new tube and placed on the magnetic to separate the beads from the solution. The supernatant was removed, and the beads were washed with 600 uL of 0.02% Tween 20 PBS (w/o calcium and magnesium).

For the direct Co-IP approach, 0.8 μg of TRAF1 1F3 antibody was added to the prewashed Dynabeads and incubated on the rotator at room temperature for 15 minutes. The tube was then placed on the magnetic, washed and combined with 250 μL of lysate. The mixture was then incubated at room temperature for 15 minutes to allow for the antigen to bind to the magnetic bead-antibody complex. Following the incubation, the supernatant was removed, and the beads were washed 3 times using 600 μL of Co-IP wash buffer (1:1 ratio between 2x Co-IP lysis buffer and double-distilled water (ddH_2O)). The beads were then washed 2-3 times with 1x ice cold PBS without magnesium and calcium and eluted with 25 μL of 2x Laemmeli Buffer. Finally, the samples were placed on a heat block set to 100°C for 5 minutes followed by a quick spin. At this point, the samples were either stored in the -20°C or a western blot was performed.

For the indirect Co-IP approach, 0.8 μg of TRAF1 1F3 antibody was added to 250 μL of lysate and incubated on the rotator at room temperature for 15 minutes to allow for the antigen to bind to the antibody. Next, 25 μL of prewashed Dynabeads was added to each lysate and incubated on the rotator at room temperature for 15 minutes to allow for the antigen-antibody complex to bind to the magnetic beads. Following the incubation, the supernatant was removed, and the beads

were washed 3 times using 600 μL of Co-IP wash buffer (1:1 ratio between 2x Co-IP lysis buffer and double-distilled water (ddH_2O)). The beads were then washed 2-3 times with 1x ice cold PBS without magnesium and calcium and eluted with 25 μL of 2x Laemmeli Buffer. Finally, the samples were placed on a heat block set to 100°C for 5 minutes followed by a quick spin. At this point, the samples were either stored in the -20°C or a western blot was performed.

3.12 – Immunoblotting

Protein samples that were stored in the -20°C were placed on a heating block set to 100°C for 5 minutes followed by either a quick spin to separate and pellet the beads from the proteins of interest (Protein A/G Agarose Beads approach) or placed on a magnetic to separate the beads from the proteins of interest (Protein G Dynabeads approach). Equal volume of protein, usually 20 μL, was loaded in each well and separated by a 10% SDS-polyacrylamide gel electrophoresis at 65 V for 30 minutes followed by 120 V for 70 minutes. The protein samples were then transferred using the Trans-Blot Turbo Transfer System (Bio-Rad) for 10 minutes onto a polyvinylidene difluoride (PVDF) membrane (Bio-Rad). The PVDF membrane was activated in 100% methanol prior to forming the transfer sandwich. After the transfer, the membrane was rinsed with water three times and then 10 mL of Ponceau stain (Thermo Scientific) was added (helpful to determine equal loading and successful transfer). The membrane was then placed on the rocker and incubated for 10-15 minutes at room temperature. The membrane was then placed in water to remove excess Ponceau stain and then an image was captured using the ChemiDoc MP Imaging System (Bio-Rad). The membrane was washed three times with 1x TBS with 0.1% Tween-20 (TBST) washing buffer and then blocked with 5% skim milk in TBST for a minimum of 1 hour at room temperature. Next, the membranes were incubated with primary antibodies, diluted in 5% BSA containing

0.02% sodium azide, overnight at 4°C. The primary antibodies that were used to assess protein expression are outlined in Table 3.12. Following the incubation with the primary antibodies, the membranes were washed three times (15 minutes, 10 minutes, and 5 minutes) with TBST. The membranes were then incubated for 1 hour at room temperature with peroxidase-conjugated secondary antibodies (1:5000 for light-chain antibodies) diluted in 5% skim milk in TBST. Following the incubation with the secondary antibodies, the membranes were washed again three times (15 minutes, 10 minutes, and 5 minutes) with TBST. Proteins of interest and housekeeping protein were detected with the Clarity (ThermoFisher Scientific) western blotting ECL detection reagent. The image was captured using the chemiluminescence feature on the ChemiDoc MP Imaging System (Bio-Rad).

Table 3.12: List of primary antibodies used to assess protein interactions by immunoblotting.

Primary Antibody	**Dilution**	**Company**	**Catalog Number**
TRAF1 (45D3)	1:1000	Cell Signaling Technology	4715S
cIAP2 (58C7)	1:1000	Cell Signaling Technology	3130S
RBCK1 (HOIL-1) (H-1)	1:200	Santa Cruz	sc-393754
Beta (β)-Actin (BA3R)	1:5000	Thermo Scientific	MA5-15739

3.13 – Statistical Analysis

All of the results were expressed as mean $\pm$ SEM with the level of statistical significance established at $p<0.05$. A two way-ANOVA with the Tukey multiple comparisons test was used for data that conformed to a normal distribution, unless otherwise stated in the figure caption. For

survival curve analysis, a log-rank (Mantel-Cox) test was performed to determine statistical significance. For data that did not fit a normal distribution, a non-parametric Mann-Whitney unpaired t-test was performed. All statistical analyses were performed with GraphPad Prism Software (10.2.0.335).

Chapter 4: Results

4.1 – TRAF1 V196A/V196A can Protect Mice from LPS-Induced Sepsis

The Sater lab has previously shown that a mutation in TRAF1, V203A, that disrupts the interaction with cIAP2 in human monocyte cells can reduce their inflammatory responses when stimulated with LPS. It has also previously been reported by Sater et al. (2016) that TRAF1 deficient mice are more susceptible to LPS-induced sepsis than their wildtype littermates. Previously, students from our lab have established various sites in TRAF1 that selectively disrupt interactions with the two binding partners of interest, cIAP2 and LUBAC. One of these sites corresponded to the mice equivalent mutation of the human TRAF1 V203A. Based on this information, we created an in vivo mouse model that is genetically engineered to have the same mutation, referred to as TRAF1 V196A. As the first step of our scientific study to establish the proof of concept that the TRAF1 V196A mice are protected from a lethal endotoxic shock, we began by determining their survival response to a lethal LPS dose. To determine the survival response, male and female mice, 6-8 weeks of age, were challenged with a lethal LPS dose of 35 mg/kg. As shown in Figure 4.1A, TRAF1 V196A/V196A male mice were completely protected compared to TRAF1 wt/wt and TRAF1 V196A/wt. On the other hand, as shown in Figure 4.1B, this protection was less pronounced in female mice. Although more TRAF1 V196A/V196A female mice survived compared to TRAF1 wt/wt and TRAF1 V196A/wt, this result was not significant. Surprisingly, fewer TRAF1 V196A/wt male and female mice survived following the intraperitoneal injection of the lethal LPS dose.

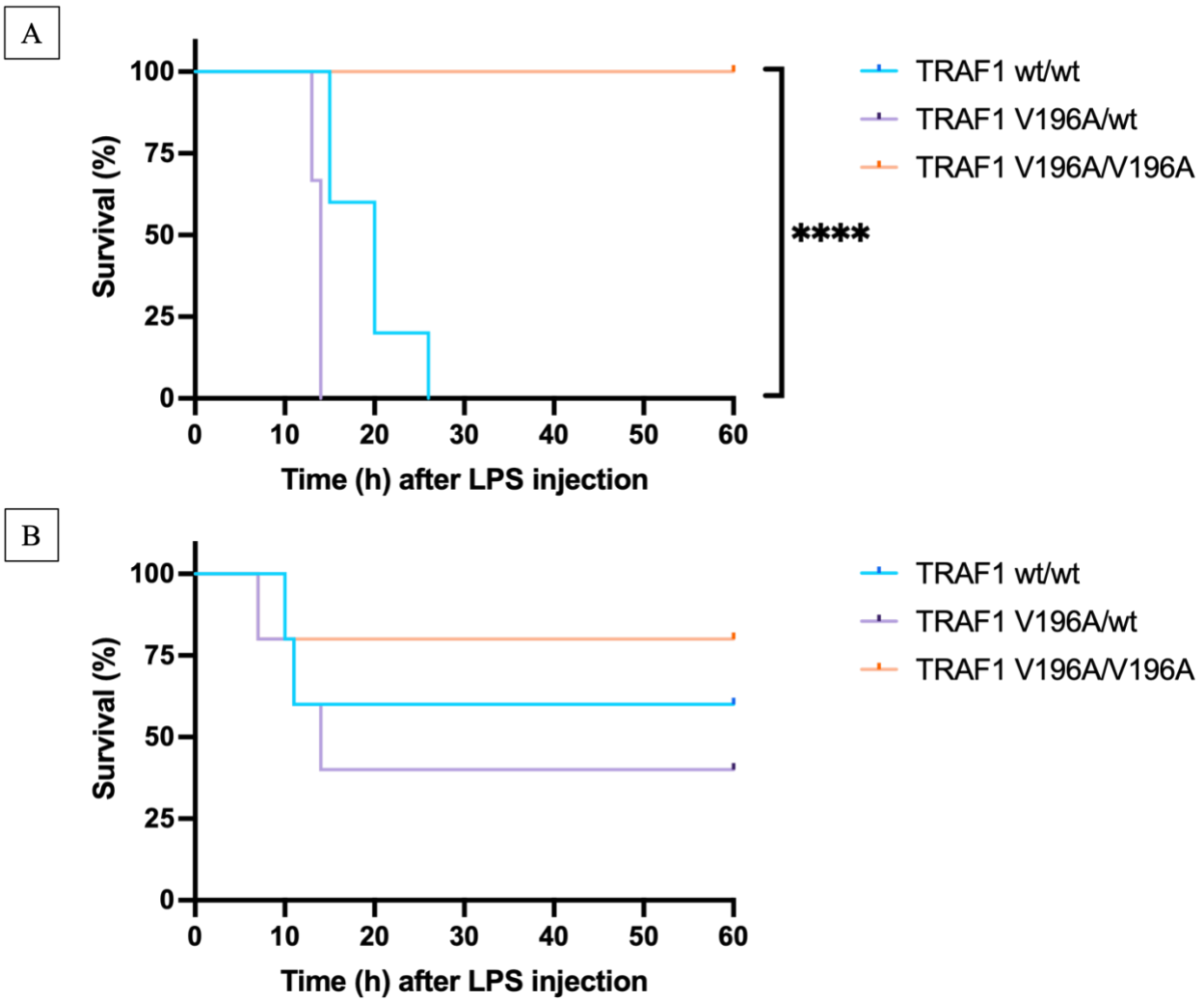

Figure 4.1: Assessing the survival of TRAF1 wt/wt, TRAF1 V196A/wt and TRAF1 V196A/V196A mice challenged with a lethal dose of lipopolysaccharide (LPS).

Mice were monitored for a total of 30-50 hours and assigned a murine sepsis score. Mice were euthanized when they met the criteria for moribund state or survived until the end of the experiment. **(A)** TRAF1 V196A/V196A male mice are protected from LPS-induced septic shock. Kaplan-Meier survival curve of TRAF1 wt/wt (n=5), TRAF1 V196A/wt (n=3) and TRAF1 V196A/V196A (n=5) male mice injected interperitoneally with 35 mg/kg LPS. **(B)** TRAF1 V196A/V196A female mice are partially protected from LPS-induced septic shock. Kaplan-Meier survival curve of TRAF1 wt/wt (n=5), TRAF1 V196A/wt (n=5) and TRAF1 V196A/V196A (n=5) female mice injected interperitoneally with 35 mg/kg LPS. Log-rank (Mantel-Cox) test was performed to determine statistical significance. *P<0.05, **P<0.01, ***P<0.001 and ****P<0.0001.

4.2 – TRAF1 V196A/V196A Delays the Progression of Symptoms during LPS-Induced Sepsis

Following the intraperitoneal lethal LPS injection, mice were monitored hourly for 30-50 hours and the murine sepsis score was recorded as a measure of sepsis severity. The murine sepsis scoring sheet consisted of parameters including activity, appearance, eyes, respiration, respiration rate, and response to stimulus. The cumulative score for the entire time course for male and female mice is shown in Figures 4.2 and 4.3, respectively. In order to evaluate the progression of symptoms and perform statistics, a shorter duration of the time course was plotted. The final timepoint plotted was set as the last timepoint with at least three mice in each genotype. As shown in Figure 4.2B and Figure 4.3B, both TRAF1 V196A/V196A male and female mice had a significantly dampened progression of sepsis severity, as indicated by the lower murine sepsis scores (MSSs) during the time course. Consistent with the survival curves, TRAF1 V196A/wt male and female mice had higher MSSs at most timepoints. The effects of TRAF1 V196A/V196A in reducing sepsis severity was more pronounced in male mice than female mice. However, we are not able to make a direct comparison between male and female mice because within each survival experiment, we only assessed the response of mice with the same sex. Interestingly, Figure 4.3B shows that at the 14-hour post-LPS timepoint, female TRAF1 V196A/V196A mice are potentially recovering at a faster rate than TRAF1 wt/wt and TRAF1 V196A/wt.

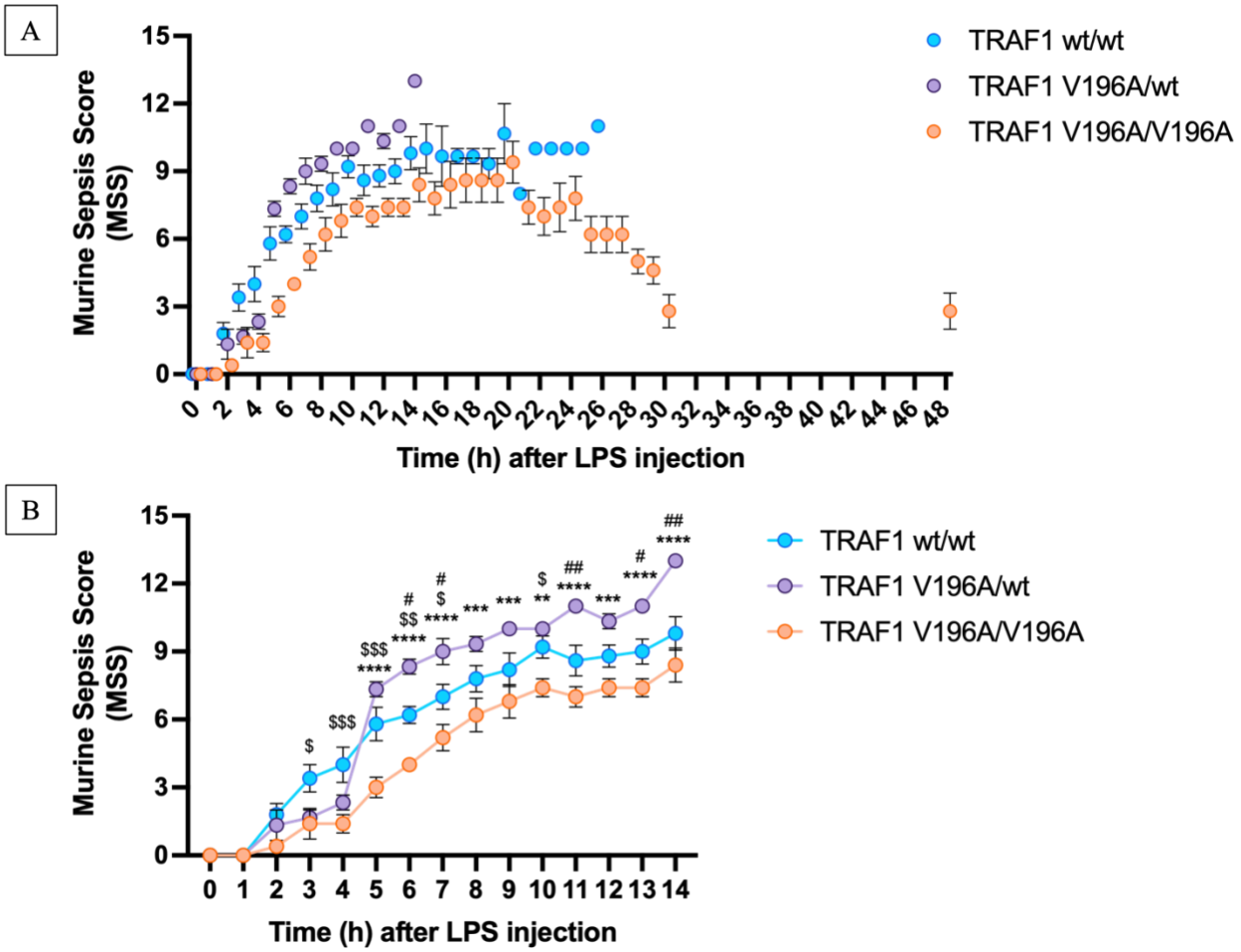

Figure 4.2: Assessing the progression of symptoms by measuring the murine sepsis score of TRAF1 wt/wt, TRAF1 V196A/wt and TRAF1 V196A/V196A male mice challenged with a lethal dose of lipopolysaccharide (LPS).

(A) TRAF1 V196A/V196A male mice exhibit reduced sepsis severity. Time course measuring sepsis severity for TRAF1 wt/wt (n=5), TRAF1 V196A/wt (n=3) and TRAF1 V196A/V196A (n=5) male mice injected interperitoneally with 35 mg/kg LPS. **(B)** Time course assessing the progression of sepsis severity until the last timepoint with at least three mice in each genotype, to perform statistical analysis. Ordinary two-way ANOVA was performed with Tukey's multiple comparisons test to determine statistical significance. The error bars represent standard error to the mean (mean ± SEM). # is used to indicate significance between TRAF1 wt/wt and TRAF1 V196A/wt, $ is used to indicate significance between TRAF1 wt/wt and TRAF1 V196A/V196A, and * is used to indicate significance between TRAF1 V196A/wt and TRAF1 V196A/V196A. #, $ or * indicate P<0.05, ##, $$ or ** indicate P<0.01 and ###, $$$ or *** indicate P<0.001.

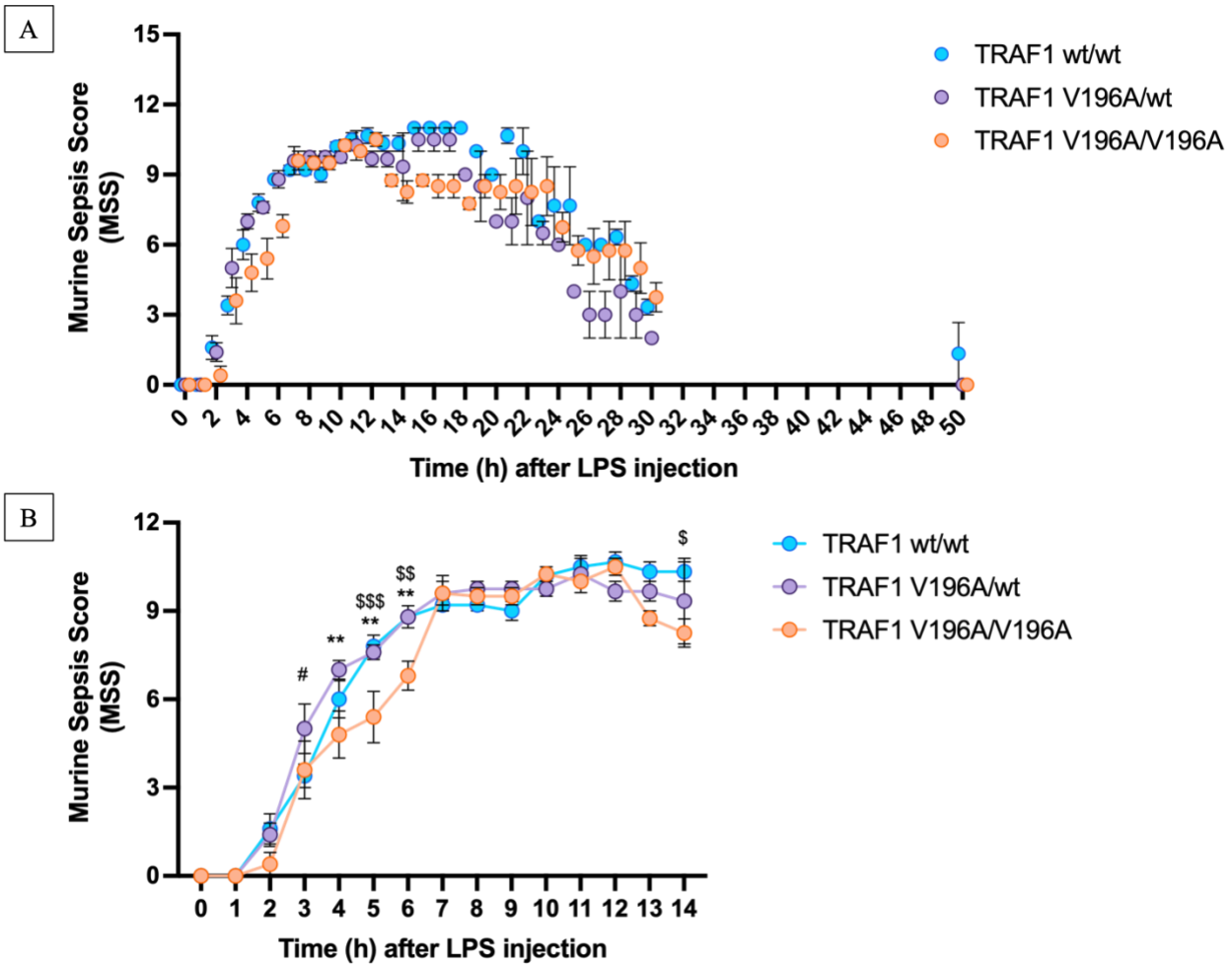

Figure 4.3: Assessing the progression of symptoms by measuring the murine sepsis score of TRAF1 wt/wt, TRAF1 V196A/wt and TRAF1 V196A/V196A female mice challenged with a lethal dose of lipopolysaccharide (LPS).

(A) TRAF1 V196A/V196A female mice exhibit reduced sepsis severity. Time course measuring sepsis severity for of TRAF1 wt/wt (n=5), TRAF1 V196A/wt (n=5) and TRAF1 V196A/V196A (n=5) female mice injected interperitoneally with 35 mg/kg LPS. **(B)** Time course assessing the progression of sepsis severity until the last timepoint with at least three mice in each genotype, to perform statistical analysis. Ordinary two-way ANOVA was performed with Tukey's multiple comparisons test to determine statistical significance. The error bars represent standard error to the mean (mean ± SEM). # is used to indicate significance between TRAF1 wt/wt and TRAF1 V196A/wt, $ is used to indicate significance between TRAF1 wt/wt and TRAF1 V196A/V196A, and * is used to indicate significance between TRAF1 V196A/wt and TRAF1 V196A/V196A. #, $ or * indicate P<0.05, ##, $$ or ** indicate P<0.01 and ###, $$$ or *** indicate P<0.001.

4.3 – Effects of TRAF1 V196A/V196A on Cytokine Production in the Sublethal LPS Model

Next, we investigated the inflammatory cytokine production following an intraperitoneal injection of a sublethal dose of LPS. TRAF1 wt/wt and TRAF1 V196A/V196A female mice were challenged with a 10 mg/kg sublethal dose of LPS. Blood was collected at the 1- and 6-hour timepoint by saphenous vein and at the 24-hour timepoint by cardiac puncture. The blood was then processed to separate the serum which was then used to perform the LEGENDplex cytokine immunoassay. As shown in Figure 4.4, the levels of IFN-β, IFN-γ, IL-1β, IL-6, IL-12 (p70), MCP-1 and TNFα were not statistically significant. This data shows that both TRAF1 wt/wt and TRAF1 V196A/V196A female mice produce relatively similar levels of cytokines. This is relatively consistent with the survival response to the lethal LPS dose where TRAF1 wt/wt and TRAF1 V196A/V196A generally had similar sepsis severity, with statically significant differences occurring between the 5- and 6-hour post-LPS injection. It is important to note that although the data demonstrates an induction across all targets, more notable differences could be observed by using a higher sublethal dose.

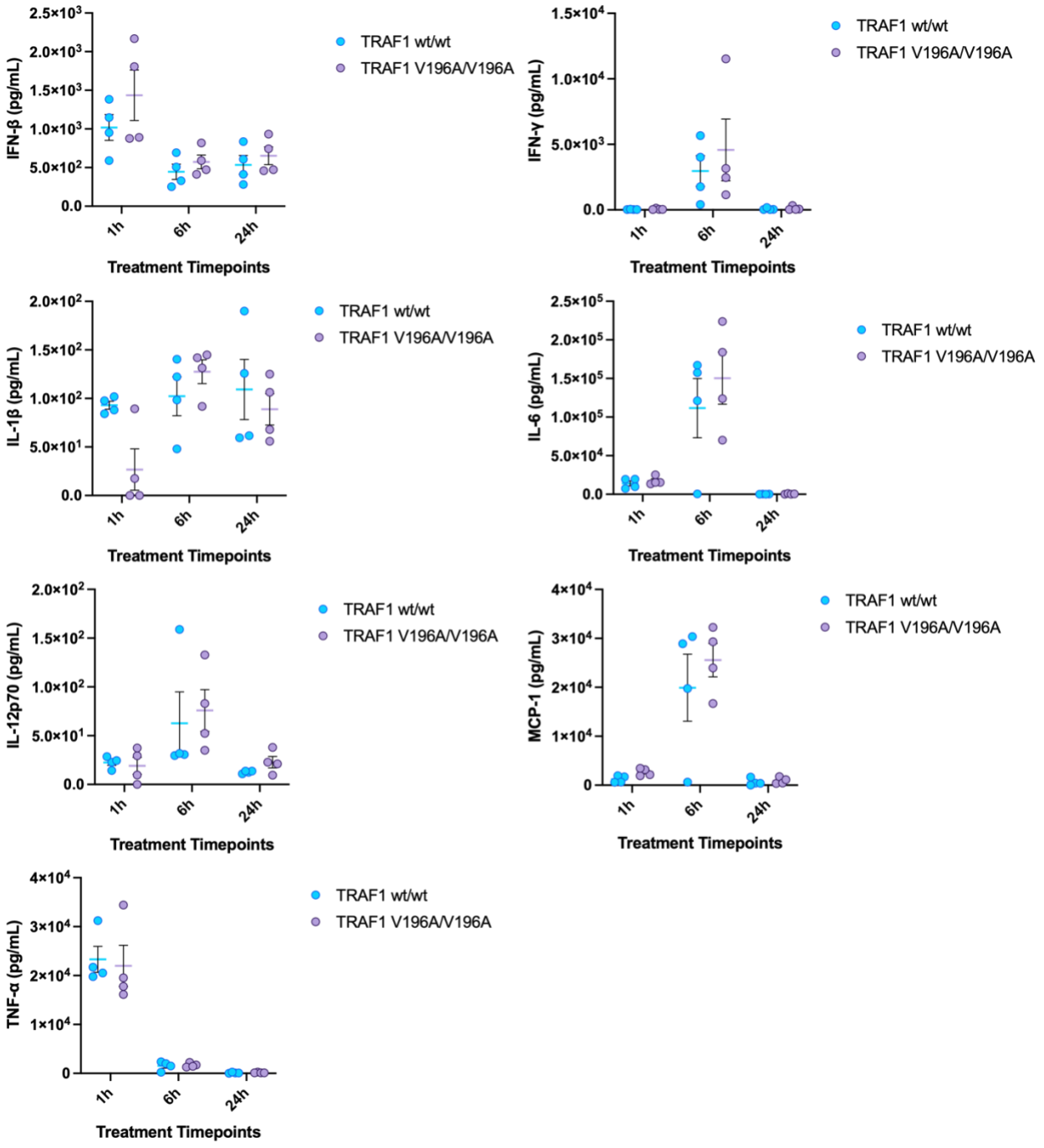

Figure 4.4: Assessing the cytokine production in TRAF1 wt/wt and V196A/V196A female mice challenged with a sublethal dose of lipopolysaccharide (LPS).

Female TRAF1 wt/wt (n=4) and TRAF1 V196A/V196A (n=4) mice were injected with a sublethal LPS dose of 10 mg/kg. Blood was collected at the 1- and 6-hour timepoint by saphenous vein and at the 24-hour timepoint by cardiac puncture. The serum was then collected and used to perform

the LEGENDplex cytokine assay by flow cytometry. Each symbol represents one mouse. A non-parametric (Mann-Whitney) unpaired t-test was performed to determine statistical significance.

4.4 – Effects of TRAF1 V196A on Gene Expression of Inflammatory Markers

In order to assess differences in the levels of inflammation, primary and immortalized bone marrow-derived macrophages (BMDMs) from TRAF1 wt/wt, TRAF1 V196A/wt, TRAF1 V196A/V196A mice were treated in vitro with 100 ng/mL LPS. The negative control was treated with equal volume of DPBS as the LPS in the treatment group. Cells were treated in reverse order beginning with the longest timepoint and harvested together once the respective timepoints were completed. To assess gene expression, cells were stimulated for 1-, 3- and 6- hour(s) and then RNA was extracted using the TRIzol method. cDNA was then synthesized from the RNA through a reverse transcription reaction. Next, RT-qPCR was performed to measure the gene expression levels of pro- and anti-inflammatory markers including IFN-β, IL-1β, IL-6, IL-10, IL-12, TGFβ and TNFα. Once the reaction was complete, the CT (cycle threshold) values were normalized to the expression of RPLP0, the housekeeping gene used in our study.

We first assessed the -ΔCT values to determine which method to analyze the data, as described in section 3.5.6. As shown in Figure 4.5A, TRAF1 V196A/wt and TRAF1 V196A/V196A have lower transcript levels, for most targets, pre-stimulation and upon LPS stimulation, exhibit a relatively dampened induction at some timepoints. Notably, for all of the targets measured, except IL-12 and TGFβ, there was a significant difference in expression levels between genotypes, indicated by a P-value that is less than 0.0001. Since there is a difference in the unstimulated expression levels for most targets between genotypes, we assessed the relative fold difference of TRAF1 V196A/wt and TRAF1 V196A/V196A with respect to TRAF1 wt/wt.

These results were reported in Figure 4.5B and the statistical analysis was performed on the fold change ($2^{-\Delta\Delta CT}$) values. The data can be interpreted as a relative comparison of the transcript for the variant genotypes compared to the wildtype at any given time. A fold difference less than 1.0 indicates that the variant genotypes have fewer transcripts than the wildtype whereas a fold difference more than 1.0 indicates that the variant genotypes have more transcripts than the wildtype. Ultimately, the amount of transcript present for a particular gene at any given timepoint is more reflective of the severity and progression of disease. As shown in Figure 4.5B, the mRNA levels for all of the target genes at most timepoints were remarkably and significantly reduced for TRAF1 V196A/V196A. Interestingly, the results also indicate that one copy of TRAF1 V196A may be sufficient at most timepoints to reduce the pro-inflammatory gene expression of IFN-β, IL-1β, and TNFα as well as the anti-inflammatory gene expression of IL-6 and IL-10. The robust increase in the expression of IL-1β at the 1-hour timepoint for TRAF1 V196A/wt is unexpected and requires further exploration to understand the underlying mechanism. Collectively, the data presented here demonstrates a remarkable reduction of key markers during an inflammatory response, indicating a significant reduction of NF-κB activation.

A

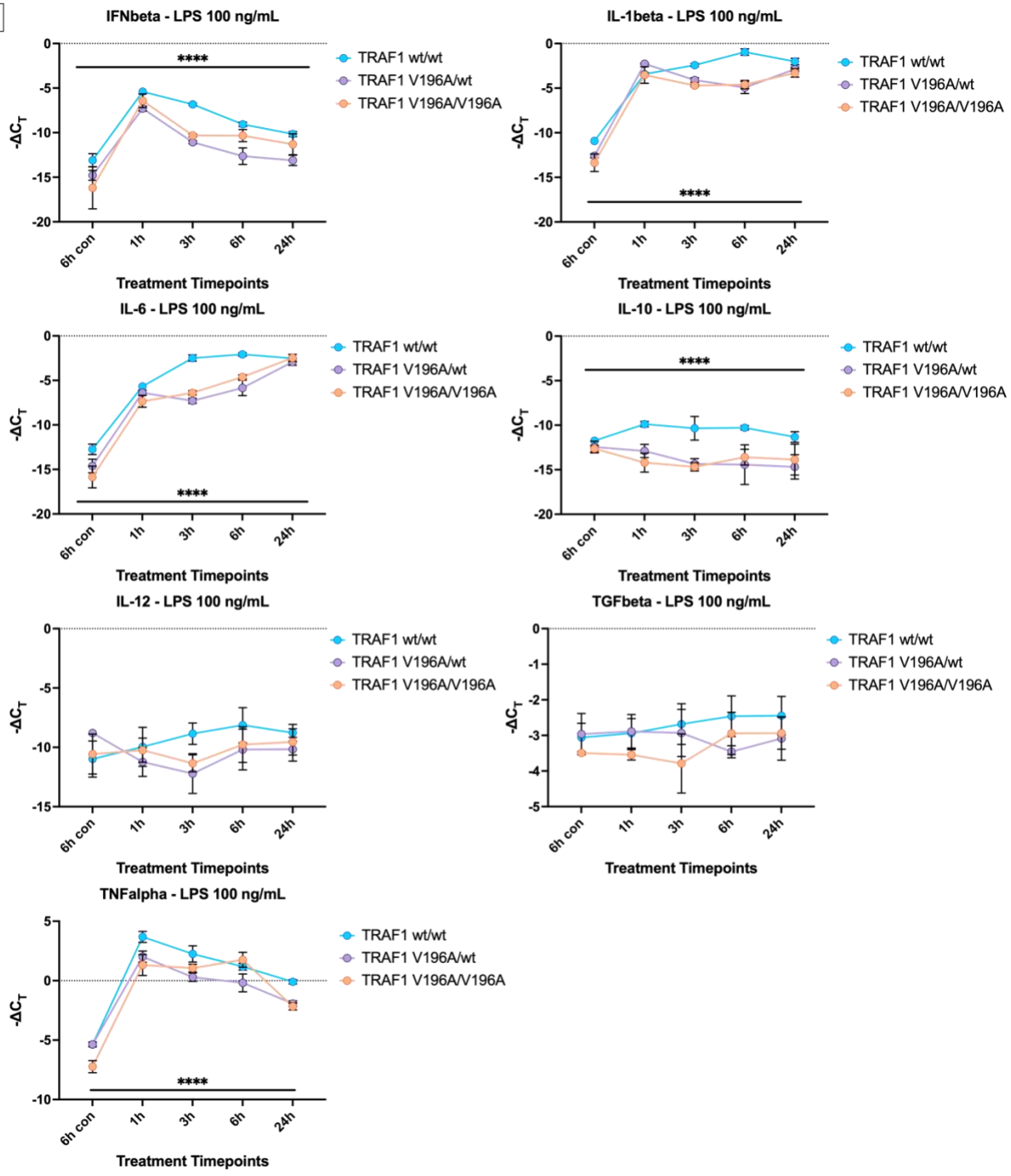
IFNbeta - LPS 100 ng/mL
IL-1beta - LPS 100 ng/mL
IL-6 - LPS 100 ng/mL
IL-10 - LPS 100 ng/mL
IL-12 - LPS 100 ng/mL
TGFbeta - LPS 100 ng/mL
TNFalpha - LPS 100 ng/mL
TRAF1 wt/wt
TRAF1 V196A/wt
TRAF1 V196A/V196A
-ΔC_T
Treatment Timepoints
6h con
1h
3h
6h
24h
****

B

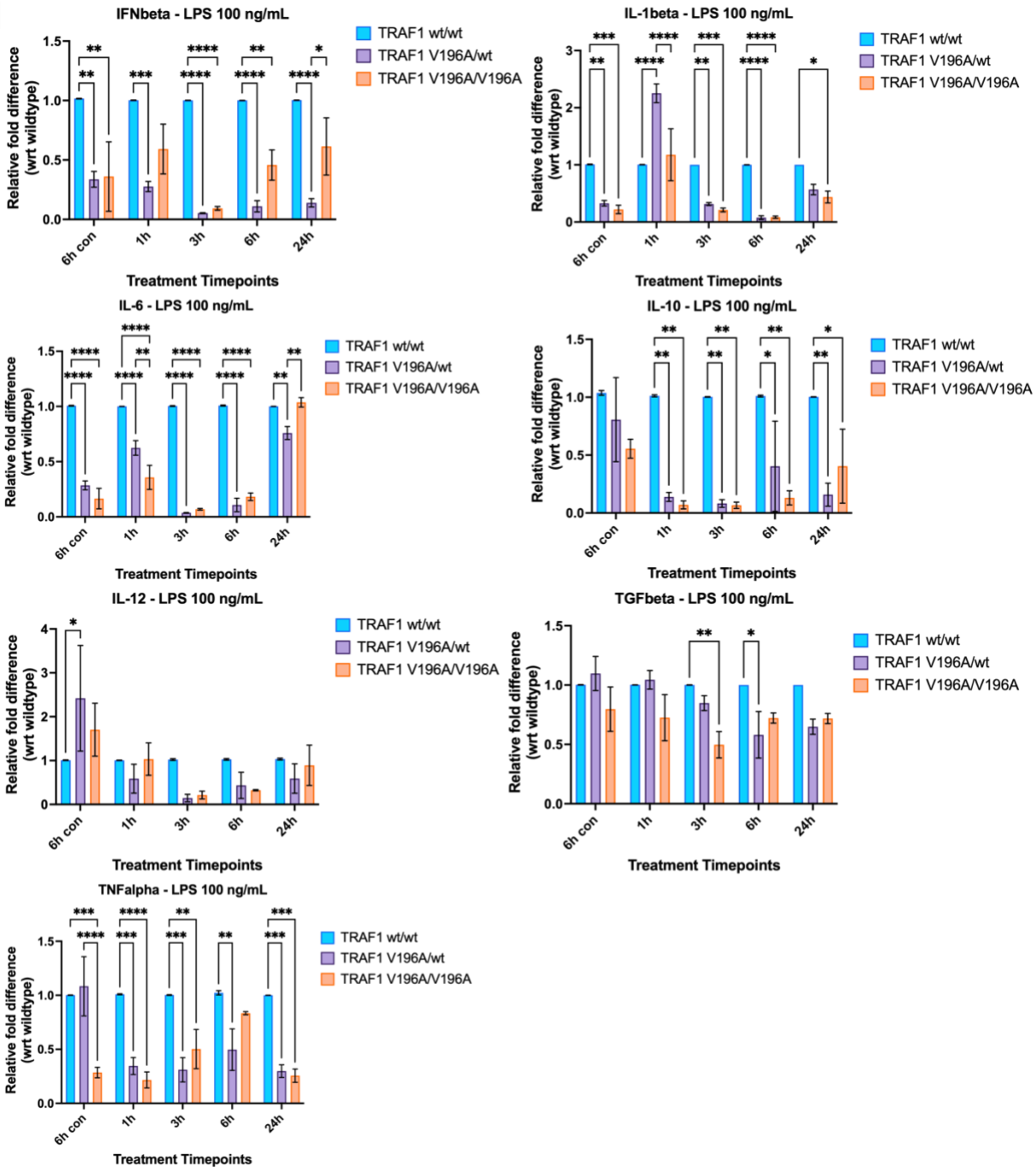
IFNbeta - LPS 100 ng/mL
IL-1beta - LPS 100 ng/mL
IL-6 - LPS 100 ng/mL
IL-10 - LPS 100 ng/mL
IL-12 - LPS 100 ng/mL
TGFbeta - LPS 100 ng/mL
TNFalpha - LPS 100 ng/mL
TRAF1 wt/wt
TRAF1 V196A/wt
TRAF1 V196A/V196A
Relative fold difference (wrt wildtype)
Treatment Timepoints
6h con
1h
3h
6h
24h

Figure 4.5: Assessing the gene expression of IFN-β, IL-1β, IL-6, IL-10, IL-12, TGFβ and TNFα by RT-qPCR following LPS stimulation of immortalized bone marrow-derived macrophages (iBMDMs).

iBMDMs from TRAF1 wt/wt, TRAF1 V196A/wt and TRAF1 V196A/V196A mice were seeded in 6-well plates and treated with or without 100 ng/mL LPS for 1-, 3- and 6-hour(s). The negative control was treated with equal volume of DPBS as the LPS in the treatment group. **(A)** TRAF1 V196A/wt and TRAF1 V196A/V196A have lower levels of transcripts for most targets pre-stimulation and exhibits a dampened response to LPS stimulation. The results are reported as -ΔCT which represent the transcript levels normalized to RPLP0. Ordinary two-way ANOVA was performed to determine statistical significance between genotypes. **(B)** TRAF1 V196A/wt and TRAF1 V196A/V196A have lower levels of gene expression of most targets compared to TRAF1 wt/wt following LPS stimulation. Analysis of the gene expression data measured by RT-qPCR was performed using the $2^{-\Delta\Delta CT}$ method. The results were normalized to RPLP0 and reported as relative fold difference with respect to the TRAF1 wt/wt genotype. A total of three independent experiments were completed. Ordinary two-way ANOVA was performed with Tukey's multiple comparisons test to determine statistical significance. The error bars represent standard error to the mean (mean $\pm$ SEM). *P<0.05, **P<0.01, ***P<0.001 and ****P<0.0001.

4.5 – Effects of TRAF1 V196A on Protein Expression of Inflammatory Markers

In order to confirm and support the RT-qPCR results indicating a reduction of NF-κB activation, we measured the protein expression of inflammatory markers. It is important to note that it is not necessary for the transcript levels to reflect similarly into changes at the protein level due to regulatory mechanisms that occur during translation. pBMDMs and iBMDMs from TRAF1 wt/wt, TRAF1 V196A/wt, TRAF1 V196A/V196A were seeded in 6-well plates and treated with or without 100 ng/mL LPS. The negative control was treated with equal volume of DPBS as the LPS in the treatment group. Cells were treated in reverse order beginning with the longest timepoint and harvested together once the respective timepoints of 15-, 30- and 60-minutes were completed. As shown in Figure 4.6A, there was a slight decrease in the expression of p-p65 in both TRAF1 V196A/wt and TRAF1 V196A/V196A pBMDMs. However, in Figure 4.6B, there was robust expression of p-p65 in TRAF1 V196A/V196A iBMDMs. This contradictory result could be due to differences in cell survival and further investigation is required to determine whether the immortalization process influences this result. As shown in Figure 4.6, both TRAF1 V196A/wt and TRAF1 V196A/V196A pBMDMs and iBMDMs, exhibited a decrease in the expression of p-SAPK/JNK. This is more notable for pBMDMs (Figure 4.6A) as the unstimulated lanes here have relatively similar levels of expression. For iBMDMs (Figure 4.6B), it is important to factor in that there is a band in the unstimulated lane for TRAF1 V196A/wt and TRAF1 V196A/V196A suggesting higher basal expression. Interestingly, both TRAF1 V196A/wt and TRAF1 V196A/V196A pBMDMs and iBMDMs expressed more IκBα than TRAF1 wt/wt. This indicates that in response to LPS, less IκBα was phosphorylated, leading to less degradation, and consequently a reduction of NF-κB activation. Cumulatively, these results indicate a reduction in LPS-induced NF-κB activation in TRAF1 V196A/wt and TRAF1 V196A/V196A.

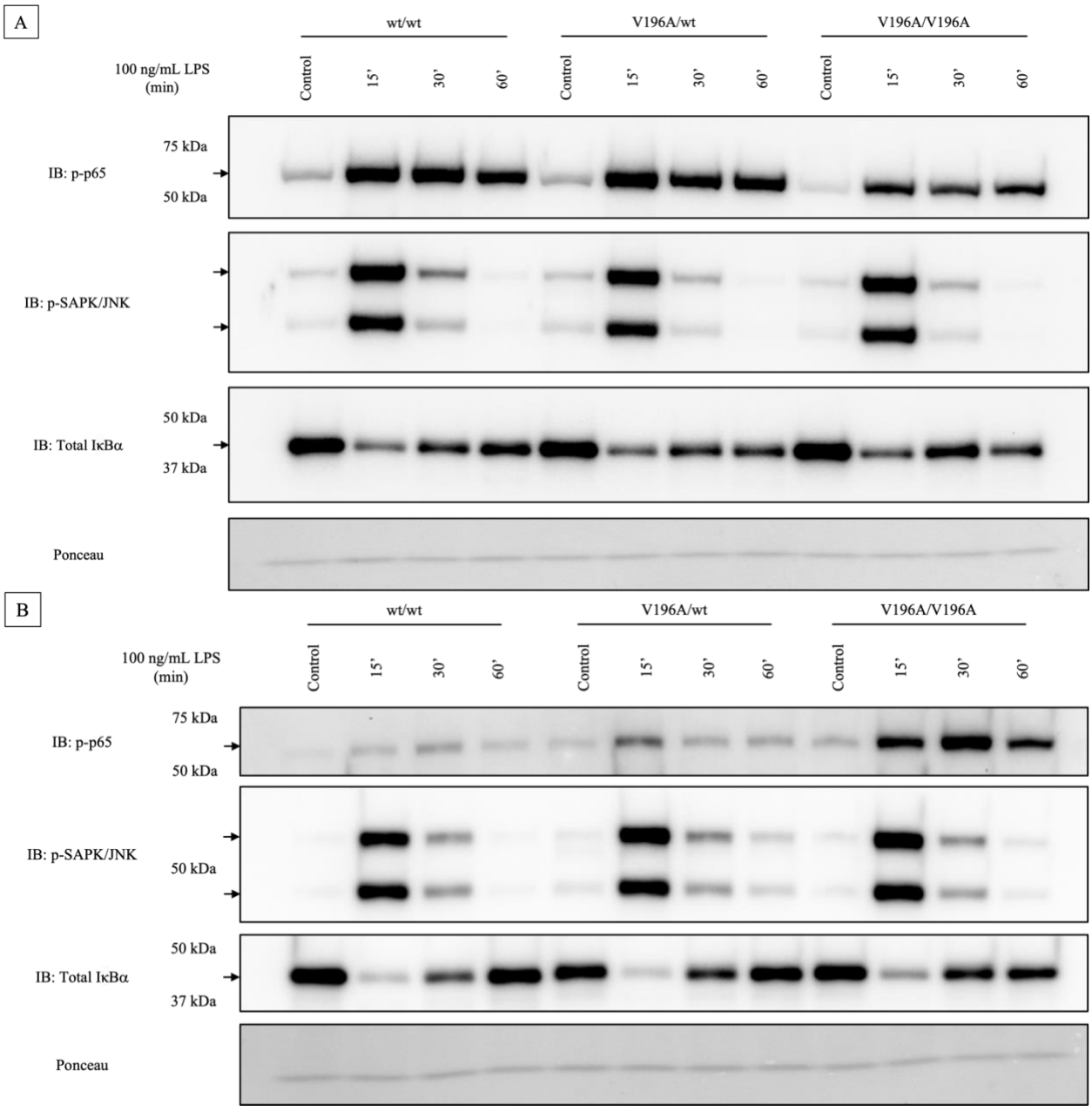

Figure 4.6: Assessing the protein expression of p-p65, p-SAPK/JNK and total IκBα by western blot following LPS stimulation of bone marrow-derived macrophages (BMDMs).

BMDMs from TRAF1 wt/wt, V196A/wt, V196A/V196A mice were seeded in 6-well plates and treated with or without 100 ng/mL LPS for 15-, 30- and 60-minutes. The negative control was treated with equal volume of DPBS as the LPS in the treatment group. Cells were treated in reverse order beginning with 60 minutes and harvested together once the respective timepoints were completed. Samples were then run on a 10% SDS-PAGE gel and transferred to a PVDF membrane using the Trans-Blot Turbo Transfer System. The membrane was immunoblotted for p-p65, p-

SAPK and total IκBα. Ponceau was used to qualitatively assess even loading of total protein since the target genes overlapped with the three housekeeping genes that were tested, β-actin, GAPDH and α-Tubulin. **(A)** TRAF1 V196A/V196A pBMDMs from male mice exhibit a slight decrease in expression of p-p-65 and p-SAPK and a reduced degradation of IκBα. A total of three independent experiments were completed and a representative western blot image is shown. **(B)** TRAF1 V196A/V196A iBMDMs exhibit a slight decrease in p-SAPK expression, reduced degradation of IκBα and a robust increase in p-p-65 expression. A total of two independent experiments were completed and a representative western blot image is shown.

4.6 – Effects of TRAF1 V196A on Phospho-Signalling

Although the western blot results support a reduction in LPS-induced NF-κB activation in TRAF1 V196A/wt and TRAF1 V196A/V196A, our western blots are not quantitative. To quantify the activation of NF-κB, we measured phosphorylation levels of p-ERK, p-p65, and p-SAPK/JNK by flow cytometry following 100 ng/mL LPS stimulation of pBMDMs and iBMDMs. The negative control was treated with equal volume of DPBS as the LPS in the treatment group. Cells were treated in reverse order beginning with the longest timepoint and harvested together once the respective timepoints of 15-, 30- and 60-minutes were completed. The results were reported as the fold change with respect to the unstimulated control. As shown in Figure 4.7, TRAF1 V196A/wt pBMDMs and iBMDMs have the highest level of p-ERK expression 15-minutes post-LPS stimulation. Additionally, TRAF1 V196A/V196A male pBMDMs have a slightly reduced p-p65 expression and TRAF1 V196A/wt iBMDMs exhibited a similar reduction (Figure 4.7). Interestingly, both TRAF1 V196A/wt and TRAF1 V196A/V196A iBMDMs exhibited a remarkably reduced level of p-SAPK/JNK expression that was statistically significant compared to TRAF1 wt/wt iBMDMs (Figure 4.7B). It is important to note that TRAF1 V196A/wt iBMDMs also had a statistically significant reduction of p-SAPK/JNK expression at the 15-minute timepoint compared to TRAF1 V196A/V196A (Figure 4.7B). Cumulatively, these results further support the proof of concept that the TRAF1 V196A variant reduces LPS-induced NF-κB activation.

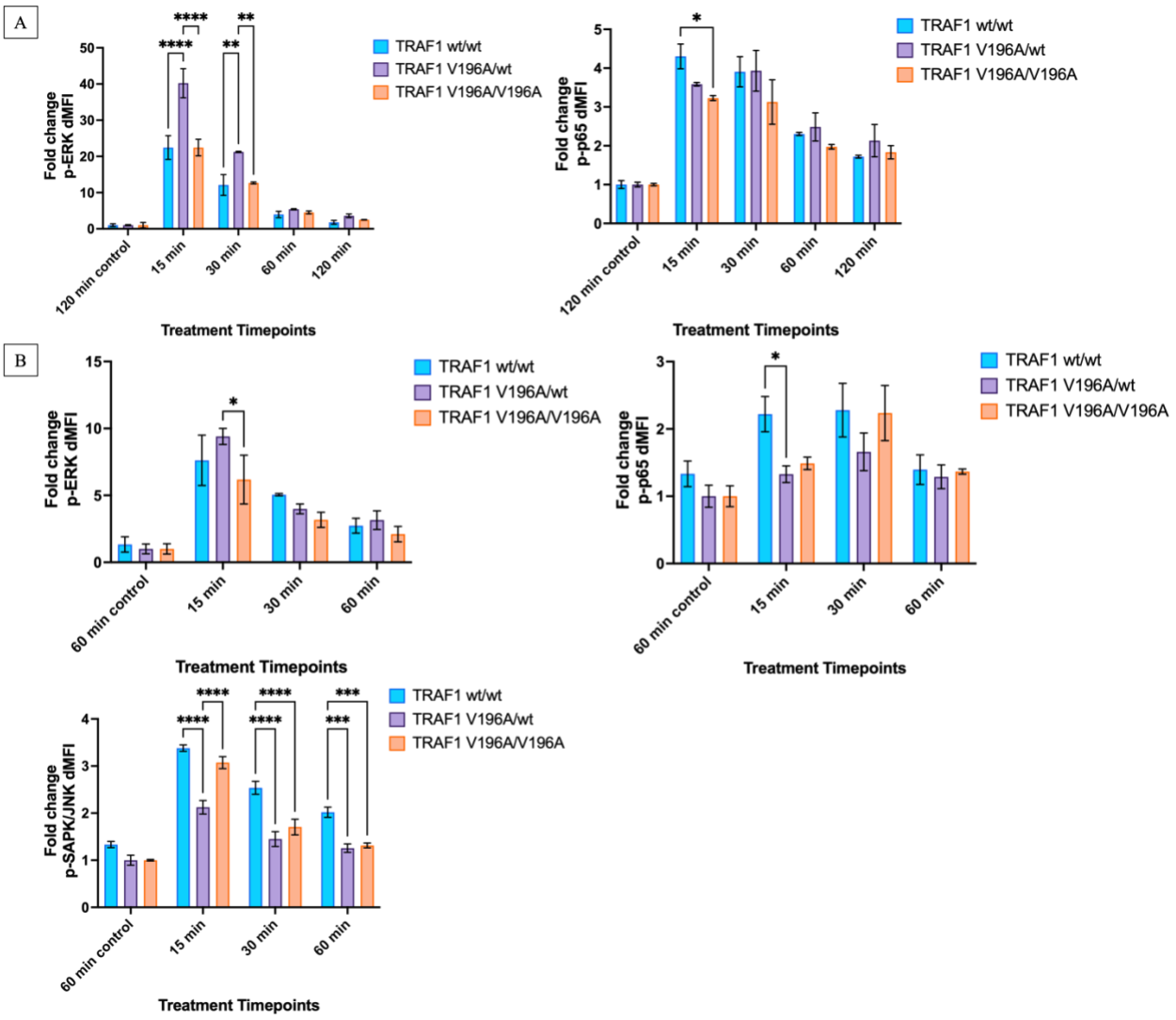

Figure 4.7: Assessing the protein expression of p-ERK, p-p65, and p-SAPK/JNK by flow cytometry following LPS stimulation of bone marrow-derived macrophages (BMDMs).

BMDMs from TRAF1 wt/wt, TRAF1 V196A/wt, TRAF1 V196A/V196A mice were seeded in 6-well plates and treated with or without 100 ng/mL LPS for 15-, 30- and 60-minutes. The negative control was treated with equal volume of DPBS as the LPS in the treatment group. Cells were treated in reverse order beginning with 60 minutes and harvested together once the respective timepoints were completed. Cells were then single-stained with p-ERK, p-p65, and p-SAPK/JNK to measure phosphorylation levels. Raw data was analyzed on FlowJo to calculate the mean fluorescence intensity (MFI) for each target. Next, the delta MFI (dMFI) was calculated by subtracting the MFI of the unstained from the MFI of the stained. **(A)** TRAF1 V196A/wt from male pBMDMs have a slightly higher p-ERK expression while TRAF1 V196A/V196A have a

slightly reduced p-p65 expression. A total of two independent experiments were completed. **(B)** TRAF1 V196A/wt iBMDMs have a slightly higher p-ERK expression, reduced p-p65 expression and both TRAF1 V196A/wt and TRAF1 V196A/V196A have lower levels of p-SAPK/JNK. A total of three independent experiments were completed. The results were reported as the fold change with respect to the unstimulated control. Ordinary two-way ANOVA was performed with Tukey's multiple comparisons test to determine statistical significance. The error bars represent standard error to the mean (mean $\pm$ SEM). *P<0.05, **P<0.01, ***P<0.001 and ****P<0.0001.

4.7 – TRAF1 V196A Reduces Inflammasome-Driven IL-1β Secretion

Our lab has previously identified the role of TRAF1 in negatively regulating inflammasome activation by restraining the LUBAC-mediated linear ubiquitination of ASC (Mirzaesmaeili et al., 2023). Moreover, previous graduate students found that inflammasome activation was inhibited in TRAF1 V203A THP-1 cells and a reduction in K63 ubiquitination. Another study reported that cIAP1/2 and TRAF2 interact with caspase-1-containing complexes and mediated nondegradative K63-linked polyubiquitination required for efficient caspase-1 activation (Labbé et al., 2011). Therefore, we hypothesized that BMDMs harbouring the TRAF1 V196A mutation will have reduced inflammasome-driven IL-1β secretion. To measure this, iBMDMs from TRAF1 wt/wt, TRAF1 V196A/wt, TRAF1 V196A/V196A mice were seeded in 6-well plates and treated with or without 100 ng/mL LPS for 3 hours (priming step). The negative control was treated with equal volume of DPBS as the LPS in the treatment group. Following the priming step, the cells were stimulated with either 5 mM ATP or stimulated with 10 μM Nigericin for 1 hour (2 hours after the priming step) and 3 hours (immediately after the priming step). As shown in Figure 4.8, there was a statistically significant reduction in inflammasome-driven IL-1β secretion in TRAF1 V196A/wt and TRAF1 V196A/V196A iBMDMs at 1-hour post-Nigericin stimulation. There were no noticeable differences with ATP stimulation. ATP-treated samples

viewed under the microscope had significant amount of cell death indicating that further optimizations may be required in either the concentration or timepoint.

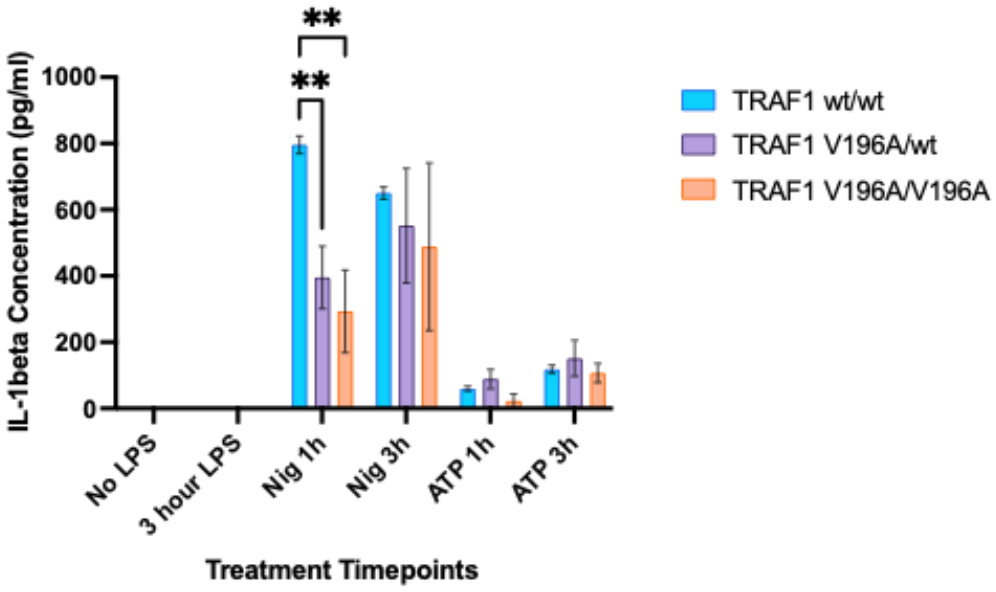

Figure 4.8: Assessing the levels of IL-1β secretion following inflammasome activation.
TRAF1 V196A/wt and TRAF1 V196A/V196A iBMDMs exhibit reduced inflammasome-driven IL-1β secretion following 1-hour Nigericin treatment. iBMDMs from TRAF1 wt/wt, TRAF1 V196A/wt, TRAF1 V196A/V196A mice were seeded in 6-well plates and treated with or without 100 ng/mL LPS for 3 hours (priming step). The negative control was treated with equal volume of DPBS as the LPS in the treatment group. Following the priming step, the cells were stimulated with either 5 mM ATP or stimulated with 10 μM Nigericin for 1 hour (2 hours after priming step) and 3 hours (immediately after priming step). The supernatant was collected and diluted 1:5 and 1:10 for Nigericin and ATP, respectively, and added to a pre-coated ELISA plate. Concentrations were obtained from a standard curve corresponding to fluorescence readings. These concentrations were adjusted accordingly by multiplying by the dilution factor to obtain the IL-1β concentration in each sample. A total of two independent experiments were performed. The results were reported as IL-1β concentration for each sample. Ordinary two-way ANOVA was performed with Tukey's multiple comparisons test to determine statistical significance. The error bars represent standard error to the mean (mean $\pm$ SEM). **P<0.01.

4.8 – TRAF1 V196A Reduces T Cell Proliferation in Response to TNFα

The dichotomous role of TRAF1 leads to both positive and negative regulatory functions in TNFR2 signaling in T cells where it interacts with both cIAP1/2 and LUBAC. Numerous studies have implicated TRAF1 to have contradictory roles in TNFR2-mediated NF-κB activation (McPherson et al., 2012; Sabbagh et al., 2008; Speiser et al., 1997; Tsitsikov et al., 2001). To identify the cell- and pathway-specific response of the TRAF1 V196A variant, T cells purified from the spleens of TRAF1 wt/wt, TRAF1 V196A/wt, TRAF1 V196A/V196A, and TRAF1 KO were labelled with 0.1 μM carboxyfluorescein succinimidyl ester (CFSE; binds to intracellular lysine residues and free primary amines) and stimulated with plate-immobilized 1 μg/mL anti-CD3 for 72 hours followed by stimulation with or without 100 ng/mL TNFα for an additional 72 hours. Proliferation was then measured on flow cytometry by measuring CFSE intensity (proliferation is indicated by the dilution of CFSE; lower levels indicate greater proliferation). The results were reported as a comparison of the dMFI values, the fold change with respect to the unstimulated control within each genotype and the fold change with respect to the CD3 only condition within each genotype. As shown in Figure 4.9, TRAF1 V196A/V196A T cells from both female and male mice exhibited significantly reduced proliferation following TNFα co-stimulation, indicating minimal activation of the TNFR2 signalling cascade. Interestingly, and to our surprise, TRAF1 V196A/V196A T cells showed a greater proliferative response to CD3 only than TRAF1 wt/wt, TRAF1 V196A/wt and TRAF1 KO. To perform statistical analysis, data from female and male experiments were pooled. As shown in Figure 4.9C, CD3-activated TRAF1 KO T cells proliferated more in response to TNFα co-stimulation. Although there was no statistical significance between CD3-activated TRAF1 V196A/V196A and TRAF1 wt/wt cells (the P-value was 0.0786), the trend shows that TRAF1 wt/wt T cells responded more to TNFα co-stimulation.

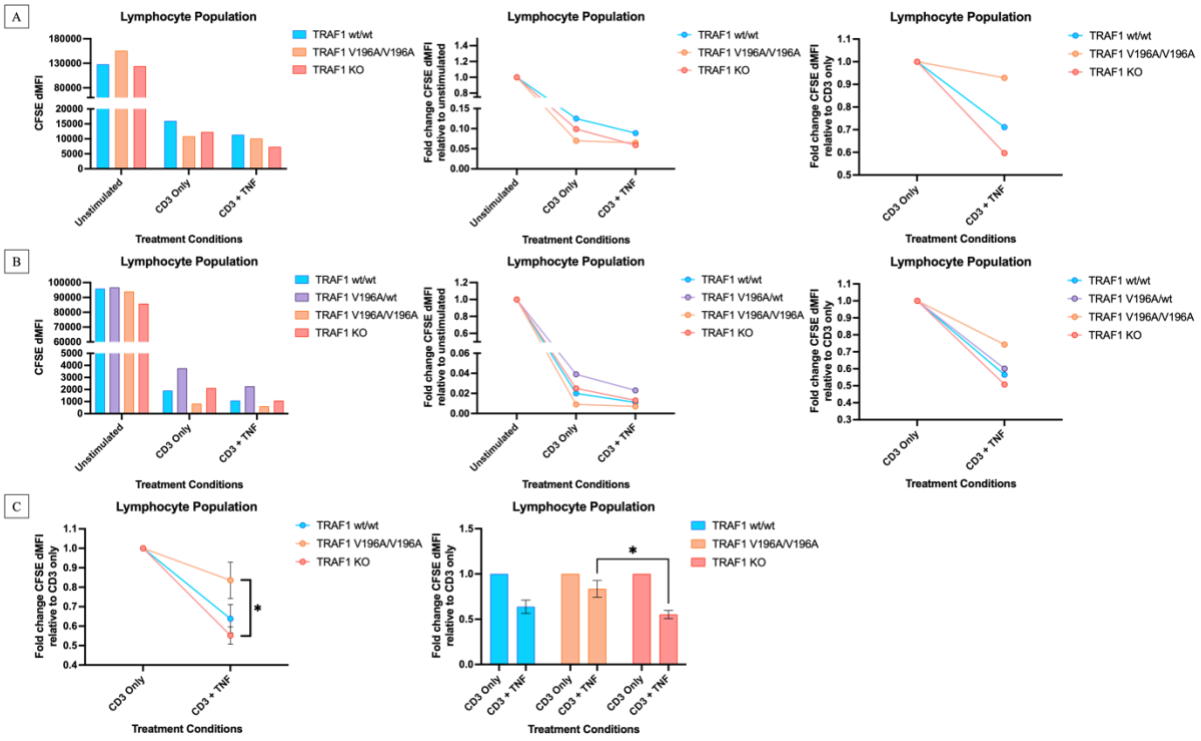

Figure 4.9: Assessing the proliferation levels of T Cells following co-stimulation with TNFα. T cells purified from the spleens of TRAF1 wt/wt, TRAF1 V196A/wt, TRAF1 V196A/V196A, and TRAF1 KO were labelled with 0.1 μM CFSE and stimulated with plate-immobilized 1 μg/mL anti-CD3 for 72 hours followed by stimulation with or without 100 ng/mL TNFα for an additional 72 hours. Cell proliferation was measured by flow cytometry and the raw data was analyzed on FlowJo to calculate the mean fluorescence intensity (MFI) for each target. Next, the delta MFI (dMFI) was calculated by subtracting the MFI of the unstained from the MFI of the stained. The results were reported as a comparison of the dMFI values, the fold change with respect to the unstimulated control within each genotype and the fold change with respect to the CD3 only condition within each genotype. TRAF1 V196A/V196A T cells from female mice **(A)** and male mice **(B)** exhibit significantly reduced proliferation following TNFα stimulation indicating minimal activation of TNFR2 signalling. A total of two independent experiments were performed, first in female mice then in male mice. The data from both female and male mice experiments were pooled to perform statistical analysis **(C).** Ordinary two-way ANOVA was performed with Tukey's multiple comparisons test to determine statistical significance. The error bars represent standard error to the mean (mean ± SEM). *P<0.05.

4.9 – Successful Validation of the hTRAF1 T268A Mutant Plasmid

As discussed in section 1.4, cIAP2 and LUBAC are both key players in the regulation of NF-κB activation. We also know that TRAF1 binds to cIAP2 through the CC domain and to LUBAC through the MATH domain. In order to dissect cell- and pathway- specific effects of TRAF1, we need to selectively disrupt these interactions. Previous graduate students have identified specific interactions in mouse and human TRAF1 that disrupt the interaction with its binding partners. However, the site where the interaction between hTRAF1 and LUBAC is abrogated and the interaction between hTRAF1 and cIAP2 is maintained is currently unknown. To determine the amino acid responsible for the interaction between hTRAF1 and LUBAC, we performed site-directed mutagenesis to create a mutated full-length hTRAF1 at residue 268 from a threonine to an alanine, referred to as hTRAF1 T268A. This amino acid corresponded to the previously identified site where the interaction between mTRAF1 and LUBAC is disrupted. Bacteria were then transformed with hTRAF1 T268A and a few clones were selected to extract the plasmid by mini-prep. This plasmid was then sent for sequencing to confirm whether the mutation was successful. Once the mutation was confirmed, midi-prep was performed to obtain a sufficient concentration of this plasmid for transient transfection. Next, we performed restriction enzyme digestion of hTRAF1 FL and all of the hTRAF1 T268A plasmid stocks from different clones to ensure that the size of the DNA fragment corresponds to the correct size of the insertion (Figure 4.10A). The correct size of the DNA fragment, the purity and the concentration were factors in selecting a suitable clone for downstream applications. Once we identified hTRAF1 T268A C5-2A as a potential clone, we confirmed the mutation through sequencing (Figure 4.10B). As such, the plasmid extracted from this clone has the correct mutation of interest and can be used for transfection and Co-IP experiments.

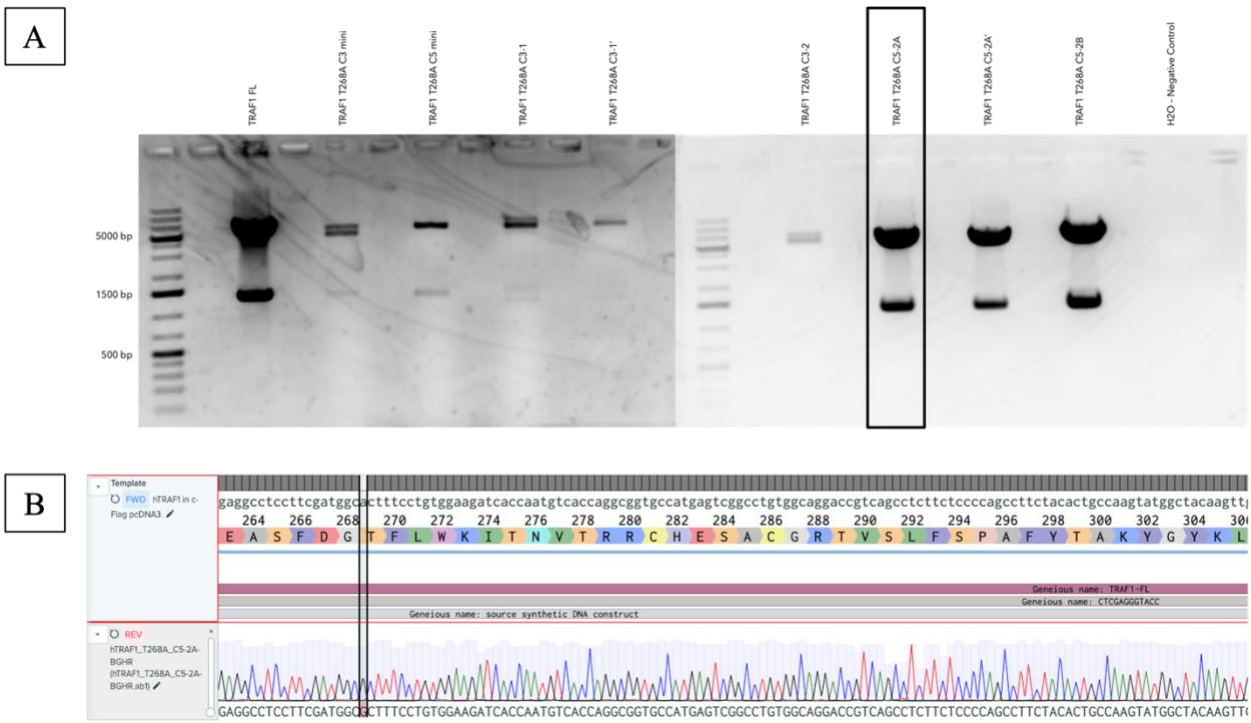

Figure 4.10: Assessing the formation of a successful site-directed mutagenesis of the human TRAF1 (hTRAF1) plasmid.

(A) Agarose gel depicting the size of the DNA fragments produced after restriction enzyme digestion of hTRAF1 full length (FL) and hTRAF1 T268A plasmids. Restriction enzyme digestion was performed using Xba1 and BamH1 restriction enzymes resulting in two bands, one at 5382 bp corresponding to the c-Flag pcDNA3 vector and the second band at 1260 bp corresponding to the hTRAF1 FL gene. The black box indicates the hTRAF1 T268A C5-2A clone that was selected as the plasmid of interest for transfection. **(B)** Sequencing results of the hTRAF1 T268A plasmid extracted and purified from the C5-2A clone. The sequence at amino acid 268 of hTRAF1 changes from ACT (threonine) to GCT (alanine). The data in this chromatogram confirms that the clone selected has the correct mutation of interest and can be used for transfection.

4.10 – hTRAF1 T268A Maintains Interaction with cIAP2

To determine whether the interaction between hTRAF1 268A and LUBAC is disrupted while the interaction between hTRAF1 T268A and cIAP2 is maintained, we performed a series of transfections in HEK293T/17 cells using plasmids for hTRAF1 T268A C5-2A, hTRAF1 FL, c-Flag, cIAP2 and LUBAC. The lysates were then collected, and Co-IP was performed using a TRAF1 specific antibody (1F3) followed by immunoblotting for our proteins of interest. As shown in Figure 4.11, the interaction between hTRAF1 T268A: LUBAC is significantly reduced and the interaction between hTRAF1 T268A: cIAP2 is maintained. While these results confirm that hTRAF1 T268A does not interfere with the stability of the interaction between hTRAF1 T268A: cIAP2, the presence of a band in the c-Flag control condition with LUBAC suggests that there is non-specific binding of LUBAC to the beads. As such, even though the non-specific binding produces a higher signal than the lane with hTRAF1 T268A: LUBAC and a lower signal than the lane with hTRAF1 FL: LUBAC, the results still require further investigation to confidently conclude the effect of this mutation on the interaction between TRAF1 and LUBAC. This is further explored and addressed in the following section 4.11.

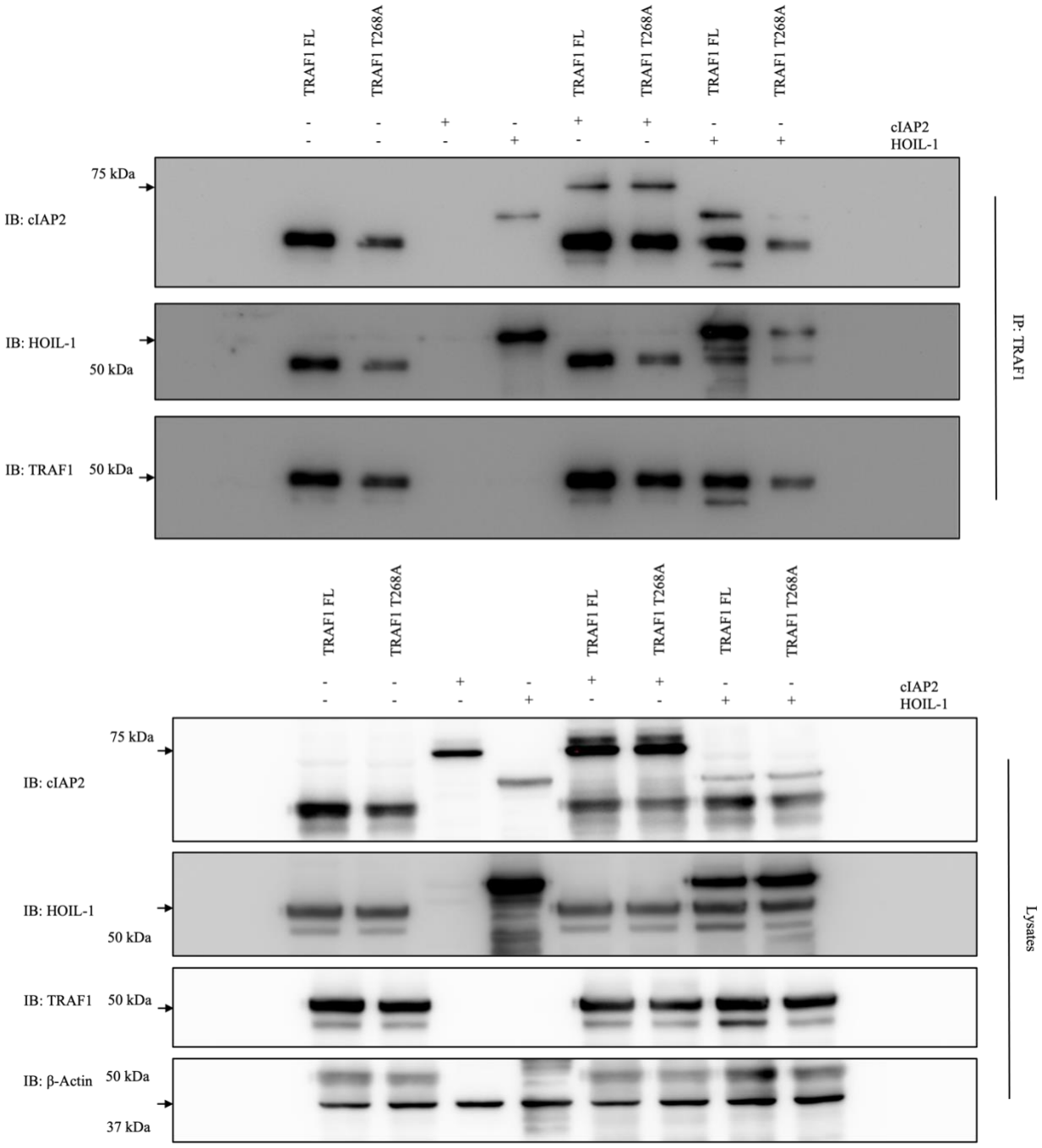

Figure 4.11: Assessing the effects of hTRAF1 T268A on the interaction with cIAP2 and HOIL-1.

hTRAF1 T268A maintains the interaction with cIAP2. HEK293T/17 cells were used to overexpress hTRAF1 T268A along with plasmids of interest. Lysates were then harvested to perform co-immunoprecipitation (Co-IP), followed by immunoblotting (IB) with cIAP2 and

HOIL-1. β-Actin was used as a loading control. The secondary antibodies consisted of light-chain specific anti-rabbit and light-chain specific anti-mouse. A total of three independent experiments were completed (one transfection was performed with 3 μg plasmid DNA transfection and two transfections were performed with 2 μg plasmid DNA) and a representative western blot image is shown from the 3 μg plasmid DNA transfection experiment (transection with either 2 or 3 μg of plasmid DNA showed similar results).

4.11 – hTRAF1 T268A Reduces Interaction with HOIL-1

In order to remove the background binding between HOIL-1 and the beads, several approaches were employed. Initially, we transfected different amounts of HOIL-1 plasmid and incubated different amounts of lysates with the antibody-bead mix during the immunoprecipitation step. From these titrations, we still observed comparable background binding relative (data not shown). Next, we employed two preclearing strategies. In the first strategy, we precleared the lysate by doing a sequential Co-IP and in the second strategy, we precleared the beads by first incubating with a c-Flag lysate before incubating the beads with the lysate of interest. Both of these strategies also showed comparable background binding (data not shown). We then discovered that there was background binding to the beads alone and the next approach involved blocking the beads with 5% BSA for one hour. As shown in Figure 4.11, we see a reduction in background binding allowing us to confidently conclude that the interaction between hTRAF1 T268A: LUBAC is significantly reduced.

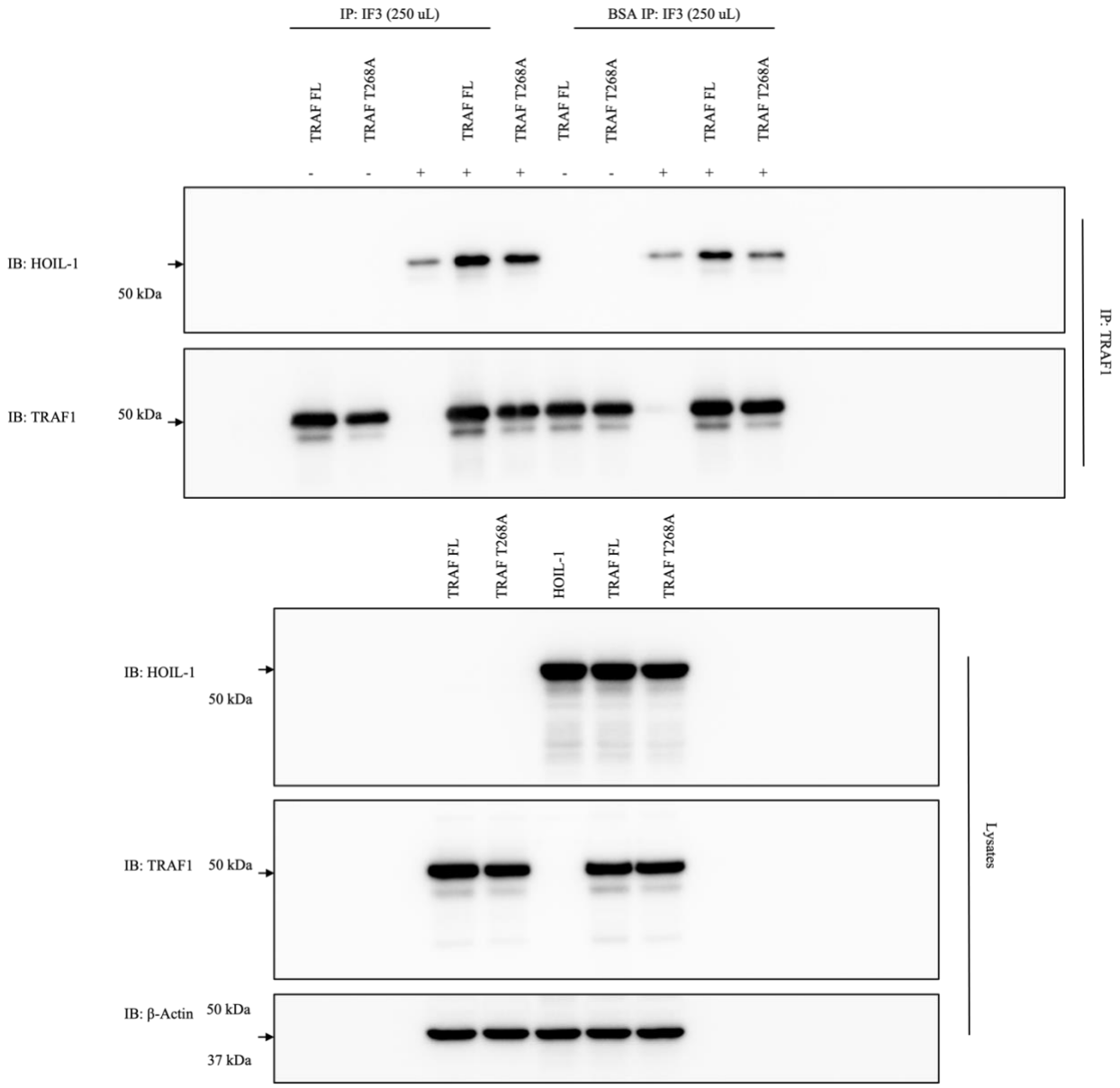

Figure 4.12: Assessing the effects of hTRAF1 T268A on the interaction with HOIL-1.

hTRAF1 T268A significantly reduces the interaction with HOIL-1. HEK293T/17 cells were used to overexpress hTRAF1 T268A along with plasmids of interest. Lysates were then harvested to perform co-immunoprecipitation (Co-IP), followed by immunoblotting (IB) with HOIL-1. β-Actin was used as a loading control. The western blot also indicates that blocking the beads with 5% BSA may help reduce the background binding for HOIL-1. The secondary antibodies consisted of light-chain specific anti-rabbit and light-chain specific anti-mouse. A total of three independent experiments were completed and a representative western blot image is shown.

Chapter 5: Discussion

TRAF1 has a multifaceted role across different immune cell types (e.g., macrophages and T lymphocytes) and receptor signalling pathways (Abdul-Sater et al., 2016; Dhillon et al., 2019; Edilova et al., 2018; McPherson et al., 2012; Speiser et al., 1997; Tsitsikov et al., 2001). In innate immune cells, such as monocytes, TRAF1 serves as a negative regulator of NF-κB activation in the TLR signalling pathway. By interacting with all three components of LUBAC, TRAF1 restrains linear ubiquitination of NEMO to inhibit NF-κB activation resulting in a dampened inflammatory response. Conversely, in adaptive immune cells, such as T lymphocytes, TRAF1 serves as a positive regulator of NF-κB activation downstream of the 4-1BB pathway. When this pathway is activated, TRAF1 forms a complex with TRAF2 and recruits cIAP2. cIAP2 is responsible for mediating K63 ubiquitination of other proteins in the signaling cascade, ultimately leading to the activation of NF-κB. The dichotomous role of TRAF1 is remarkably pronounced downstream of TNFR2 receptors where it interacts with both LUBAC and cIAP2.

Recently, Abdul-Sater et al. (2016) showed that a RA-associated SNP in the TRAF1 gene results in lower levels of TRAF1 protein but higher amounts of inflammatory cytokines. Individuals with this genetic variant of TRAF1 had lower levels of TRAF1 protein in both macrophages and T lymphocytes. As a result, these individuals had less activated T lymphocytes and produced lower levels of destructive cytokines. In contrast, their macrophages produced significantly higher levels of pro-inflammatory cytokines which led to an excessive inflammatory response. RA Patients with this SNP were also at a higher risk of mortality from sepsis (Panoulas et al., 2009). Due to the dichotomous role of TRAF1, broadly targeting it poses several challenges since that would result in increased inflammation from macrophages and reduced lymphocyte survival which could increase susceptibility to other infections. Moreover, Abdul-Sater et al.

(2016) reported that TRAF1 -/- mice are more susceptible to LPS-induced sepsis than their wildtype littermates. Nonetheless, this unexpected finding highlights the challenges of targeting TRAF1 indiscriminately and the importance of studying the mechanisms underlying the disparate roles to promote and maintain a balanced immune response.

Notably, TRAF1 is an excellent candidate to selectively target in the development of sepsis and RA therapies due to its dichotomous role of regulating of NF-κB activation in the immune system. Our lab has recently identified a mutation in TRAF1, V203A, that disrupts the interaction with cIAP2 in human monocyte cells which can reduce their inflammatory responses when stimulated with LPS. Interestingly, through Co-IP assays, the V203A mutation was identified by a previous graduate student as V196A in mouse TRAF1 (mTRAF1); V196A disrupted the interaction between mTRAF1 and cIAP2 while maintaining the interaction between mTRAF1 and LUBAC. Using CRISPR/Cas12a gene editing, we have genetically engineered a mouse model with this TRAF1 V196A mutation. By disrupting the TRAF1/cIAP2/NF-κB axis, this mutation prevents TRAF1-mediated activation of NF-κB in lymphocytes while enhancing TRAF1-mediated inhibition of NF-κB in monocytes.

To begin our scientific study, we first established the proof of concept that the TRAF1 V196A mice were protected from a lethal endotoxic shock. We challenged male and female mice, 6-8 weeks of age, with a lethal LPS dose of 35 mg/kg to determine the survival response. Here, we showed that TRAF1 V196A/V196A male mice were completely protected compared to TRAF1 wt/wt and TRAF1 V196A/wt, and that this protection was less pronounced in female mice (Figure 4.1). To our surprise, TRAF1 V196A/wt male and female mice were more susceptible following the intraperitoneal injection of the lethal LPS dose. Throughout the time course of this experiment, mice were monitored hourly for 30-50 hours and the murine sepsis score, indicative of sepsis

severity, was recorded along with general observations. The murine sepsis scoring sheet consisted of parameters including activity, appearance, eyes, respiration, respiration rate, and response to stimulus. Consistent with the survival curves, TRAF1 V196A/V196A male and female mice had a significantly dampened progression of sepsis severity, as indicated by the lower MSSs during the time course, and TRAF1 V196A/wt male and female mice had higher MSSs at most timepoints (Figures 4.2 and 4.3). However, we are not able to make a direct comparison between male and female mice because we only assessed the response of mice with the same sex within one survival experiment.

In order to assess the role of TRAF1 V196A in regulating inflammatory cytokine production, we challenged TRAF1 wt/wt and TRAF1 V196A/V196A female mice with a sublethal dose of 10 mg/kg LPS. We showed that the levels of IFN-β, IFN-γ, IL-1β, IL-6, IL-12 (p70), MCP-1 and TNFα were not statistically significant indicating that both TRAF1 wt/wt and TRAF1 V196A/V196A female mice produce relatively similar levels of cytokines (Figure 4.4). Despite the insignificant result, these findings are relatively consistent with the survival response to the lethal LPS dose where TRAF1 wt/wt and TRAF1 V196A/V196A generally had similar sepsis severity, with statically significant differences occurring between the 5- and 6-hour post-LPS injection. One recent study reported that male mice have significantly higher levels of IL-6, IL-10 and TNFα than female mice and that there are no differences in cytokine production between sexes in pre-puberty young mice (Kuo, 2016). Another study discovered a sex difference in the phenotype of resident leukocytes in females that allows for a more efficient acute inflammatory response that protects them from mortality that is associated with severe sepsis (Scotland et al., 2011).

Undoubtedly, the results of our in vivo experiments necessitated investigating cell- and pathway- specific effects of the TRAF1 V196A variant. We employed various in vitro techniques to measure the expression of inflammatory markers at both the gene and protein level in pBMDMs and iBMDMs from TRAF1 wt/wt, TRAF1 V196A/wt and TRAF1 V196A/V196A mice stimulated with 100 ng/mL LPS. We began by performing RT-qPCR to measure the gene expression levels of pro- and anti-inflammatory markers including IFN-β, IL-1β, IL-6, IL-10, IL-12, TGFβ and TNFα. It is important to note that the amount of transcript present for a particular gene at any given timepoint is more reflective of the severity and progression of disease. Moreover, we identified differential gene expression in the unstimulated condition between genotypes. As such, we decided to report data as the relative fold difference of TRAF1 V196A/wt and TRAF1 V196A/V196A with respect to TRAF1 wt/wt. We have shown that TRAF1 V196A/wt and TRAF1 V196A/V196A have lower transcript levels, for most targets, pre-stimulation and upon LPS stimulation, exhibit a relatively dampened induction at some timepoints (Figure 4.5A). Notably, the mRNA levels for all of the target genes at most timepoints were remarkably and significantly reduced for TRAF1 V196A/V196A (Figure 4.5B). We also determined that one copy of TRAF1 V196A may be sufficient at most timepoints to reduce the pro-inflammatory gene expression of IFN-β, IL-1β, and TNFα as well as the anti-inflammatory gene expression of IL-6 and IL-10. Surprisingly, the TRAF1 V196A/wt exhibited a robust expression of IL-1β at the 1-hour timepoint which requires further exploration. This could be one of the factors underlying the increased susceptibility of the TRAF1 V196A/wt mice in the survival experiment.

To further confirm and support the reduction of NF-κB activation measured through RT-qPCR, we assessed the protein expression of inflammatory markers following 100 ng/mL LPS stimulation by performing western blots. We assessed the levels of p-p65, p-SAPK/JNK and IκBα

in pBMDMs and iBMDMs. Interestingly, both TRAF1 V196A/wt and TRAF1 V196A/V196A pBMDMs (Figure 4.6A) and iBMDMs (Figure 4.6B) exhibited a slight decrease in the expression of p-SAPK/JNK and expressed more IκBα than TRAF1 wt/wt. This indicates that in response to LPS, less IκBα was phosphorylated, leading to less degradation, and consequently a reduction of NF-κB activation. However, pBMDMs and iBMDMs differed in their expression of p-p65 expression. While TRAF1 V196A/wt and TRAF1 V196A/V196A pBMDMs exhibited a reduction in p-p65 expression compared to TRAF1 wt/wt pBMDMs, TRAF1 V196A/V196A iBMDMs had a robust increase in p-p65 expression compared to TRAF1 V196A/wt and TRAF1 V196A/V196A iBMDMs. The increase in p-p65 expression requires further investigation to determine the role of cell survival and identify any potential effects of the immortalization process. Interestingly, pBMDMs with the TRAF1 V196A mutation showed lower levels of p-p65 and p-SAPK/JNK in the unstimulated lane suggesting that the basal inflammation is lower than wildtype TRAF1. On the contrary, iBMDMs with the TRAF1 V196A mutation showed slightly higher levels of p-p65 and p-SAPK/JNK in the unstimulated lane suggesting that the basal inflammation is higher than wildtype TRAF1. Overall, the western blot results support a reduction in LPS-induced NF-κB activation in TRAF1 V196A/wt and TRAF1 V196A/V196A.

Our next aim was to quantify the LPS-induced activation of NF-κB by measuring the phosphorylation levels of p-ERK, p-p65, and p-SAPK/JNK by flow cytometry. We have shown that TRAF1 V196A/wt pBMDMs and iBMDMs have the highest level of p-ERK expression 15-minutes post-LPS stimulation (Figure 4.7). Similar to the western blot results, we have also shown that TRAF1 V196A/V196A male pBMDMs have a slightly reduced p-p65 expression and TRAF1 V196A/wt iBMDMs exhibited a similar reduction (Figure 4.7A). More importantly, we have shown that both TRAF1 V196A/wt and TRAF1 V196A/V196A iBMDMs had remarkably reduced

level of p-SAPK/JNK expression that was statistically significant compared to TRAF1 wt/wt iBMDMs (Figure 4.7B). Cumulatively, the RT-qPCR, western blot, and phospho-flow results support the proof of concept that TRAF1 V196A reduces LPS-induced NF-κB activation.

Recent literature has identified the importance of cIAP1/2 and TRAF2 interaction with caspase-1 containing complexes for efficient caspase-1 activation through cIAP2-mediated nondegradative K63-linked polyubiquitination (Labbé et al., 2011). Our lab has previously identified the role of TRAF1 in negatively regulating inflammasome activation by restraining LUBAC's ability to mediate linear ubiquitination of ASC (Mirzaesmaeili et al., 2023). Previous graduate students have found that inflammation activation was inhibited in TRAF V203A THP-1 cells, cIAP2 was more prone to degradation and K63-ubiquitination was reduced. We assessed the levels of inflammasome-driven IL-1β secretion following 100 ng/mL LPS priming for 3 hours followed by stimulation with either 5 mM ATP or stimulated with 10 μM Nigericin for 1 hour (2 hours after priming step) and 3 hours (immediately after priming step). We have shown that iBMDMs harbouring the TRAF1 V196A mutation have a statistically significant reduction of IL-1β after 1 hour following nigericin stimulation (Figure 4.8). This supports the findings of previous graduate students and aligns with the current literature. Stimulation with ATP did not result in any noticeable differences. One possible explanation is owing to the significant amount of cell death observed under the microscope indicating that a shorter time course needs to be explored or that we need to find a new optimal concentration of ATP for our samples.

The next focus of our study was to investigate the role of TRAF1 V196A in T cell signalling. TRAF1 has been characterized for its dichotomous role of positively and negatively regulating TNFR signalling in T cells by interacting with cIAP1/2 and LUBAC. In the past three decades, numerous studies have reported the complex and contradictory roles of TRAF1 in T-cell

signalling, particularly in TNFR2-mediated NF-κB activation (McPherson et al., 2012; Sabbagh et al., 2008; Speiser et al., 1997; Tsitsikov et al., 2001). It is important to note that these studies employed either TRAF1 knockout models or specific agonists and antagonists targeting key players of the TNFR2 signalling cascade. We have shown here that TRAF1 V196A/V196A T cells from both female and male mice exhibited significantly reduced proliferation following TNFα co-stimulation, indicating minimal activation of the TNFR2 signalling cascade (Figure 4.9). Borghi et al. (2018) reported that both HOIP and cIAP1 and their associated M1- and K63-linked polyubiquitination are required for TNFR2-induced canonical NF-κB activation. Previous graduate students have found that disrupting the interaction between TRAF1 and cIAP2 lead to a reduction in K63-ubiquitination and a loss of TRAF1-mediated protection of cIAP2, thus making cIAP2 more vulnerable to degradation. With these findings, we suspect that the reduced proliferation observed here is due to TRAF1's inhibition on LUBAC-mediated M1-ubiquitination as well as a reduction in the levels of K63-ubiquitination. Interestingly, and to our surprise, TRAF1 V196A/V196A T cells showed a greater proliferative response to stimulation with CD3 only than TRAF1 wt/wt, TRAF1 V196A/wt and TRAF1 KO (Figure 4.9). Previously, it was reported that CD3-activated TRAF1-deficient T cells exhibit increased proliferation to CD3 due to endogenous TNF resulting in the activation of the TNFR2 pathway (Tsitsikov et al., 2001). There are a few potential explanations underlying the increased proliferation of TRAF1 V196A/V196A T cells to CD3 alone. Wallis et al. (2017) identified the role of TRAF3 for effective TC3 signalling by regulating two inhibitors, namely, the C-terminal Src kinase (Csk) and the protein tyrosine phosphatase N22 (PTPN22). A previous student in our lab identified that the TRAF1 V203A mutation prevents TRAF3 degradation. Although we have not tested this, there is a possibility that the TRAF1 V196A variant prevents TRAF3 degradation as well, resulting in enhanced TCR

signaling. The next explanation is that there may be activation of the alternative NF-κB pathway and the role of cIAP1 needs to be further explored in our model. Another explanation could be the contribution of Tregs. According to literature, stimulation of CD4+ T cells by plate bound anti-CD3 can selectively induce the expansion of Tregs (Abraham et al., 2008; Singh et al., 2009). This would require further investigation and it is important to note that there is likely impaired Treg signalling because TRAF1 V196A potentially hinders TNFR2 signalling axis by disrupting the interaction between TRAF1 and cIAP2.

To perform statistical analysis, data from female and male experiments were pooled. As expected, CD3-activated TRAF1 KO T cells proliferated more than TRAF1 V196A/V196A T cells in response to TNFα co-stimulation. Despite there being no statistical significance between CD3-activated TRAF1 V196A/V196A and TRAF1 wt/wt cells (the P-value was 0.0786), there was a clear trend that TRAF1 wt/wt T cells responded more to TNFα co-stimulation. Overall, this is a very important experiment that needs to be performed at least two more times for both male and female mice to increase the statistical power and to elucidate the cell- and pathway- specific role of TRAF1 V196A.

The final focus of our study was to identify the site where the interaction between hTRAF1 and LUBAC is disrupted while the interaction between hTRAF1 and cIAP2 is maintained. cIAP2 and LUBAC are both key players that interact with TRAF1 to regulate NF-κB activation. We also know that TRAF1 binds to cIAP2 through the CC domain and to LUBAC through the MATH domain. Previous graduate students have identified specific interactions in mouse and human TRAF1 that disrupt the interaction with its binding partners. We performed site-directed mutagenesis to create a mutated full-length hTRAF1 at residue 268 from a threonine to an alanine, referred to as hTRAF1 T268A. This amino acid corresponded to the previously identified

mTRAF1-T261A in mice where the interaction between mTRAF1 and LUBAC was disrupted without affecting the interaction between mTRAF1 and cIAP2. The hTRAF1 T268A plasmid was validated by first performing restriction enzyme digestion to ensure the correct size (Figure 4.10A) and then through sequencing to confirm the mutation (Figure 4.10B). Next, we transfected HEK293T/17 cells according to the various conditions and then collected the lysates to perform co-immunoprecipitation (Co-IP) and subsequent immunoblotting for our proteins of interest. We have shown that hTRAF1 268A maintains the interaction between hTRAF1 and cIAP2 (Figure 4.11) while significantly reducing the interaction between hTRAF1 and LUBAC (Figure 4.12). Despite several optimizations to mitigate the background binding with HOIL-1, we were only able to reduce and not completely eliminate this. This experiment could be repeated in the future with different HOIL-1 antibodies to further elucidate whether hTRAF1 268A significantly reduces or completely abrogates the interaction between hTRAF1 and LUBAC.

Figure 5.1 provides an overview of the multifaceted role of TRAF1 to elucidate the pathway-specific role of mTRAF1 V196A and hTRAF1 T268A in regulating inflammation through NF-κB activation.

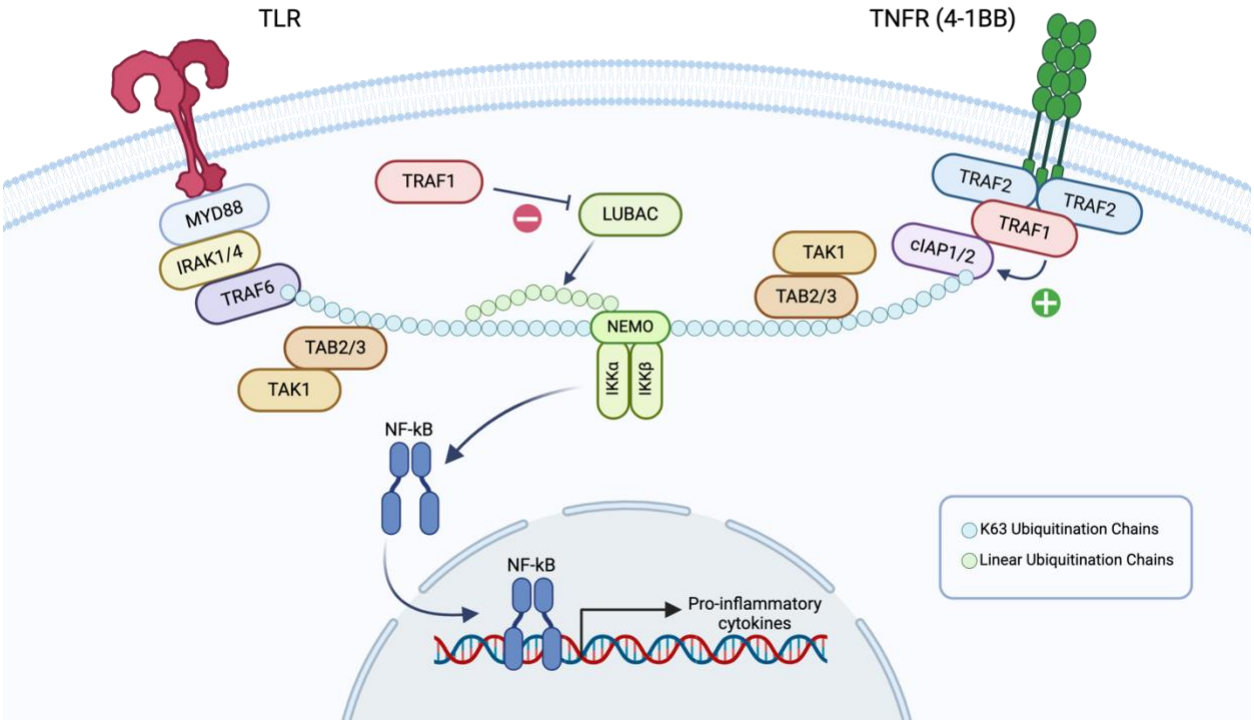

Figure 5.1: An overview of the pathway-specific role of TRAF1 in regulating inflammation through NF-κB activation.

Figure adapted from Abdul-Sater et al. (2016) and Edilova et al. (2018). Created with BioRender.com.

Chapter 6: Conclusions and Future Directions

6.1 – Future Directions

Our study has confirmed through various experiments that TRAF1 V196A leads to a remarkable reduction of key markers during an inflammatory response, indicating a significant reduction of NF-κB activation. There are a few aspects of this scientific study that can be further investigated. One important piece is to perform gene and protein expression analysis on the organs that were harvested during the lethal and sublethal experiments. Future experiments should also include histology to assess immune-cell infiltration and flow cytometry to identify and quantify different subsets of immune cells. We also suggest investigating the response of TRAF1 V196A BMDMs to TNFα stimulation with the addition of TNFR1 and TNFR2 antagonists which would allow us to understand pathway-specific activation. Moreover, to support the reduction in inflammasome-driven IL-1β secretion, protein levels of pro-caspase-1, caspase-1, pro-IL-1β and IL-1β can be assessed by western blot. It would also be insightful to assess the role of TRAF1 V196A by measuring markers of cell death by RT-qPCR and western blot as well as performing an LDH assay.

Furthermore, more biological replicates of the T cell assay need to be completed to concretely establish a significant reduction in proliferation and response to TNF co-stimulation. In addition to measuring proliferation and cytokine production, the cells can be lysed at various timepoints to monitor the levels of M-1 and K63-ubiquitination, providing more meaningful insight on the underlying molecular mechanisms. Further experimentation is also required to understand the reason TRAF1 V196A/V196A T cells proliferate more than the other genotypes in

response to CD3 only. One experiment that can be employed here is to block TNFR1 and TNFR2, individually, to assess the role of endogenous TNF and potentially the role of Treg expansion.

Lastly, now that we have identified hTRAF1 T268A as the site of interaction that significantly reduces the interaction between TRAF1 and LUBAC while maintaining the interaction with cIAP2, we can use CRISPR/CRISPR-associated protein 9 (Cas9) homology-directed repair (HDR) to create a mutation in THP-1 monocytic leukemia cells to determine the cellular and molecular effects of this mutant on NF-κB activation.

6.2 – Conclusions

The significance of this scientific study is to understand the dichotomous role of TRAF1 in regulating NF-κB activation. There are numerous studies linking TRAF1 to chronic and uncontrolled inflammation which leads to serious health conditions such as autoimmune diseases, cancer, and cardiovascular disease as well as an increased risk of mortality due to severe sepsis (Abdul-Sater et al., 2016; Dhillon et al., 2019; Edilova et al., 2018, 2018; Madahar et al., 2023; Panoulas et al., 2009). Undoubtedly, targeting TRAF1 indiscriminately can lead to several unwarranted challenges such as an increase in inflammation coupled with a decrease in lymphocyte survival. Therefore, it follows that TRAF1 should be selectively targeted to achieve a balanced immune response. In our study, we employed in vivo and in vitro experiments to evaluate a TRAF1 mutant, V196A, where the interaction between TRAF1 and cIAP2 is disrupted and the interaction between TRAF1 and LUBAC is maintained. Through a series of experiments including assessing the survival and cytokine production of mice in the lethal and sublethal LPS model, gene and protein expression of inflammatory markers, phosphorylation status of key players in the signaling cascade, inflammasome-driven 1β-secretion, and proliferation of T cells, we prove that the TRAF1 V196A variant limits lymphocyte activation and reduces the production of pro-

inflammatory cytokines in macrophages. In our study, we also identified a potential site of interaction, hTRAF1 T268A, that significantly reduces the interaction between TRAF1 and LUBAC while maintaining the interaction between TRAF1 and cIAP2. It is important to evaluate the cellular and molecular responses of this mutant in regulating NF-κB activation. Ultimately, identifying the sites of protein-protein interactions between TRAF1 and its binding partners will create the foundation for future studies exploring the role of TRAF1. This will support the development of new treatments that target specific functions of TRAF1 to improve the quality of life of RA and sepsis patients.

References

Abdul-Sater, A. A., Edilova, M. I., Clouthier, D. L., Mbanwi, A., Kremmer, E., & Watts, T. H. (2016). The signaling adaptor TRAF1 negatively regulates Toll-like receptor signaling and this underlies its role in rheumatic disease. *Nature Immunology*, 12.

Abraham, M., Karni, A., Dembinsky, A., Miller, A., Gandhi, R., Anderson, D., & Weiner, H. L. (2008). In vitro induction of regulatory T cells by anti-CD3 antibody in humans. *Journal of Autoimmunity*, *30*(1–2), 21–28. https://doi.org/10.1016/j.jaut.2007.11.007

Akira, S., & Takeda, K. (2004). Toll-like receptor signalling. *Nature Reviews Immunology*, *4*(7), 499–511. https://doi.org/10.1038/nri1391

Altavilla, D., Squadrito, G., Minutoli, L., Deodato, B., Bova, A., Sardella, A., Seminara, P., Passaniti, M., Urna, G., Venuti, S. F., Caputi, A. P., & Squadrito, F. (2002). Inhibition of nuclear factor-κB activation by IRFI 042, protects against endotoxin-induced shock. *Cardiovascular Research*, *54*(3), 684–693. https://doi.org/10.1016/S0008-6363(02)00276-6

Babaeijandaghi, F., Paiero, A., Long, R., Tung, L. W., Smith, S. P., Cheng, R., Smandych, J., Kajabadi, N., Chang, C.-K., Ghassemi, A., Kennedy, W. D. M., Soliman, H., Schutz, P. W., & Rossi, F. M. V. (2022). TNFα and IFNγ cooperate for efficient pro- to anti-inflammatory transition of macrophages during muscle regeneration. *Proceedings of the National Academy of Sciences of the United States of America*, *119*(44), e2209976119. https://doi.org/10.1073/pnas.2209976119

Barichello, T., Generoso, J. S., Singer, M., & Dal-Pizzol, F. (2022). Biomarkers for sepsis: More than just fever and leukocytosis—a narrative review. *Critical Care*, *26*(1), 14. https://doi.org/10.1186/s13054-021-03862-5

Basodan, N., Mehmadi, A. E. A., Mehmadi, A. E. A., Aldawood, S. M., Hawsawi, A., Fatini, F., Mulla, Z. M., Nawwab, W., Alshareef, A., Almhmadi, A. H., Ahmed, A., Bokhari, A., Alzahrani, A. G., Basodan, N., Mehmadi, A. E. A., Mehmadi, A. E. A., Aldawood, S., Hawsawi, A., Fatini, F., … Alzahrani, A. (2022). Septic Shock: Management and Outcomes. *Cureus*, *14*(12). https://doi.org/10.7759/cureus.32158

Bennett, J., Capece, D., Begalli, F., Verzella, D., D'Andrea, D., Tornatore, L., & Franzoso, G. (2018). NF-κB in the crosshairs: Rethinking an old riddle. *The International Journal of Biochemistry & Cell Biology*, *95*, 108–112. https://doi.org/10.1016/j.biocel.2017.12.020

Bernard, G. R., Vincent, J. L., Laterre, P. F., LaRosa, S. P., Dhainaut, J. F., Lopez-Rodriguez, A., Steingrub, J. S., Garber, G. E., Helterbrand, J. D., Ely, E. W., Fisher, C. J., & Recombinant human protein C Worldwide Evaluation in Severe Sepsis (PROWESS) study group. (2001). Efficacy and safety of recombinant human activated protein C for severe sepsis. *The New England Journal of Medicine*, *344*(10), 699–709. https://doi.org/10.1056/NEJM200103083441001

Bhagwani, A., Thompson, A. A. R., & Farkas, L. (2020). When Innate Immunity Meets Angiogenesis—The Role of Toll-Like Receptors in Endothelial Cells and Pulmonary Hypertension. *Frontiers in Medicine*, *7*, 352. https://doi.org/10.3389/fmed.2020.00352

Bishop, G. A., & Xie, P. (2007). Multiple roles of TRAF3 signaling in lymphocyte function. *Immunologic Research*, *39*(1–3), 22–32. https://doi.org/10.1007/s12026-007-0068-1

Blasi, E., Mathieson, B. J., Varesio, L., Cleveland, J. L., Borchert, P. A., & Rapp, U. R. (1985). Selective immortalization of murine macrophages from fresh bone marrow by a raf/myc recombinant murine retrovirus. *Nature*, *318*(6047), 667–670. https://doi.org/10.1038/318667a0

Borghi, A., Haegman, M., Fischer, R., Carpentier, I., Bertrand, M. J. M., Libert, C., Afonina, I. S., & Beyaert, R. (2018). The E3 ubiquitin ligases HOIP and cIAP1 are recruited to the TNFR2 signaling complex and mediate TNFR2-induced canonical NF-κB signaling. *Biochemical Pharmacology*, *153*, 292–298. https://doi.org/10.1016/j.bcp.2018.01.039

Brenner, D., Blaser, H., & Mak, T. W. (2015). Regulation of tumour necrosis factor signalling: Live or let die. *Nature Reviews Immunology*, *15*(6), 362–374. https://doi.org/10.1038/nri3834

Bullock, J., Rizvi, S. A. A., Saleh, A. M., Ahmed, S. S., Do, D. P., Ansari, R. A., & Ahmed, J. (2018). Rheumatoid Arthritis: A Brief Overview of the Treatment. *Medical Principles and Practice*, *27*(6), 501–507. https://doi.org/10.1159/000493390

Cao, L., Zhu, T., Lang, X., Jia, S., Yang, Y., Zhu, C., Wang, Y., Feng, S., Wang, C., Zhang, P., Chen, J., & Jiang, H. (2020). Inhibiting DNA Methylation Improves Survival in Severe Sepsis by Regulating NF-κB Pathway. *Frontiers in Immunology*, *11*. https://doi.org/10.3389/fimmu.2020.01360

Cao, M., Wang, G., & Xie, J. (2023). Immune dysregulation in sepsis: Experiences, lessons and perspectives. *Cell Death Discovery*, *9*(1), 1–11. https://doi.org/10.1038/s41420-023-01766-7

Chen, R.-H., Chen, Y.-H., & Huang, T.-Y. (2019). Ubiquitin-mediated regulation of autophagy. *Journal of Biomedical Science*, *26*(1), 80. https://doi.org/10.1186/s12929-019-0569-y

Cockram, P. E., Kist, M., Prakash, S., Chen, S.-H., Wertz, I. E., & Vucic, D. (2021). Ubiquitination in the regulation of inflammatory cell death and cancer. *Cell Death and Differentiation*, *28*(2), 591–605. https://doi.org/10.1038/s41418-020-00708-5

Cohen, J., Vincent, J.-L., Adhikari, N. K. J., Machado, F. R., Angus, D. C., Calandra, T., Jaton, K., Giulieri, S., Delaloye, J., Opal, S., Tracey, K., van der Poll, T., & Pelfrene, E. (2015). Sepsis: A roadmap for future research. *The Lancet. Infectious Diseases*, *15*(5), 581–614. https://doi.org/10.1016/S1473-3099(15)70112-X

Conze, D. B., Albert, L., Ferrick, D. A., Goeddel, D. V., Yeh, W.-C., Mak, T., & Ashwell, J. D. (2005). Posttranscriptional downregulation of c-IAP2 by the ubiquitin protein ligase c-IAP1 in vivo. *Molecular and Cellular Biology*, *25*(8), 3348–3356. https://doi.org/10.1128/MCB.25.8.3348-3356.2005

Das, A., Ariyakumar, G., Gupta, N., Kamdar, S., Barugahare, A., Deveson-Lucas, D., Gee, S., Costeloe, K., Davey, M. S., Fleming, P., & Gibbons, D. L. (2024). Identifying immune signatures of sepsis to increase diagnostic accuracy in very preterm babies. *Nature Communications*, *15*(1), 388. https://doi.org/10.1038/s41467-023-44387-5

De Nardo, D., Kalvakolanu, D. V., & Latz, E. (2018). Immortalization of Murine Bone Marrow-Derived Macrophages. In G. Rousselet (Ed.), *Macrophages: Methods and Protocols* (pp. 35–49). Springer. https://doi.org/10.1007/978-1-4939-7837-3_4

Deane, K. D., Demoruelle, M. K., Kelmenson, L. B., Kuhn, K. A., Norris, J. M., & Holers, V. M. (2017). Genetic and environmental risk factors for rheumatoid arthritis. *Best Practice & Research Clinical Rheumatology*, *31*(1), 3–18. https://doi.org/10.1016/j.berh.2017.08.003

Dempsey, P. W., Doyle, S. E., He, J. Q., & Cheng, G. (2003). The signaling adaptors and pathways activated by TNF superfamily. *Cytokine & Growth Factor Reviews*, *14*(3), 193–209. https://doi.org/10.1016/S1359-6101(03)00021-2

Dhillon, B., Aleithan, F., Abdul-Sater, Z., & Abdul-Sater, A. A. (2019). The Evolving Role of TRAFs in Mediating Inflammatory Responses. *Frontiers in Immunology*, *10*, 104. https://doi.org/10.3389/fimmu.2019.00104

Doherty, G. M., Lange, J. R., Langstein, H. N., Alexander, H. R., Buresh, C. M., & Norton, J. A. (1992). Evidence for IFN-gamma as a mediator of the lethality of endotoxin and tumor necrosis factor-alpha. *Journal of Immunology (Baltimore, Md.: 1950)*, *149*(5), 1666–1670.

Eckelman, B. P., & Salvesen, G. S. (2006). The human anti-apoptotic proteins cIAP1 and cIAP2 bind but do not inhibit caspases. *The Journal of Biological Chemistry*, *281*(6), 3254–3260. https://doi.org/10.1074/jbc.M510863200

Edilova, M. I., Abdul-Sater, A. A., & Watts, T. H. (2018). TRAF1 Signaling in Human Health and Disease. *Frontiers in Immunology*, *9*, 2969. https://doi.org/10.3389/fimmu.2018.02969

Edilova, M. I., Akram, A., & Abdul-Sater, A. A. (2021). Innate immunity drives pathogenesis of rheumatoid arthritis. *Biomedical Journal*, *44*(2), 172–182. https://doi.org/10.1016/j.bj.2020.06.010

Edman-Wallér, J., Ljungström, L., Jacobsson, G., Andersson, R., & Werner, M. (2016). Systemic symptoms predict presence or development of severe sepsis and septic shock. *Infectious Diseases (London, England)*, *48*(3), 209–214. https://doi.org/10.3109/23744235.2015.1104719

Emmerich, C. H., Bakshi, S., Kelsall, I. R., Ortiz-Guerrero, J., Shpiro, N., & Cohen, P. (2016). Lys63/Met1-hybrid ubiquitin chains are commonly formed during the activation of innate

immune signalling. *Biochemical and Biophysical Research Communications*, *474*(3), 452–461. https://doi.org/10.1016/j.bbrc.2016.04.141

Entezami, P., Fox, D. A., Clapham, P. J., & Chung, K. C. (2011). Historical Perspective on the Etiology of Rheumatoid Arthritis. *Hand Clinics*, *27*(1), 1–10. https://doi.org/10.1016/j.hcl.2010.09.006

Fajgenbaum, D. C., & June, C. H. (2020). Cytokine Storm. *The New England Journal of Medicine*, *383*(23), 2255–2273. https://doi.org/10.1056/NEJMra2026131

Finfer, S., & Machado, F. R. (2016). The Global Epidemiology of Sepsis. Does It Matter That We Know So Little? *American Journal of Respiratory and Critical Care Medicine*, *193*(3), 228–230. https://doi.org/10.1164/rccm.201510-1976ED

Fitzgerald, K. A., & Kagan, J. C. (2020). Toll-like Receptors and the control of immunity. *Cell*, *180*(6), 1044–1066. https://doi.org/10.1016/j.cell.2020.02.041

Fohner, A. E., Greene, J. D., Lawson, B. L., Chen, J. H., Kipnis, P., Escobar, G. J., & Liu, V. X. (2019). Assessing clinical heterogeneity in sepsis through treatment patterns and machine learning. *Journal of the American Medical Informatics Association: JAMIA*, *26*(12), 1466–1477. https://doi.org/10.1093/jamia/ocz106

Fujita, H., Rahighi, S., Akita, M., Kato, R., Sasaki, Y., Wakatsuki, S., & Iwai, K. (2014). Mechanism Underlying IκB Kinase Activation Mediated by the Linear Ubiquitin Chain Assembly Complex. *Molecular and Cellular Biology*, *34*(7), 1322–1335. https://doi.org/10.1128/MCB.01538-13

Giamarellos-Bourboulis, E. J., Aschenbrenner, A. C., Bauer, M., Bock, C., Calandra, T., Gat-Viks, I., Kyriazopoulou, E., Lupse, M., Monneret, G., Pickkers, P., Schultze, J. L., van der Poll, T., van de Veerdonk, F. L., Vlaar, A. P. J., Weis, S., Wiersinga, W. J., & Netea,

M. G. (2024). The pathophysiology of sepsis and precision-medicine-based immunotherapy. *Nature Immunology*, *25*(1), 19–28. https://doi.org/10.1038/s41590-023-01660-5

Graber, T. E., & Holcik, M. (2011). Distinct roles for the cellular inhibitors of apoptosis proteins 1 and 2. *Cell Death & Disease*, *2*(3), e135–e135. https://doi.org/10.1038/cddis.2011.20

Haraoui, B., & Bykerk, V. (2007). Etanercept in the treatment of rheumatoid arthritis. *Therapeutics and Clinical Risk Management*, *3*(1), 99–105.

Howard, M., Muchamuel, T., Andrade, S., & Menon, S. (1993). Interleukin 10 protects mice from lethal endotoxemia. *The Journal of Experimental Medicine*, *177*(4), 1205–1208. https://doi.org/10.1084/jem.177.4.1205

Ikezoe, T., Yang, Y., Heber, D., Taguchi, H., & Koeffler, H. P. (2003). PC-SPES: A Potent Inhibitor of Nuclear Factor-κB Rescues Mice from Lipopolysaccharide-Induced Septic Shock. *Molecular Pharmacology*, *64*(6), 1521–1529. https://doi.org/10.1124/mol.64.6.1521

Iwai, K. (2021). Discovery of linear ubiquitination, a crucial regulator for immune signaling and cell death. *The FEBS Journal*, *288*(4), 1060–1069. https://doi.org/10.1111/febs.15471

Jacobi, J. (2002). Pathophysiology of sepsis. *American Journal of Health-System Pharmacy: AJHP: Official Journal of the American Society of Health-System Pharmacists*, *59 Suppl 1*, S3-8. https://doi.org/10.1093/ajhp/59.suppl_1.S3

Kaiser, P., & Huang, L. (2005). Global approaches to understanding ubiquitination. *Genome Biology*, *6*(10), 233. https://doi.org/10.1186/gb-2005-6-10-233

Karki, R., Sharma, B. R., Tuladhar, S., Williams, E. P., Zalduondo, L., Samir, P., Zheng, M., Sundaram, B., Banoth, B., Malireddi, R. K. S., Schreiner, P., Neale, G., Vogel, P.,

Webby, R., Jonsson, C. B., & Kanneganti, T.-D. (2021). Synergism of TNF-α and IFN-γ Triggers Inflammatory Cell Death, Tissue Damage, and Mortality in SARS-CoV-2 Infection and Cytokine Shock Syndromes. *Cell*, *184*(1), 149-168.e17. https://doi.org/10.1016/j.cell.2020.11.025

Kaur, B. P., & Secord, E. (2019). Innate Immunity. *Pediatric Clinics of North America*, *66*(5), 905–911. https://doi.org/10.1016/j.pcl.2019.06.011

Kawai, T., & Akira, S. (2007). Signaling to NF-κB by Toll-like receptors. *Trends in Molecular Medicine*, *13*(11), 460–469. https://doi.org/10.1016/j.molmed.2007.09.002

Kawai, T., & Akira, S. (2010). The role of pattern-recognition receptors in innate immunity: Update on Toll-like receptors. *Nature Immunology*, *11*(5), 373–384. https://doi.org/10.1038/ni.1863

Kawasaki, T., & Kawai, T. (2014). Toll-Like Receptor Signaling Pathways. *Frontiers in Immunology*, *5*. https://doi.org/10.3389/fimmu.2014.00461

Kelly, A., Vereker, E., Nolan, Y., Brady, M., Barry, C., Loscher, C. E., Mills, K. H. G., & Lynch, M. A. (2003). Activation of p38 plays a pivotal role in the inhibitory effect of lipopolysaccharide and interleukin-1 beta on long term potentiation in rat dentate gyrus. *The Journal of Biological Chemistry*, *278*(21), 19453–19462. https://doi.org/10.1074/jbc.M301938200

Kirisako, T., Kamei, K., Murata, S., Kato, M., Fukumoto, H., Kanie, M., Sano, S., Tokunaga, F., Tanaka, K., & Iwai, K. (2006). A ubiquitin ligase complex assembles linear polyubiquitin chains. *The EMBO Journal*, *25*(20), 4877–4887. https://doi.org/10.1038/sj.emboj.7601360

Kumar, V. (2020). Toll-like receptors in sepsis-associated cytokine storm and their endogenous negative regulators as future immunomodulatory targets. *International Immunopharmacology*, *89*, 107087. https://doi.org/10.1016/j.intimp.2020.107087

Kuo, S.-M. (2016). Gender Difference in Bacteria Endotoxin-Induced Inflammatory and Anorexic Responses. *PLoS ONE*, *11*(9), e0162971. https://doi.org/10.1371/journal.pone.0162971

Labbé, K., McIntire, C. R., Doiron, K., Leblanc, P. M., & Saleh, M. (2011). Cellular Inhibitors of Apoptosis Proteins cIAP1 and cIAP2 Are Required for Efficient Caspase-1 Activation by the Inflammasome. *Immunity*, *35*(6), 897–907. https://doi.org/10.1016/j.immuni.2011.10.016

Lalani, A. I., Zhu, S., Gokhale, S., Jin, J., & Xie, P. (2018). TRAF Molecules in Inflammation and Inflammatory Diseases. *Current Pharmacology Reports*, *4*(1), 64–90. https://doi.org/10.1007/s40495-017-0117-y

Li, D., & Wu, M. (2021). Pattern recognition receptors in health and diseases. *Signal Transduction and Targeted Therapy*, *6*(1), 1–24. https://doi.org/10.1038/s41392-021-00687-0

Liao, G., Zhang, M., Harhaj, E. W., & Sun, S.-C. (2004). Regulation of the NF-kappaB-inducing kinase by tumor necrosis factor receptor-associated factor 3-induced degradation. *The Journal of Biological Chemistry*, *279*(25), 26243–26250. https://doi.org/10.1074/jbc.M403286200

Lin, Y.-J., Anzaghe, M., & Schülke, S. (2020). Update on the Pathomechanism, Diagnosis, and Treatment Options for Rheumatoid Arthritis. *Cells*, *9*(4), Article 4. https://doi.org/10.3390/cells9040880

Liu, D., Huang, S.-Y., Sun, J.-H., Zhang, H.-C., Cai, Q.-L., Gao, C., Li, L., Cao, J., Xu, F., Zhou, Y., Guan, C.-X., Jin, S.-W., Deng, J., Fang, X.-M., Jiang, J.-X., & Zeng, L. (2022). Sepsis-induced immunosuppression: Mechanisms, diagnosis and current treatment options. *Military Medical Research*, *9*(1), 56. https://doi.org/10.1186/s40779-022-00422-y

Liu, G., & Zhao, Y. (2007). Toll-like receptors and immune regulation: Their direct and indirect modulation on regulatory CD4+ CD25+ T cells. *Immunology*, *122*(2), 149–156. https://doi.org/10.1111/j.1365-2567.2007.02651.x

Liu, J., Xiang, J., Li, X., Blankson, S., Zhao, S., Cai, J., Jiang, Y., Redmond, H. P., & Wang, J. H. (2017). NF-κB activation is critical for bacterial lipoprotein tolerance-enhanced bactericidal activity in macrophages during microbial infection. *Scientific Reports*, *7*(1), 40418. https://doi.org/10.1038/srep40418

Liu, P., Gan, W., Su, S., Hauenstein, A. V., Fu, T.-M., Brasher, B., Schwerdtfeger, C., Liang, A. C., Xu, M., & Wei, W. (2018). K63-linked polyubiquitin chains bind to DNA to facilitate DNA damage repair. *Science Signaling*, *11*(533), eaar8133. https://doi.org/10.1126/scisignal.aar8133

Liu, S., & Chen, Z. J. (2011). Expanding role of ubiquitination in NF-κB signaling. *Cell Research*, *21*(1), 6–21. https://doi.org/10.1038/cr.2010.170

Liu, S. F., & Malik, A. B. (2006). NF-κB activation as a pathological mechanism of septic shock and inflammation. *American Journal of Physiology-Lung Cellular and Molecular Physiology*, *290*(4), L622–L645. https://doi.org/10.1152/ajplung.00477.2005

Liu, S. F., Ye, X., & Malik, A. B. (1999). Pyrrolidine dithiocarbamate prevents I-kappaB degradation and reduces microvascular injury induced by lipopolysaccharide in multiple organs. *Molecular Pharmacology*, *55*(4), 658–667.

Liu, T., Zhang, L., Joo, D., & Sun, S.-C. (2017). NF-κB signaling in inflammation. *Signal Transduction and Targeted Therapy*, *2*(1), 1–9. https://doi.org/10.1038/sigtrans.2017.23

Liu, V. X., Bhimarao, M., Greene, J. D., Manickam, R. N., Martinez, A., Schuler, A., Barreda, F., & Escobar, G. J. (2021). The Presentation, Pace, and Profile of Infection and Sepsis Patients Hospitalized Through the Emergency Department: An Exploratory Analysis. *Critical Care Explorations*, *3*(3), e0344. https://doi.org/10.1097/CCE.0000000000000344

Ma, G., Wu, X., Qi, C., Yu, X., & Zhang, F. (2024). Development of macrophage-associated genes prognostic signature predicts clinical outcome and immune infiltration for sepsis. *Scientific Reports*, *14*(1), 2026. https://doi.org/10.1038/s41598-024-51536-3

Madahar, S. S., Gideon, A., & Abdul-Sater, A. A. (2023). Nod-like receptors in inflammatory arthritis. *Biomedical Journal*, *47*(1), 100655. https://doi.org/10.1016/j.bj.2023.100655

Mahoney, D. J., Cheung, H. H., Mrad, R. L., Plenchette, S., Simard, C., Enwere, E., Arora, V., Mak, T. W., Lacasse, E. C., Waring, J., & Korneluk, R. G. (2008). Both cIAP1 and cIAP2 regulate TNFα-mediated NF-κB activation. *Proceedings of the National Academy of Sciences*, *105*(33), 11778–11783. https://doi.org/10.1073/pnas.0711122105

Marshall, J. S., Warrington, R., Watson, W., & Kim, H. L. (2018). An introduction to immunology and immunopathology. *Allergy, Asthma & Clinical Immunology*, *14*(2), 49. https://doi.org/10.1186/s13223-018-0278-1

McPherson, A. J., Snell, L. M., Mak, T. W., & Watts, T. H. (2012). Opposing Roles for TRAF1 in the Alternative versus Classical NF-κB Pathway in T Cells *. *Journal of Biological Chemistry*, *287*(27), 23010–23019. https://doi.org/10.1074/jbc.M112.350538

Mirzaesmaeili, A., Zangiabadi, S., Raspanti, J., Akram, A., Inman, R. D., & Abdul-Sater, A. A. (2023). Cutting Edge: Negative Regulation of Inflammasome Activation by TRAF1 Can Limit Gout. *Journal of Immunology (Baltimore, Md.: 1950)*, *210*(5), 531–535. https://doi.org/10.4049/jimmunol.2200465

Mithal, L. B., Arshad, M., Swigart, L. R., Khanolkar, A., Ahmed, A., & Coates, B. M. (2022). Mechanisms and modulation of sepsis-induced immune dysfunction in children. *Pediatric Research*, *91*(2), 447–453. https://doi.org/10.1038/s41390-021-01879-8

Nakamura, N. (2018). Ubiquitin System. *International Journal of Molecular Sciences*, *19*(4), 1080. https://doi.org/10.3390/ijms19041080

Panoulas, V. F., Smith, J. P., Nightingale, P., & Kitas, G. D. (2009). Association of the TRAF1/C5 locus with increased mortality, particularly from malignancy or sepsis, in patients with rheumatoid arthritis. *Arthritis and Rheumatism*, *60*(1), 39–46. https://doi.org/10.1002/art.24176

Pocock, J., Gómez-Guerrero, C., Harendza, S., Ayoub, M., Hernández-Vargas, P., Zahner, G., Stahl, R. A. K., & Thaiss, F. (2003). Differential activation of NF-kappa B, AP-1, and C/EBP in endotoxin-tolerant rats: Mechanisms for in vivo regulation of glomerular RANTES/CCL5 expression. *Journal of Immunology (Baltimore, Md.: 1950)*, *170*(12), 6280–6291. https://doi.org/10.4049/jimmunol.170.12.6280

Poll, T. van der, Shankar-Hari, M., & Wiersinga, W. J. (2021). The immunology of sepsis. *Immunity*, *54*(11), 2450–2464. https://doi.org/10.1016/j.immuni.2021.10.012

Pritts, T. A., Moon, M. R., Wang, Q., Hungness, E. S., Salzman, A. L., Fischer, J. E., & Hasselgren, P. O. (2000). Activation of NF-kappaB varies in different regions of the gastrointestinal tract during endotoxemia. *Shock (Augusta, Ga.)*, *14*(2), 118–122. https://doi.org/10.1097/00024382-200014020-00007

Rosenthal, V. D., Maki, D. G., Mehta, Y., Leblebicioglu, H., Memish, Z. A., Al-Mousa, H. H., Balkhy, H., Hu, B., Alvarez-Moreno, C., Medeiros, E. A., Apisarnthanarak, A., Raka, L., Cuellar, L. E., Ahmed, A., Navoa-Ng, J. A., El-Kholy, A. A., Kanj, S. S., Bat-Erdene, I., Duszynska, W., … Anh, D. P. P. (2014). International Nosocomial Infection Control Consortiu (INICC) report, data summary of 43 countries for 2007-2012. Device-associated module. *American Journal of Infection Control*, *42*(9), 942–956. https://doi.org/10.1016/j.ajic.2014.05.029

Rothe, M., Wong, S. C., Henzel, W. J., & Goeddel, D. V. (1994). A novel family of putative signal transducers associated with the cytoplasmic domain of the 75 kDa tumor necrosis factor receptor. *Cell*, *78*(4), 681–692. https://doi.org/10.1016/0092-8674(94)90532-0

Roy, N., Deveraux, Q. L., Takahashi, R., Salvesen, G. S., & Reed, J. C. (1997). The c-IAP-1 and c-IAP-2 proteins are direct inhibitors of specific caspases. *The EMBO Journal*, *16*(23), 6914–6925. https://doi.org/10.1093/emboj/16.23.6914

Rudd, K. E., Johnson, S. C., Agesa, K. M., Shackelford, K. A., Tsoi, D., Kievlan, D. R., Colombara, D. V., Ikuta, K. S., Kissoon, N., Finfer, S., Fleischmann-Struzek, C., Machado, F. R., Reinhart, K. K., Rowan, K., Seymour, C. W., Watson, R. S., West, T. E., Marinho, F., Hay, S. I., … Naghavi, M. (2020). Global, regional, and national sepsis incidence and mortality, 1990–2017: Analysis for the Global Burden of Disease Study.

Lancet (London, England), *395*(10219), 200–211. https://doi.org/10.1016/S0140-6736(19)32989-7

Russell, D. A., Tucker, K. K., Chinookoswong, N., Thompson, R. C., & Kohno, T. (1995). Combined inhibition of interleukin-1 and tumor necrosis factor in rodent endotoxemia: Improved survival and organ function. *The Journal of Infectious Diseases*, *171*(6), 1528–1538. https://doi.org/10.1093/infdis/171.6.1528

Sabbagh, L., Pulle, G., Liu, Y., Tsitsikov, E. N., & Watts, T. H. (2008). ERK-Dependent Bim Modulation Downstream of the 4-1BB-TRAF1 Signaling Axis Is a Critical Mediator of CD8 T Cell Survival In Vivo1. *The Journal of Immunology*, *180*(12), 8093–8101. https://doi.org/10.4049/jimmunol.180.12.8093

Scotland, R. S., Stables, M. J., Madalli, S., Watson, P., & Gilroy, D. W. (2011). Sex differences in resident immune cell phenotype underlie more efficient acute inflammatory responses in female mice. *Blood*, *118*(22), 5918–5927. https://doi.org/10.1182/blood-2011-03-340281

Sheehan, M., Wong, H. R., Hake, P. W., & Zingarelli, B. (2003). Parthenolide improves systemic hemodynamics and decreases tissue leukosequestration in rats with polymicrobial sepsis*. *Critical Care Medicine*, *31*(9), 2263. https://doi.org/10.1097/01.CCM.0000085186.14867.F7

Sheikh, F., Chechulina, V., Garber, G., Hendrick, K., Kissoon, N., Proulx, L., Russell, K., Fox-Robichaud, A. E., Schwartz, L., Barrett, K. A., & Sepsis Canada. (2024). Reducing the burden of preventable deaths from sepsis in Canada: A need for a national sepsis action plan. *Healthcare Management Forum*, 8404704241240956. https://doi.org/10.1177/08404704241240956

Siegmund, D., Kums, J., Ehrenschwender, M., & Wajant, H. (2016). Activation of TNFR2 sensitizes macrophages for TNFR1-mediated necroptosis. *Cell Death & Disease*, *7*(9), e2375–e2375. https://doi.org/10.1038/cddis.2016.285

Silman, A. J., & Pearson, J. E. (2002). Epidemiology and genetics of rheumatoid arthritis. *Arthritis Research & Therapy*, *4*(3), S265. https://doi.org/10.1186/ar578

Singh, N., Yamamoto, M., Takami, M., Seki, Y., Takezaki, M., Mellor, A. L., & Iwashima, M. (2009). CD4+CD25+ Regulatory T Cells Resist a Novel Form of CD28- and Fas-Dependent p53-Induced T Cell Apoptosis. *The Journal of Immunology*, *184*(1), 94–104. https://doi.org/10.4049/jimmunol.0900753

So, T., & Ishii, N. (2019). The TNF–TNFR Family of Co-signal Molecules. In M. Azuma & H. Yagita (Eds.), *Co-signal Molecules in T Cell Activation: Immune Regulation in Health and Disease* (pp. 53–84). Springer. https://doi.org/10.1007/978-981-32-9717-3_3

Speiser, D. E., Lee, S. Y., Wong, B., Arron, J., Santana, A., Kong, Y.-Y., Ohashi, P. S., & Choi, Y. (1997). A Regulatory Role for TRAF1 in Antigen-induced Apoptosis of T Cells. *The Journal of Experimental Medicine*, *185*(10), 1777–1783.

Sun, M., & Zhang, X. (2022). Current methodologies in protein ubiquitination characterization: From ubiquitinated protein to ubiquitin chain architecture. *Cell & Bioscience*, *12*, 126. https://doi.org/10.1186/s13578-022-00870-y

Sun, S.-C. (2010). Controlling the fate of NIK: A central stage in noncanonical NF-kappaB signaling. *Science Signaling*, *3*(123), pe18. https://doi.org/10.1126/scisignal.3123pe18

Sun, S.-C. (2011). Non-canonical NF-κB signaling pathway. *Cell Research*, *21*(1), 71–85. https://doi.org/10.1038/cr.2010.177

Sun, S.-C., Chang, J.-H., & Jin, J. (2013). Regulation of NF-κB in Autoimmunity. *Trends in Immunology*, *34*(6), 282–289. https://doi.org/10.1016/j.it.2013.01.004

Sun, T., Liu, Z., & Yang, Q. (2020). The role of ubiquitination and deubiquitination in cancer metabolism. *Molecular Cancer*, *19*(1), 146. https://doi.org/10.1186/s12943-020-01262-x

Takahama, M., Patil, A., Richey, G., Cipurko, D., Johnson, K., Carbonetto, P., Plaster, M., Pandey, S., Cheronis, K., Ueda, T., Gruenbaum, A., Kawamoto, T., Stephens, M., & Chevrier, N. (2024). A pairwise cytokine code explains the organism-wide response to sepsis. *Nature Immunology*, *25*(2), 226–239. https://doi.org/10.1038/s41590-023-01722-8

Takeda, K., & Akira, S. (2005). Toll-like receptors in innate immunity. *International Immunology*, *17*(1), 1–14. https://doi.org/10.1093/intimm/dxh186

Tokunaga, F., Nakagawa, T., Nakahara, M., Saeki, Y., Taniguchi, M., Sakata, S., Tanaka, K., Nakano, H., & Iwai, K. (2011). SHARPIN is a component of the NF-κB-activating linear ubiquitin chain assembly complex. *Nature*, *471*(7340), 633–636. https://doi.org/10.1038/nature09815

Tokunaga, F., Sakata, S., Saeki, Y., Satomi, Y., Kirisako, T., Kamei, K., Nakagawa, T., Kato, M., Murata, S., Yamaoka, S., Yamamoto, M., Akira, S., Takao, T., Tanaka, K., & Iwai, K. (2009). Involvement of linear polyubiquitylation of NEMO in NF-κB activation. *Nature Cell Biology*, *11*(2), 123–132. https://doi.org/10.1038/ncb1821

Tsitsikov, E. N., Laouini, D., Dunn, I. F., Sannikova, T. Y., Davidson, L., Alt, F. W., & Geha, R. S. (2001). TRAF1 is a negative regulator of TNF signaling. Enhanced TNF signaling in TRAF1-deficient mice. *Immunity*, *15*(4), 647–657. https://doi.org/10.1016/s1074-7613(01)00207-2

Vallabhapurapu, S., Matsuzawa, A., Zhang, W., Tseng, P.-H., Keats, J. J., Wang, H., Vignali, D. A. A., Bergsagel, P. L., & Karin, M. (2008). Non-redundant and complementary functions of adaptor proteins TRAF2 and TRAF3 in a ubiquitination cascade that activates NIK-dependent alternative NF-κB signaling. *Nature Immunology*, *9*(12), 1364–1370. https://doi.org/10.1038/ni.1678

van der Poll, T., van de Veerdonk, F. L., Scicluna, B. P., & Netea, M. G. (2017). The immunopathology of sepsis and potential therapeutic targets. *Nature Reviews Immunology*, *17*(7), 407–420. https://doi.org/10.1038/nri.2017.36

Vince, J. E., Pantaki, D., Feltham, R., Mace, P. D., Cordier, S. M., Schmukle, A. C., Davidson, A. J., Callus, B. A., Wong, W. W.-L., Gentle, I. E., Carter, H., Lee, E. F., Walczak, H., Day, C. L., Vaux, D. L., & Silke, J. (2009). TRAF2 Must Bind to Cellular Inhibitors of Apoptosis for Tumor Necrosis Factor (TNF) to Efficiently Activate NF-κB and to Prevent TNF-induced Apoptosis. *The Journal of Biological Chemistry*, *284*(51), 35906–35915. https://doi.org/10.1074/jbc.M109.072256

Vincent, J.-L. (2022). Current sepsis therapeutics. *eBioMedicine*, *86*, 104318. https://doi.org/10.1016/j.ebiom.2022.104318

Waage, A., & Espevik, T. (1988). Interleukin 1 potentiates the lethal effect of tumor necrosis factor alpha/cachectin in mice. *The Journal of Experimental Medicine*, *167*(6), 1987–1992. https://doi.org/10.1084/jem.167.6.1987

Wajant, H., Pfizenmaier, K., & Scheurich, P. (2003). Tumor necrosis factor signaling. *Cell Death & Differentiation*, *10*(1), 45–65. https://doi.org/10.1038/sj.cdd.4401189

Wajant, H., & Siegmund, D. (2019). TNFR1 and TNFR2 in the Control of the Life and Death Balance of Macrophages. *Frontiers in Cell and Developmental Biology*, *7*, 91. https://doi.org/10.3389/fcell.2019.00091

Watts, T. H. (2005). TNF/TNFR family members in costimulation of T cell responses. *Annual Review of Immunology*, *23*, 23–68. https://doi.org/10.1146/annurev.immunol.23.021704.115839

Wicovsky, A., Henkler, F., Salzmann, S., Scheurich, P., Kneitz, C., & Wajant, H. (2009). Tumor necrosis factor receptor-associated factor-1 enhances proinflammatory TNF receptor-2 signaling and modifies TNFR1–TNFR2 cooperation. *Oncogene*, *28*(15), 1769–1781. https://doi.org/10.1038/onc.2009.29

Xie, P. (2013). TRAF molecules in cell signaling and in human diseases. *Journal of Molecular Signaling*, *8*, 7. https://doi.org/10.1186/1750-2187-8-7

Yang, Y., Feng, R., Wang, Y.-Z., Sun, H.-W., Zou, Q.-M., & Li, H.-B. (2020). Toll-like receptors: Triggers of regulated cell death and promising targets for cancer therapy. *Immunology Letters*, *223*, 1–9. https://doi.org/10.1016/j.imlet.2020.04.002

Zhang, H., & Sun, S.-C. (2015). NF-κB in inflammation and renal diseases. *Cell & Bioscience*, *5*(1), 63. https://doi.org/10.1186/s13578-015-0056-4

Zheng, C., Kabaleeswaran, V., Wang, Y., Cheng, G., & Wu, H. (2010). Crystal Structures of the TRAF2: cIAP2 and the TRAF1: TRAF2: cIAP2 Complexes: Affinity, Specificity, and Regulation. *Molecular Cell*, *38*(1), 101–113. https://doi.org/10.1016/j.molcel.2010.03.009

Zhu, Y., Chen, X., Liu, Z., Peng, Y.-P., & Qiu, Y.-H. (2015). Interleukin-10 Protection against Lipopolysaccharide-Induced Neuro-Inflammation and Neurotoxicity in Ventral

Mesencephalic Cultures. *International Journal of Molecular Sciences*, *17*(1), 25. https://doi.org/10.3390/ijms17010025

Appendix A

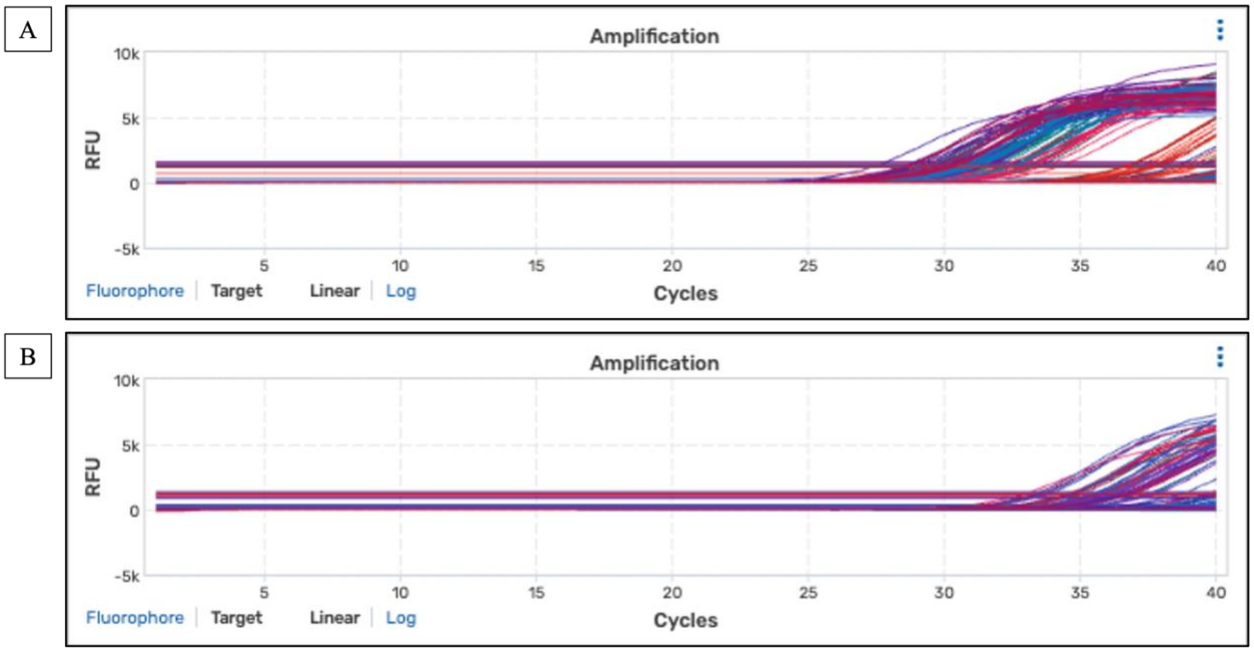

Supplementary Figure 1.0: RT-qPCR amplification curves for the no reverse transcriptase control corresponding to the genes of interest.

The RNA extraction protocol was optimized by including a second extraction with acid phenol chloroform that helps minimize DNA contamination. **(A)** Amplification curves for unmodified protocol show significant contribution of genomic DNA amplification. **(B)** Amplification curves for the modified protocol shows minimal or insignificant genomic DNA amplification.